



## **TASK 27**

# **Performance of Solar Facade Components**

## **Performance, durability and sustainability**

of advanced windows and solar components for building envelopes

**Final Report**

## **Subtask A: Performance**

**Project A3:**

**Solar building components and integrated assemblies**

March 2006

**Operating Agent:**

**Michael Köhl**

**Fraunhofer Institute for Solar Energy Systems**

**for PTJ Jülich, Germany**

## Table of content

|  |           |
|--|-----------|
| <b>Table of content .....</b>  | <b>2</b>  |
| <b>Project A3: Solar building components and integrated assemblies .....</b> | <b>7</b>  |
| <b>Case study 1: Solar shading devices.....</b>                              | <b>8</b>  |
| <b>1 Introduction.....</b>   | <b>8</b>  |
| <b>2 Performance indicators.....</b>   | <b>9</b>  |
| <b>2.1 Concept.....</b>  | <b>9</b>  |
| <b>2.2 Materials .....</b>   | <b>9</b>  |
| <b>2.3 Shading devices.....</b>  | <b>10</b> |
| <b>2.4 Combination of shading device and glazing.....</b>                    | <b>11</b> |
| <b>3 Measurement and modelling of shading performance.....</b>               | <b>11</b> |
| <b>3.1 Optical and calorimetric measurements.....</b>                        | <b>11</b> |
| 3.1.1 Measured shading devices.....  | 12        |
| 3.1.2 Solar calorimeter at ISE .....   | 13        |
| 3.1.3 Measurement results.....   | 13        |
| <b>3.2 Outdoor testing .....</b>   | <b>17</b> |
| 3.2.1 Exterior shading .....   | 18        |
| 3.2.2 Interior shading.....  | 24        |
| <b>3.3 Numerical modelling of optical properties and TSET.....</b>           | <b>25</b> |
| 3.3.1 EN 13363 .....   | 25        |
| 3.3.2 ISO 15099 .....  | 25        |
| 3.3.3 View factor model extensions .....                                     | 25        |
| 3.3.4 Optical ray-tracing .....  | 26        |
| <b>3.4 Comparison of experimental and numerical results .....</b>            | <b>27</b> |
| 3.4.1 Comparison of laboratory based experiments and modelling results ..... | 27        |

|  |           |
|--|-----------|
| Comparison of outdoor testing results with other methods.....                          | 31        |
| <b>3.5 Requirements/recommendations .....</b>  | <b>33</b> |
| 3.5.1 Calorimetric TSET-measurement.....   | 33        |
| 3.5.1.3 Component specific recommendation.....   | 34        |
| 3.5.2 Outdoor testing.....   | 36        |
| 3.5.3 Modelling .....  | 37        |
| <b>4 Shading devices and building performance.....</b>                                 | <b>37</b> |
| <b>4.1 Impact of solar shading on thermal comfort.....</b>                             | <b>37</b> |
| 4.1.1 Measured thermal comfort in an office.....                                       | 38        |
| 4.1.2 Calculation of the operative temperature in the sun .....                        | 40        |
| 4.1.3 Conclusions.....   | 42        |
| <b>4.2 Impact of solar shading on heating – cooling – lighting energy demand .....</b> | <b>42</b> |
| 4.2.1 Location.....  | 46        |
| 4.2.2 Façade orientation.....  | 46        |
| 4.2.3 Optical properties and geometry .....  | 47        |
| 4.2.4 Shading position.....  | 48        |
| 4.2.5 Control strategies .....   | 49        |
| <b>5. Conclusions .....</b>  | <b>51</b> |
| <b>5 Shading data for building EPAM .....</b>  | <b>52</b> |
| <b>5.1 Simplified performance indicators for EPAM.....</b>                             | <b>52</b> |
| <b>5.2 Shading concepts in building design .....</b>                                   | <b>53</b> |
| 5.2.1 Energy and comfort related requirements.....                                     | 54        |
| 5.2.2 Recommendations regarding building design.....                                   | 54        |
| <b>6 References .....</b>  | <b>56</b> |
| <b>Case Study 2: Double Envelope Facades.....</b>                                      | <b>58</b> |
| <b>1 Introduction.....</b>   | <b>58</b> |
| <b>2 State-of-the-art of double envelope facades .....</b>                             | <b>59</b> |

|  |           |
|--|-----------|
| <b>3 Performance characterisation .....</b>  | <b>60</b> |
| <b>4 Simulations and modelling of double envelope facades .....</b>                      | <b>61</b> |
| <b>4.1 Case study - IEA Task 27 common simulation exercise .....</b>                     | <b>62</b> |
| <b>5 Evaluation of existing double envelope facades .....</b>                            | <b>66</b> |
| <b>6 Development of the design tools and integration into existing design tools.....</b> | <b>67</b> |
| <b>7 Publications .....</b>  | <b>68</b> |
| <b>8 Working documents .....</b>   | <b>68</b> |
| <b>Case study 3: Performance of TI façades .....</b>                                     | <b>70</b> |
| <b>1 Introduction.....</b>   | <b>70</b> |
| <b>2 TI façade systems .....</b>   | <b>71</b> |
| <b>2.1 What is “transparent insulation”?.....</b>  | <b>71</b> |
| <b>2.2 Principles and examples .....</b>   | <b>71</b> |
| <b>2.3 Typical layout of structures .....</b>  | <b>72</b> |
| <b>2.4 Estimation of performance .....</b>   | <b>74</b> |
| <b>3 Concept of performance indicators .....</b>   | <b>75</b> |
| <b>3.1 Layer model.....</b>  | <b>75</b> |
| <b>3.2 Detailed and simplified indicators.....</b>                                       | <b>75</b> |
| <b>4 Performance indicators.....</b>   | <b>76</b> |
| <b>4.1 Basic materials.....</b>  | <b>76</b> |
| <b>4.2 TI structures .....</b>   | <b>77</b> |
| <b>4.3 TI façade element with integrated absorber .....</b>                              | <b>78</b> |

|  |            |
|--|------------|
| <b>4.4 Combination of TI-façade and wall.....</b>                                  | <b>78</b>  |
| <b>5 Building integration effects .....</b>  | <b>82</b>  |
| 5.1 Heat loss through the frame .....  | 83         |
| 5.2 Heat loss through internal convection .....                                    | 85         |
| 5.3 Shading effects, solar absorption by the frame.....                            | 87         |
| 5.4 Thermal comfort, overheating .....   | 89         |
| 5.5 Durability .....   | 90         |
| 5.6 Further aspects .....  | 91         |
| <b>6 Performance assessment recommendations.....</b>                               | <b>91</b>  |
| 6.1 Solar / thermal performance .....  | 91         |
| 6.2 Durability .....   | 92         |
| <b>7 References .....</b>  | <b>93</b>  |
| <b>Case Study 4: Daylighting elements .....</b>                                    | <b>95</b>  |
| 1 Optical performance characterization: principle of virtual goniophotometry ..... | 95         |
| 2 Redirecting daylight material description .....                                  | 97         |
| 3 Characterization results: light source equivalent distributions .....            | 98         |
| 4 Daylighting simulations .....  | 100        |
| 5 Real case study setup : daylighting within the Twincells .....                   | 102        |
| 6 Conclusion .....   | 102        |
| <b>Case study 5: Window – Wall/Roof Assembly .....</b>                             | <b>103</b> |

---

|  |            |
|--|------------|
| <b>1 Introduction</b> .....  | <b>103</b> |
| <b>2 Thermal transmittance for window - wall/roof assembly</b> .....                                       | <b>104</b> |
| <b>2.1 Characterization according to standards</b> .....   | <b>104</b> |
| <b>2.2 The expanded linear thermal transmittance</b> .....   | <b>105</b> |
| <b>2.3 Thermal transmittance case study</b> .....  | <b>108</b> |
| 2.3.1 Geometry and thermal properties of the reference window-wall assembly .....                          | 110        |
| 2.3.2 Results.....   | 113        |
| <b>2.4 Thermal transmittance of typical window - wall/roof assemblies in participating countries</b> ..... | <b>115</b> |
| 2.4.1 Netherlands.....   | 115        |
| 2.4.2 Finland.....   | 117        |
| <b>3 Effects of window wall/roof assembly on solar transmittance</b> .....                                 | <b>119</b> |
| <b>3.1 Correction for incidence angle and self-shading</b> .....   | <b>119</b> |
| <b>3.2 Characterizing self-shading by linear shading coefficients</b> .....                                | <b>121</b> |
| <b>3.3 Evaluation of the shaded area caused by self-shading</b> .....                                      | <b>122</b> |
| <b>3.4 Example</b> .....   | <b>127</b> |
| <b>3.5 Investigation of the linear shading coefficient</b> .....   | <b>128</b> |
| <b>3.6 Relation to other methods</b> .....   | <b>128</b> |
| <b>3.7 Simplifications and further work</b> .....  | <b>129</b> |
| <b>3.8 Ray tracing</b> .....   | <b>131</b> |
| 3.8.1 Model description .....  | 131        |
| 3.8.2 Simple method compared to results from ray tracing with zero reflectance .....                       | 132        |
| 3.8.3 Influence of reflectance .....   | 133        |
| <b>4 References</b> .....  | <b>139</b> |

---

## **Project A3: Solar building components and integrated assemblies**

Partners:

| <b>Country</b> |       | <b>Participant</b>  |
|----------------|-------|---------------------|
| B              | UCL   | Magali Bodart       |
| CH             | EMPA  | Hans Simmler        |
| CH             | EMPA  | Heinrich Manz       |
| CAN            | NRC   | Hakim Elmahdy       |
| DE             | IFT   | Nobert Sack         |
| DE             | IFT   | Michael Feinberger  |
| DE             | IFT   | Philip Plathner     |
| DE             | ISE   | Michael Köhl        |
| DE             | ISE   | Werner Platzer      |
| DK             | DTU   | Karsten Duer        |
| DK             | DTU   | Ole Holck           |
| DK             | DTU   | Svend Svendsen      |
| DK             | DTU   | Toke-Rammer Nielson |
| DK             | DTU   | Jean L.J. Rosenfeld |
| DK             | SBI   | Hanne Krogh         |
| DK             | Velux | Jan Franson         |
| DK             | Velux | Lone Moller S       |
| FR             | CSTB  | Jean-Luc Chevalier  |
| FR             | CSTB  | Francois Olive      |
| FR             | EDF   | Géraldine Corredera |
| FR             | EDF   | Denis Covalet       |
| FR             | EDF   | Remi Le Berre       |
| FR             | ENTPE | Richard Mitanchey   |
| FR             | ENTPE | Marc Fontoynt       |
| FR             | CSTB  | Francois Olive      |

---

|     |       |                   |
|-----|-------|-------------------|
| FIN | VTT   | Ismo Heimonen     |
| IT  | ENEA  | Augusto Maccari   |
| IT  | ENEA  | Michele Zinzi     |
| NL  | TNO   | Henk Oversloot    |
| NL  | TNO   | Dick van Dijk     |
| NOR | E & H | Catherine Peyrouy |
| SWE | LU    | Hakan Hakansson   |
| USA | ARC   | James Fairman     |
| USA | UMASS | Dragan Curcija    |
| USA | LBNL  | Mike Rubin        |

## Case study 1: Solar shading devices

Prepared by:

Ida Bryn, Erichsen&Horgen AS, Norway

Werner J. Platzer, Fraunhofer Institute for Solar Energy Systems, Germany

Hans Simmler, EMPA Building Technologies Laboratory. Switzerland

### 1 Introduction

Solar shading is a special topic in building physics and design. Historically it was the first “smart” component in the building envelope in the sense that it allowed to control (solar) energy transfer from outside to the inside of the building. As known from personal experience the switching efficiency can be very high, but traditional (manual) control efficiency is sometimes low. Another speciality of the widely used slat type devices is the large anisotropy of the transmission properties with respect to the incidence angle.

The capability of blocking or letting pass solar radiation into the building makes the proper handling of a shading system rather complex, even without angle-selective properties. Solar gain may significantly reduce the heating energy demand, but may also cause glare, overheating problems and large cooling loads. Blocking radiation may reduce these problems, but strongly increase the lighting energy demand. Also, daylight and view through is appreciated by most occupants.

Solar shading thus becomes a multi-dimensional optimisation task, which is more and more important since many new office buildings have a highly glazed envelope, making

the indoor climate very sensitive to solar irradiation. But for all that, knowledge about characteristics and impact of shading devices on comfort and energy performance of buildings is still on a rather simple level. For example, building simulation tools often use just a user defined shading factor or total solar energy transmittance for a glazing with activated shading device. Aims of this project were therefore to improve and validate measurement and modelling techniques for solar and thermal properties, and to get more insight regarding the performance of shading systems in buildings.

Due to available resources much lower than assumed by participants during the definition phase, some topics of the work plan could not be investigated in depth within this project. The work is also limited to a number of typical systems on the market: Venetian blind devices (rotatable profiled coloured slats), roller blinds or fabric glare protection screens. Light-guiding systems and switchable glazing are investigated in other projects of IEA Task 27.

## 2 Performance indicators

### 2.1 Concept

For the general assessment of the energy performance of a particular building envelope component a large number of data and model relations are needed. An energy performance assessment methodology (EPAM) is relating the measured physical data to the performance of the component installed in a building and climatic environment. The performance of a building is characterised by a number of aspects, namely heating, cooling, lighting and comfort (visual, thermal, and air quality). More details on the methodology and relevant indicators are given in [1].

In the following paragraph, performance indicators are listed and briefly commented for the various levels bottom-up (from materials to building). Information on measurement and calculation methods and standards can be found e.g. in [2].

### 2.2 Materials

Optical properties of the shading materials are the basis for the calculation of the optical and thermal properties of shading devices. Normally, direct-hemispherical data are used, as surfaces are mostly non-specular. Spectral or integral properties are used in modelling of structures. Relevant properties are listed in table 1.

Angular dependence on the materials level is generally not determined, but can be useful in detailed modelling such as ray-tracing.

Table 1: Properties for characterisation of basic shading materials

| Parameter   | Symbol, details  | Relevance, comments  |
|---|--|--|
| IR-emissivity<br>ev. IR-transmittance                         | $\varepsilon(\lambda, \text{far IR}), \varepsilon$ (integral, far IR)<br>$\tau(\lambda, \text{far IR}), \tau$ (integral, far IR) | radiative heat exchange (thermal transmittance)<br>normally integral values used in modelling    |
| solar transmittance<br>solar reflectance<br>solar absorptance | $\tau(\lambda, \text{solar band})$ or $\tau_e$ (solar)<br>$\rho(\lambda, \text{solar band})$ or $\rho_e$ (solar)                 | solar radiation propagation through shading layer or enclosure<br>modelling: spectral (integral) |
| visual transmittance<br>visual reflectance                    | $\tau_v$ (visual)<br>$\rho_v$ (visual)   | used for modelling of daylight properties  |

## 2.3 Shading devices

In principle, the properties of a geometric structure like a Venetian blind can be calculated from geometry and basic materials data. In practise, the properties are often determined by spectral or broadband optical measurements on the whole structure.

Table 2: Properties for characterisation of shading devices

| Parameter  | Symbol, details  | Relevance, comments  |
|--|--|--|
| solar transmittance (direct-hemispherical)                 | $\tau_{dh}(\lambda, \text{solar band})$ or $\tau_{dh}$ (solar)<br>incl. angular dependence | angular dependence is needed to calculate the transmittance for diffuse irradiation              |
| solar reflectance (direct-hemispherical)                   | $\rho_{dh}(\lambda, \text{solar band})$ or $\rho_{dh}$ (solar)<br>incl. angular dependence | used to calculate multiple reflection effects between glazing and shading ev. both sides         |
| visual transmittance<br>visual reflectance                 | $\tau_v$ (visual)<br>$\rho_v$ (visual)<br>incl. angular dependence                         | used for modelling of daylight properties  |
| total solar energy transmittance TSET (direct irradiation) | $g_{dir}$ (solar)<br>incl. angular dependence  | normally with glazing angular dependence is needed to calculate the TSET for diffuse irradiation |
| total solar energy transmittance (diffuse irradiation)     | $g_{dif}$ (solar)  | hemispherical irradiation: often calculated from $g_{dir}$                                       |

## 2.4 Combination of shading device and glazing

The parameters in table 2 are also relevant for the combination of shading and glazing. In particular calorimetric measurements of g-values are normally done on a shading – glazing combination. In order to define simplified performance indicators it is useful to determine parameters for a specific set of configurations (Table 3) that can be evaluated e.g. according to European standards [3][4][5] as indicated.

Table 3: Specific configurations for energy performance assessment

| Configuration                       | Parameters   | Method       |
|-------------------------------------|--|--------------|
| Glazing                             | $g, \tau_v, q_i$   | EN 410       |
| Glazing+shading cut-off             | $g_{\text{cut-off}}, \tau_{v,\text{cut-off}}, q_{i,\text{cut-off}}$          | EN 13363-1/2 |
| Glazing+shading closed              | $g_{\text{closed}}, \tau_{v,\text{closed}}, q_{i,\text{closed}}$             | EN 13363-1/2 |
| Glazing+glare protection (interior) | $g_{\text{glare-prot}}, \tau_{v,\text{glare-prot}}, q_{i,\text{glare-prot}}$ | EN 13363-1/2 |

The cut-off position for a Venetian blind is defined as the slat tilt angle for which direct transmission of incident radiation is just blocked. A typical incidence angle is  $45^\circ$ . This configuration is assumed to be representative for the transmission properties of a façade with solar shading system upon direct irradiance.

## 3 Measurement and modelling of shading performance

A variety of experimental and calculation methods is available. They all include a number of assumptions and conditions, limitations and simplifications that are not always known in detail. Therefore the aim of component measuring and modelling within this project was not to build up a data base of a large number of components and devices, but to check the consistency of the various methods and to improve or further develop experimental and numerical methods.

### 3.1 Optical and calorimetric measurements

Optical spectrophotometer or visual band measurements with or without integrating sphere were widely performed to characterise shading materials. Spectra data were produced by ISE, ENEA and Empa. Since there were no special surface materials involved, the results are not further discussed here. The laboratory measurements described in the following paragraphs were performed at ISE.

### 3.1.1 Measured shading devices

#### Exterior Venetian blinds

- Three types of lamella with similar complex cross-section (Figure 1-1), white, white perforated, dark brown, width: 90 mm, vertical distance: 80 mm
- measured with a double glazing unit (DGU) 4/16 Ar/4, coating surface 2  
 $g=48\%$ ,  $U=1.3 \text{ W}/(\text{m}^2\text{K})$

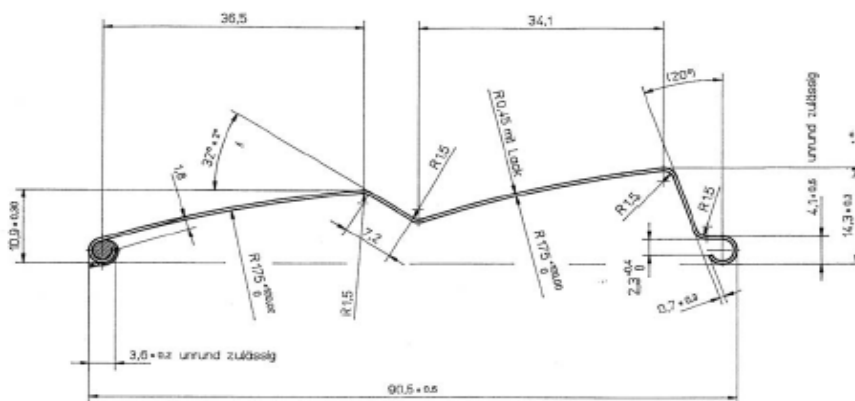


Figure 1-1: Cross-section of the massive external Venetian blind lamella.

#### Interior sun and glare protection systems

- White Venetian blind with 25 mm wide slats, vertical distance 22mm
- Light guiding Venetian blind with specular reflecting slat
- Fabric roller blind, silver (outside) and white (inside)

measured with a DGU 4/16 Ar/4, coating surface 2,  $g=48\%$ ,  $U=1.3 \text{ W}/(\text{m}^2\text{K})$

measured with a DGU 4/16 Ar/4, coating surface 3,  $g=35\%$ ,  $U=1.1 \text{ W}/(\text{m}^2\text{K})$

### Integrated systems

- White Venetian blind with 15 mm wide slats, vertical distance 13mm
- Fabric roller blind bright grey (both sides)

integrated in DGU (pos. 2, 27mm air),  $g=47\%$ ,  $U=1.5 \text{ W}/(\text{m}^2\text{K})$ , and

integrated in DGU (pos. 2, 27mm air),  $g=32\%$ ,  $U=1.4 \text{ W}/(\text{m}^2\text{K})$

### 3.1.2 Solar calorimeter at ISE

The measurements reported here were done by means of the solar calorimeter at Fraunhofer ISE (Figure 1-2). In principle the  $g$ -value is determined by measuring the (local) heat flux on an absorber plate behind the specimen in relation to the incident irradiance at defined temperature and convection conditions. For the angle selective shading systems the directional divergence perpendicular to the slat rotation axis was reduced by mounting the radiation sources in a row parallel to the slats.



Figure 1-2: Solar calorimeter (ISE) with mounted exterior Venetian blind (left). Test frame for interior Venetian blinds (right).

### 3.1.3 Measurement results

Result of measurements on the exterior shading configuration are summarised in Tabel 4. A large difference of the  $g$ -value between the white and the dark colour can be seen. The perforation of the white slats gives only a small difference.

Table 4: Results of calorimetric measurements on exterior Venetian blinds

| System                                    | Incidence angle | Azimuth angle | Tilt angle | U [W/m <sup>2</sup> K] | $\Delta U$ [W/m <sup>2</sup> K] | g [-] | $\Delta g$ [-] |
|---|-----------------|---------------|------------|------------------------|---------------------------------|-------|----------------|
| Glazing without Venetian blind            | 0               | 0             | 0          | 1.29                   | 0.02                            | 0.484 | 0.010          |
|   | 45              | 0             | 0          | 1.29                   | 0.02                            | 0.435 | 0.020          |
|   | 60              | 0             | 0          | 1.29                   | 0.02                            | 0.369 | 0.030          |
| Glazing + white Venetian blind            | 0               | 0             | 0          | 1.22                   | 0.02                            | 0.432 | 0.008          |
|   | 0               | 0             | 45         | 1.14                   | 0.02                            | 0.150 | 0.008          |
|   | 45              | 0             | 0          | 1.22                   | 0.02                            | 0.099 | 0.006          |
|   | 45              | 0             | 30         | 1.14                   | 0.02                            | 0.059 | 0.001          |
|   | 45              | 0             | 45         | 1.14                   | 0.02                            | 0.039 | 0.003          |
|   | 54              | 45            | 45         | 1.14                   | 0.02                            | 0.033 | 0.002          |
|   | 60              | 0             | 0          | 1.22                   | 0.02                            | 0.072 | 0.001          |
| Glazing + white perforated Venetian blind | 0               | 0             | 45         | 1.22                   | 0.02                            | 0.158 | 0.009          |
|   | 45              | 0             | 30         | 1.14                   | 0.02                            | 0.064 | 0.002          |
|   | 45              | 0             | 45         | 1.14                   | 0.02                            | 0.047 | 0.002          |
|   | 54              | 45            | 45         | 1.14                   | 0.02                            | 0.036 | 0.003          |
|   | 60              | 0             | 0          | 1.22                   | 0.02                            | 0.075 | 0.002          |
| Glazing + brown Venetian blind            | 0               | 0             | 45         | 1.14                   | 0.02                            | 0.096 | 0.007          |
|   | 45              | 0             | 30         | 1.14                   | 0.02                            | 0.010 | 0.001          |
|   | 45              | 0             | 45         | 1.14                   | 0.02                            | 0.008 | 0.001          |
|   | 54              | 45            | 45         | 1.14                   | 0.02                            | 0.005 | 0.002          |
|   | 60              | 0             | 0          | 1.22                   | 0.02                            | 0.014 | 0.001          |

NB: The uncertainties  $\Delta U$  and  $\Delta g$  do not include systematic errors

The influence of the slat shape is easily seen at zero incidence and horizontal slats. The reduction of the g-value compared to the bare glazing is more than 10 %, which would not be the case for a flat slat (the beam divergence contribution was estimated to be less than 2.5 %). Results of measurements on interior systems are shown in

Table 5. Here the solar transmittance of the outside glazing system has a big influence. Therefore the measurements were done with various types of glazing.

Table 6 contains results of measurements on glazing with integrated shading systems. The results show clearly the relation between the position of the shading device and the g-value: From exterior to interior position the band of TSET values is shifted upwards significantly.

Table 5: Results of calorimetric measurements on interior Venetian blinds

| Glazing    | Shading system      | Position | Incidence angle | g [-] | U [W/m <sup>2</sup> K] |
|------------|---------------------|----------|-----------------|-------|------------------------|
| Ipasol     | None                |          | 0               | 0.352 | 1.09                   |
|            |                     |          | 30              | 0.346 | 1.09                   |
|            |                     |          | 45              | 0.333 | 1.09                   |
|            |                     |          | 60              | 0.310 | 1.09                   |
| Ipasol     | Jalousie white      | 0        | 0               | 0.329 | 1.19                   |
|            |                     | 0        | 30              | 0.271 | 1.19                   |
|            |                     | 0        | 45              | 0.228 | 1.19                   |
|            |                     | 0        | 60              | 0.191 | 1.19                   |
|            |                     | 45       | 0               | 0.242 | 1.15                   |
|            |                     | 45       | 45              | 0.161 | 1.15                   |
|            |                     | 90       | 0               | 0.157 | 1.15                   |
| Ipasol     | Roller blind silver | Open     | 0               | 0.352 | 1.09                   |
|            |                     | Closed   | 0               | 0.218 | 1.06                   |
|            |                     | Closed   | 45              | 0.206 | 1.06                   |
|            |                     | Closed   | 60              | 0.184 | 1.06                   |
| Silverstar | None                | Open     | 0               | 0.484 | 1.29                   |
|            |                     |          | 45              | 0.435 | 1.29                   |
|            |                     |          | 60              | 0.369 | 1.29                   |
| Silverstar | Jalousie white      | 0        | 0               | 0.455 | 1.34                   |
|            |                     | 0        | 30              | 0.377 | 1.34                   |
|            |                     | 0        | 45              | 0.324 | 1.34                   |
|            |                     | 0        | 60              | 0.275 | 1.34                   |
|            |                     | 45       | 0               | 0.338 | 1.30                   |
|            |                     | 45       | 45              | 0.161 | 1.30                   |
|            |                     | 90       | 0               | 0.161 | 1.30                   |
| Silverstar | Roller blind silver | Open     | 0               | 0.484 | 1.29                   |
|            |                     | Closed   | 0               | 0.305 | 1.21                   |
|            |                     | Closed   | 60              | 0.258 | 1.21                   |

NB: U-value measurements with interior Systems include edge heat loss of the glazing. U-values without or with “open” shading were determined at the center without edge effect.

Table 6: Results of calorimetric measurements on integrated shading systems

| Glazing   | Shading system | Position   | Incidence angle | g [-] | U [W/m <sup>2</sup> K] |
|-----------|----------------|------------|-----------------|-------|------------------------|
| Suncool   | None           | Open       | 0               | 0.331 | 1.47                   |
| Suncool   | Venetian blind | Horizontal | 0               | 0.327 | 1.44                   |
|           |                | Horizontal | 60              | 0.082 | 1.44                   |
|           |                | Closed     | 0               | 0.135 | 1.27                   |
|           |                | Closed     | 60              | 0.082 | 1.27                   |
|           |                | Closed     | 60              | 0.082 | 1.27                   |
| Suncool   | Roller blind   | Open       | 0               | 0.331 | 1.47                   |
|           |                | Closed     | 0               | 0.129 | 1.60                   |
|           |                | Closed     | 60              | 0.123 | 1.60                   |
| Optitherm | None           | Open       | 0               | 0.482 | 1.55                   |
| Optitherm | Venetian blind | Horizontal | 0               | 0.476 | 1.54                   |
|           |                | Horizontal | 60              | 0.297 | 1.54                   |
|           |                | Horizontal | 0               | 0.196 | 1.37                   |
|           |                | Horizontal | 60              | 0.106 | 1.37                   |
|           |                | Horizontal | 60              | 0.106 | 1.37                   |
| Optitherm | Roller blind   | Open       | 0               | 0.482 | 1.55                   |
|           |                | Horizontal | 0               | 0.164 | 1.63                   |
|           |                | Horizontal | 60              | 0.160 | 1.63                   |

### 3.2 Outdoor testing

In the actual work within IEA Task 27, a number of Venetian blind shading devices in combination with insulating glazing were investigated in the calorimetric outdoor test facility (Fig. 1-3) on the EMPA campus near Zurich (Switzerland) [6]. The facility is designed for measurements on lightweight façade components under a quasi-constant test cell temperature with little impact of test cell dynamics. In the following, standard evaluation of measurements is shown for external shading with various slat colours and tilt angles. Because of the strong angular dependence of the shading transmittance it is obvious that an identified single g-value will be influenced by the range of solar incidence angles during the measuring period. For a reference case, a comparison between different measuring periods (seasonal effects) and results from more detailed identification models are shown. In addition, measurements on an interior Venetian blind are summarised. Experimental and numerical results are compared in paragraph 3.4.

Measurements on glass double façades with integrated shading were performed and analyzed by means of a coupled thermal - fluid mechanical model. These results are addressed in IEA Task 27 Project A3.2.



Figure 1-3: EMPA outdoor test facility. Two test cells are built in a wooden building. Temperature controlled indoor air is flowing around the cell walls except for the test face which is exposed to the environment. Climate data sensors including a tracker for direct normal radiation are located between the two test faces.

### 3.2.1 Exterior shading

The experimental set-up is shown schematically in Figure. A double-pane insulating glazing unit (IGU) was installed in a highly insulated surround panel, the outside glazing surface nearly flush with the exterior surface of the surround panel. The installation follows the recommendations given in paragraph 0 to minimize shading effects by the surround panel. The properties of the glazing are:

- Outside: Sunstop Combi Neutral 62/45, 6 mm  
Solar protective, low- $\varepsilon$  coating on surface 2  
( $\tau_e = 49\%$ ,  $\rho_{1,2} = 24\%$ ,  $27\%$ ,  $\varepsilon_{1,2} = 89\%$ ,  $6\%$ )
- Gap: 16 mm, argon 90 %
- Inside: float glass 6 mm
- Glazing area: 1.50 m x 1.25 m, including edge  
1.45 m x 1.20 m = 1.74 m<sup>2</sup>, transparent area A (installed)
- U-value: 1.2 W/m<sup>2</sup>K, UA = 2.1 W/K
- g-value: 47 % at normal incidence, g·A = 0.82 m<sup>2</sup>

Details of the installation of the Venetian blind are indicated also in figure 1-4. The pivot of the slat is placed 70 mm in front of the exterior surface of the glazing. To prevent lateral

effects with large solar incidence angles an overlap between slats and frame of about 200 mm was included around the glazing.

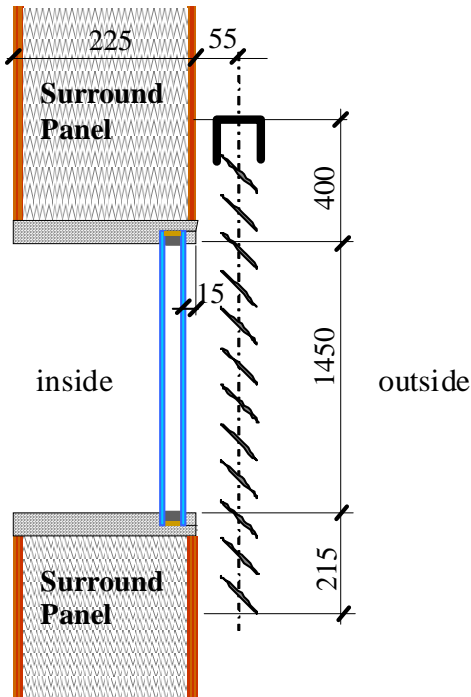


Figure 1-4: Vertical section through the mounted glazing and the external shading device (left). Right: view of the test frame with the mounted shading during a measuring period.

The shading device consists of painted profiled aluminium slats shown in Fig. 4. Major properties are:

|                    |   |
|--------------------|---|
| Width:             | 90 mm   |
| Vertical distance: | 80 mm   |
| Surface:           | white ( $\rho_e = 70\%$ ), brown ( $\rho_e = 7\%$ ), white perforated (5% hole area fraction). The perforation allows for visible contact to the outside also in the closed position. |

### 3.2.1.1 Average TSET identification model and results

The thermal network model shown in figure 1-5 was used for the identification of an average total solar energy transmittance (TSET, g-value) in the experimental data. A single potential divider (node 4) represents the test component between test cell air (node 1) and exterior air (node 5). The solar input  $G_V \cdot A$  (global vertical solar irradiation times area) is linked to node 4. A small parallel conductance H1-10 accounts for a lateral heat flow to the environment through the wooden surface layer of the test frame. Since the temperature of the service room air (node 3) around the test cell is quite homogeneous

and close to the test cell temperature the test cell walls can be taken into account just by another potential divider between node 1 and node 3. The parameters not related to the test component were determined in advance by detailed calibration procedures within the IQ-TEST project [7]. The component parameters were evaluated by means of the thermal network identification software LORD [8].

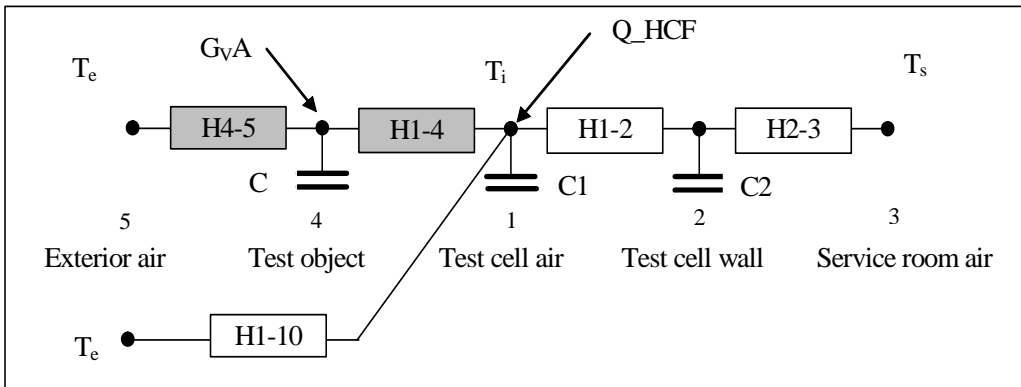


Figure 1-5: Thermal network model used for the basic analysis.  $Q_{HCF}$  is the sum of heating power, cooling power and heat flow through the surround panel. More details are described in the text.

The three shading devices (white, brown, white perforated) with identical slat geometry were measured for three different slat tilt angles. As the measuring periods for the non-closed slat positions are within a few weeks, the results can be assigned mainly to the characteristics of the shading device. The g-values are summarized for comparison in Table 7.

Table 1-7: TSET of the insulating glazing with different exterior shading devices as described in the text.

| Slat angle       | g (-) for slat colour |       |                  |
|------------------|-----------------------|-------|------------------|
|                  | white                 | brown | white perforated |
| 0° (closed)      | 0.009                 | 0.035 | 0.040            |
| 45°              | 0.067                 | 0.039 | 0.071            |
| 90° (horizontal) | 0.155                 | 0.100 | 0.125            |

As expected the solar gain strongly depends on the slat position as well as on the slat type. The white slat shows the most dynamic behaviour: the gain is almost zero in the closed position because of the large reflectance. In the horizontal position the gain is rather high due to the light-guide capability of the white surface. The brown slat gives clearly a higher gain than the white type in the closed state, caused by a larger secondary heat gain through the hot absorbing surface. In the non-closed positions the gain is lower compared to the white slat because of the missing light-guide effect. For the "view-through" white slat a non-negligible gain has to be accepted in the closed position. In the horizontal position however the solar gain is quite similar to the non-perforated white slat.

Using black embrasures and a vented dark absorber surface behind the glazing a solar gain  $g = 0.385$  was determined for the bare glazing in the beginning of July. This is about 15 % less than declared by the manufacturer for normal incidence, which is a reasonable reduction factor for hemispherical and direct radiation at about 60°-incidence angle.

In order to estimate the influence of the varying average sun elevation in different measurement periods, the most critical configuration with white slats at 90° (horizontal) was measured three times between March and June 2003. Because of small temperature differences in May and June a fixed U-value was used in all identification runs. The results are listed in Table 8. A relative decrease of the average solar gain of about 13 % is observed.

Reasons are:

i) For a shading device with horizontal slat rotation axis the sun elevation projected to the window direction determines the transmittance of the shading. During maximum irradiation in the window orientation (30° west at EMPA) the projected elevation is in the range from 40° to 60°, i.e. only a minor fraction of the whole angular range contributes to the identified solar heat gain.

ii) The angular distribution of the diffuse sky and Albedo fraction is rather independent from the measurement period. Thus the impact of the period dependent direct radiation fraction is further reduced.

We conclude that in a practical sense the radiation environment for our test site does not change too much between spring and autumn in this case. The results reasonably represent the average solar heat gain in an approximately hemispherical radiation distribution.

Table 1-8: Results for the white shading device with horizontal slats measured in March, May and June.

| Slat position | UA (W/K) | average global g-value (-) | measurement period |         |
|---------------|----------|----------------------------|--------------------|---------|
|               |          |                            | from:              | to:     |
| horizontal    | 2.1      | 0.155 ± 1.1 %              | 11.3.03            | 21.3.03 |
| horizontal    | 2.1      | 0.147 ± 3.2 %              | 06.5.03            | 27.5.03 |
| horizontal    | 2.1      | 0.136 ± 7.4 %              | 06.6.03            | 20.6.03 |

1) with relative statistical uncertainty of the identified value

An even smaller seasonal effect was expected for the slat angle 45° because no direct radiation enters the test cell. The analysis yielded  $g = 0.07$  for middle of March, but  $g = 0.09$  for middle of July. That is, the solar gain is 25 % lower in March than in July! Assuming a technical problem at first, it could be observed by eye that in July the test cell inside was brighter with the 45° than with the 90° slat position on sunny days. The light grey concrete slabs in front of the test wall reflected solar beam radiation into the test cell in periods with high solar intensity. The lesson learned is that ground reflection must be taken into account in particular with angle-selective devices, for instance by adjusting the

reflectance of the ground in front of the test wall and / or by measuring the Albedo part separately.

### 3.2.1.2 Evaluation of an angle-dependent TSET

The evaluation of an average global g-value, which is influenced by time dependent boundary conditions, is a rather strong simplification. The angular selectivity of louver type shading obviously causes a strong dependence between the directional distribution of the incident solar radiation and the effective TSET. Therefore the direct and non-direct radiation components must be separated and linked to different component properties. The model and the decomposed radiation quantities are shown in 1-6.

During the selected sunny period, the non-direct component was only a small fraction of the global irradiation on the shading plane. Therefore we focus the evaluation on the direct component, measured with a pyrliometer on a computer-controlled tracker.

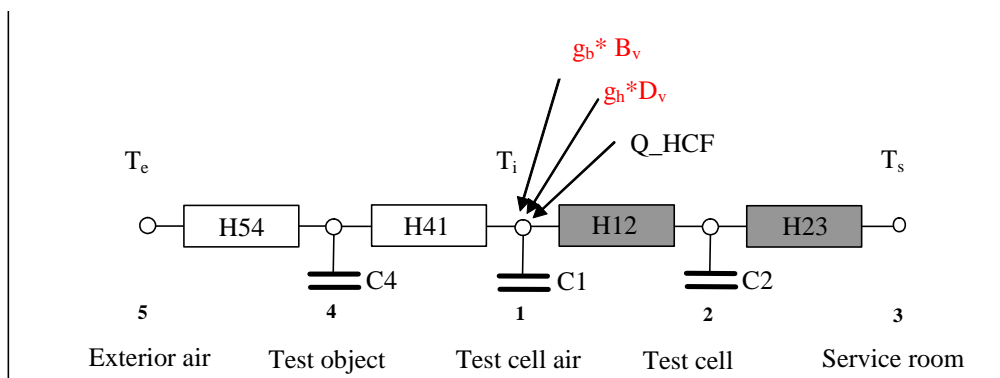


Figure 1-6: Thermal network model and input of the solar radiation components for a more detailed analysis of the angle dependent solar heat gain through the shading.

Radiation components and g-values were split as follows:

$$g_g \cdot G_v = g_b \cdot B_v + g_h \cdot D_v \quad (1)$$

Here  $B_v$  is the direct and  $D_v$  is the diffuse radiation component in the window plane, both multiplied with respective g-values to be determined. In reality the g-value for the direct component changes dynamically with the sun elevation projected into the vertical plane in the window direction. In a certain range of incidence angles the slat structure is partly transparent to solar radiation (figure 1-7). A second fraction of reflected radiation is transmitted also at larger incidence angles. An attempt to such an analysis has been made on data from white, horizontal lamellae taken around middle of March, where direct transmittance occurs for a few hours at the test site..

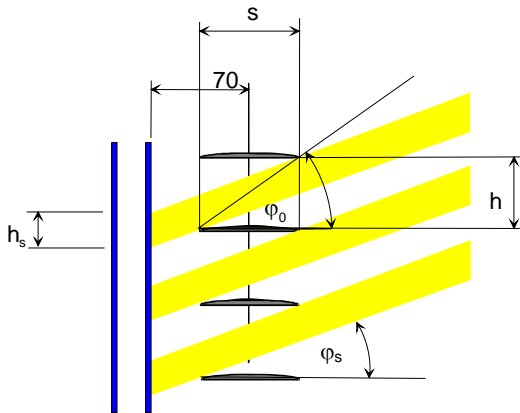


Figure 1-7: Geometric sketch of the transmitted portion of direct solar radiation. No radiation is directly transmitted when the projected elevation angle  $\varphi$  is larger than  $\varphi_0$ , which is about  $45^\circ$  in our case.

Based on geometric considerations the following simplified angular dependence for the direct total solar energy transmittance was assumed:

$$g_b \approx a \cdot f(\varphi, \varphi_0) + b \cdot g(\varphi, \varphi_0) \tag{2}$$

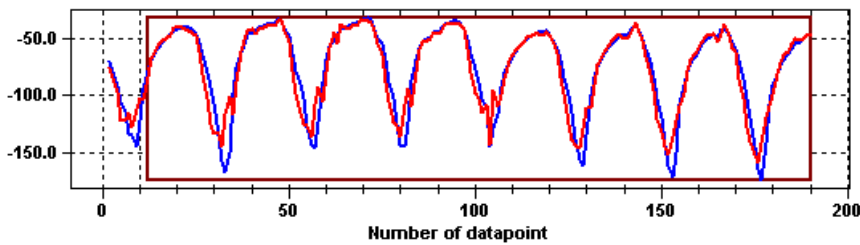
where  $a$  and  $b$  are constants to be identified and

$$f \approx h_s / h = 1 - \frac{w}{h} \cdot \tan(\varphi) = 1 - \frac{\tan(\varphi)}{\tan(\varphi_0)} \approx 1 - \frac{\varphi}{\varphi_0} \text{ for } (0 \leq \varphi < \varphi_0)$$

$$\text{otherwise } f = 0 \tag{3}$$

$$g = \frac{1 - \varphi / (\pi / 2)}{1 - \varphi_0 / (\pi / 2)} \text{ for } (\varphi \geq \varphi_0), \text{ otherwise } g = 1 \tag{4}$$

A simplified approximation function consisting of two linear sections with a different slope is suggested also by numerical models described in paragraph 0.



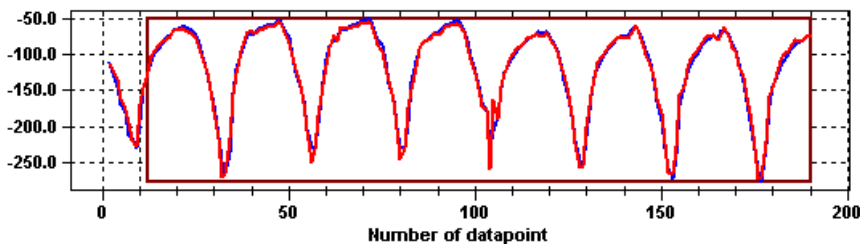


Figure 1-8: Quality of the cooling power fit using the basic average TSET model (top) and the extended model described in the text (bottom).

The result of the identification is shown in figure 1-8. The cooling power peaks measured during the hours with a directly transmitted portion of the solar irradiation are missed if the basic model (single global  $g$ -value) is used, but they are well reproduced with the model involving an angle-dependent gain.

Accordingly the residual at the end of the identification process is significantly lower with the extended identification model. The result is now a simplified angular function for the solar heat gain

$$g_b = 0.363(1 - \varphi/\varphi_0) + 0.078 \quad (5)$$

in the range  $0 \leq \varphi \leq \varphi_0$ . The (statistical) uncertainty of the parameters is  $< 3\%$ .

### 3.2.2 Interior shading

A series of measurements was done on the same glazing and an interior Venetian blind shading with the following properties: solar reflectance 71 % (white), slat width 25 mm, bending 2 mm, vertical distance 22 mm. The glazing was mounted flush with the inside surface of the test cell. It was placed with an air gap of 70 mm between glazing and slat pivot. In the closed position two options for convective heat exchange with the room were tested: i) gap blocked on top and on both sides, ii) gap fully open (free hanging shading device). The identified  $g$ -values are summarized in Tabel 9. A somewhat reduced TSET identified for the bare glazing is caused by the shading effect of the embrasures.

Table 1-9: Measured  $g$ -values of an interior shading device with a double pane IGU.

| Shading condition                      | $g$ -value |
|--|------------|
| Without shading                        | 0.39       |
| 90° (horizontal)                       | 0.32       |
| 45°                                    | 0.28       |
| Closed (ca. 20°)<br>Maximum convection | 0.25       |
| Closed (ca. 20°)<br>Blocked convection | 0.23       |

A minor effect of blocked or free convection between shading gap and room can be identified from the data. The identified change of the g-value is about 0.02. Last but not least it should be noted that the measured g-values are above the recommended range even with closed shading and with the well highly lamella surface present in the actual measurements.

### 3.3 Numerical modelling of optical properties and TSET

Several numerical calculation schemes and tools are available, mainly based on the standards EN 13363 or ISO 15099, which describe basically the same view factor approach for the calculation of the optical properties of a slat type shading “layer” with diffuse reflectance. For arbitrary slat shapes and non-diffuse surfaces ray-tracing methods are used. These options are briefly addressed in the following paragraphs.

#### 3.3.1 EN 13363

EN 13363-1 [4] describes a simplified method combining the g-value of the glazing with transmittance / reflectance values of the shading. Equations are given for exterior, interior and integrated shading. The air gap between shading layer and glazing is assumed closed for exterior position and fully ventilated for interior position of the shading layer, which is on the upper side regarding thermal gains.

In EN 13363-2 [5] view factor based equations are given for the calculation of transmittance / reflectance properties of shading with tilted flat slats with diffuse surface reflection. The application is however limited as the slat are assumed perpendicular to the solar beam (no direct transmittance) and view factors are given just for 45° tilt angle. The thermal model is similar to ISO 15099.

#### 3.3.2 ISO 15099

ISO 15099 [9] describes a general view factor approach for flat slats with diffuse reflection. As the slat is divided into five elements on each side of the enclosure no explicit expressions are given for the view factors. The thermal model includes a simple heat exchanger model to calculate heat transfer in ventilated gaps and between gaps e.g. on both sides of a shading layer. The algorithms are implemented for example in the program WIS [10].

#### 3.3.3 View factor model extensions

An obvious drawback of the optical model in ISO 15099 is the missing “thickness” or profile of the slat, which may be in the range of 10 to 20 % of the width for mechanical stability reasons. This additional shading effect of the slats is relevant mainly for beam

directions nearly parallel to the slat surface, and is larger for tilted slats, where the distance between the slats is smaller.

In principle a view factor method can be used similarly to the flat slat case. However the calculation is more complex because some sections of the surface may be hidden (particularly in nearly closed position) or are visible to each other due to the bending (concave side of a lamella). Also the calculation of the directly transmitted fraction has to be modified.

Based on the assumption of lamella with a spherical cross-section extended view factor models were implemented during this project at ISE and Empa. In these internal tools the enclosure for the calculation of the radiation exchange consists of six parts according to EN 13363 (figure 1-9).

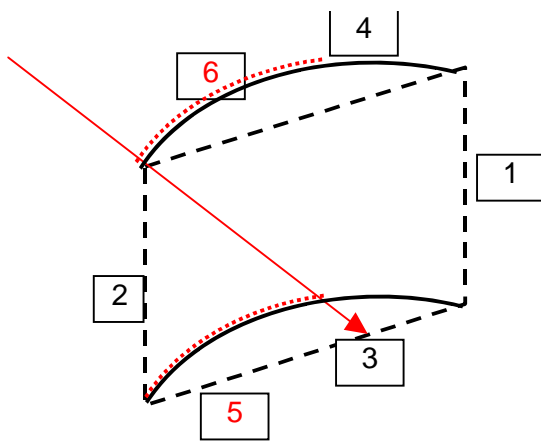


Figure 1-9: Sketch of a shading device consisting of lamella with spherical cross-section.

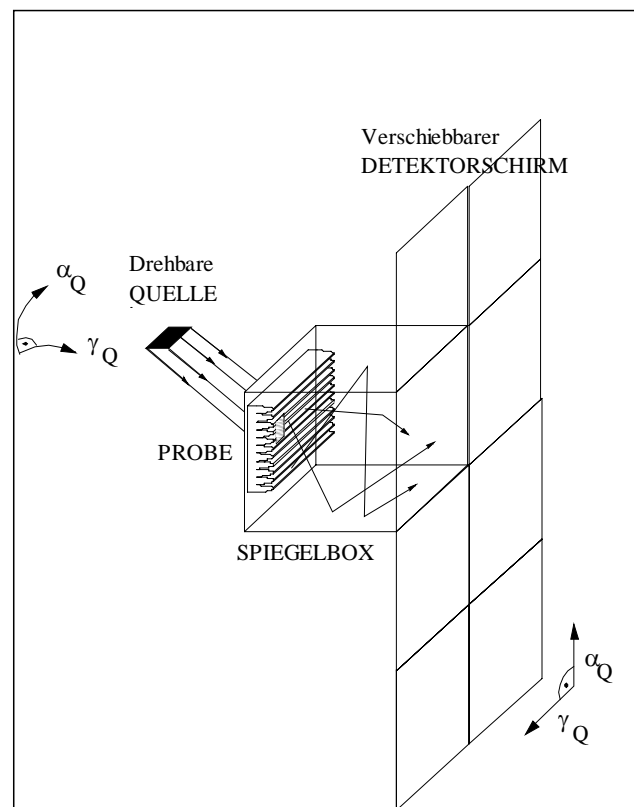


Figure 1-10: Virtual optical measuring unit built up with the ray-tracing tool OptiCAD ®.

### 3.3.4 Optical ray-tracing

By means of optical ray tracing transmission / reflection characteristics of shading – glazing systems can be modelled using the exact geometry and diffuse as well as specular optical properties of surfaces. Such a virtual measuring unit (figure 1-10) was built at ISE.

## 3.4 Comparison of experimental and numerical results

### 3.4.1 Comparison of laboratory based experiments and modelling results

Solar transmittance data measured with an integrating sphere on an interior white Venetian blind are compared with numerical calculations in figure 1-11, which shows generally good agreement between the methods. At larger tilt angles the flat slat approximation in WIS is visible.

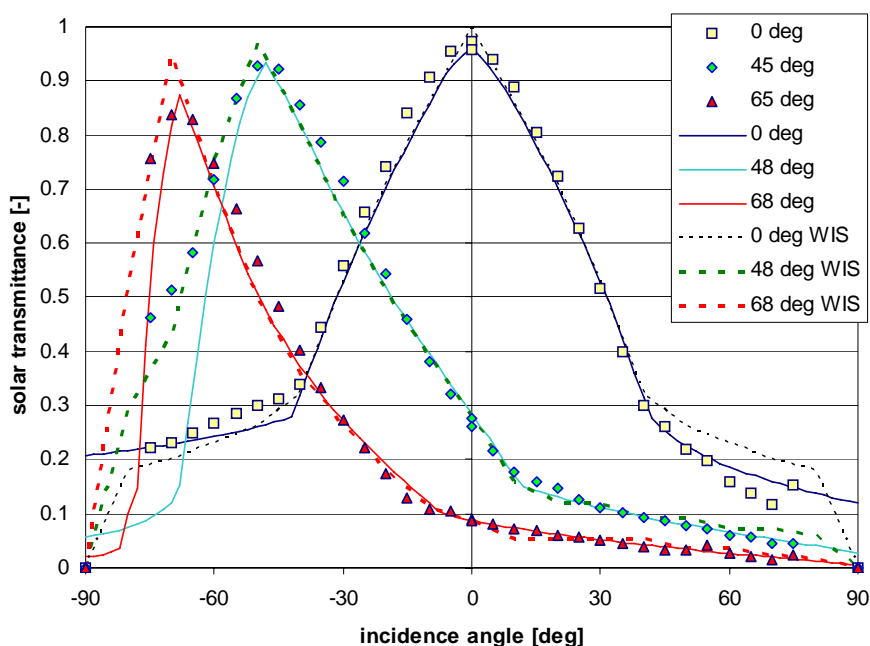


Figure 1-11: Comparison of solar transmittance measurements on a Venetian blind (25mm white) at various tilt angles and values calculated by an extended view factor method (ISE) and WIS.

#### 3.4.1.1 TSET of exterior Venetian blinds

Measured and calculated g-values on exterior Venetian blinds with a DGU are shown in figure 1-12 and figure 1-13. The “thick” profiled lamella gives large differences between the extended view factor model and the flat slat approximation in WIS, in particular with tilted slats.

The divergence becomes smaller as the angle between slat surface and incident beam becomes larger. The difference is also moderated by involved glazing.

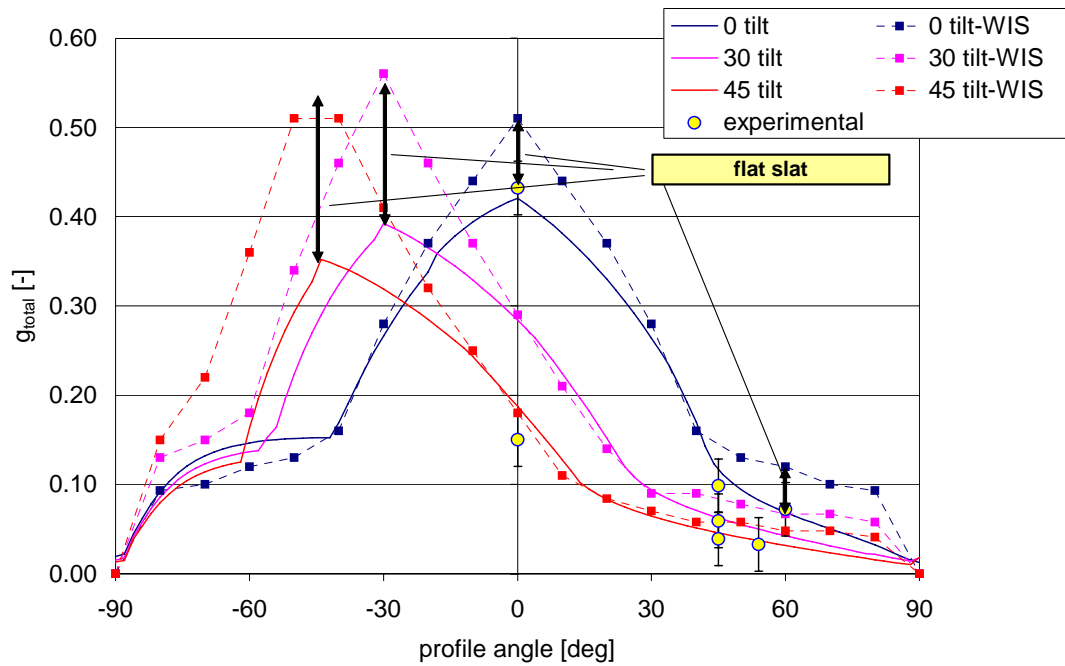


Figure 1-12: Experimental data for white exterior Venetian blind with low-e glazing, compared with  
 a) WIS-Model (flat slats)  
 b) ISE-Model (curved slats)

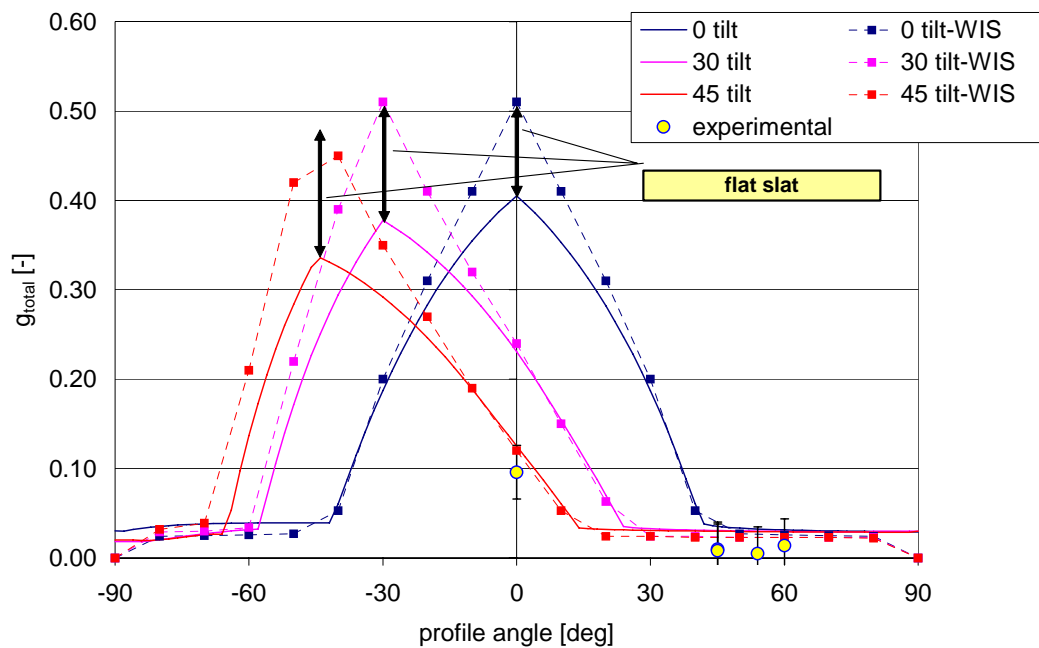


Figure 1-13: Experimental data for brown exterior Venetian blind with low-e glazing, compared with  
 a) WIS-Model (flat slats)  
 b) ISE-Model (curved slats)



### 3.4.1.2 TSET of interior shading devices

Interior Venetian blinds were measured with two different solar protection DGUs. The comparison of measured and modelled results shows good agreement (Figure 1-14 and figure 1-15). Also a comparison of measured and modelled g-values for an internal roller blind gives good agreement.

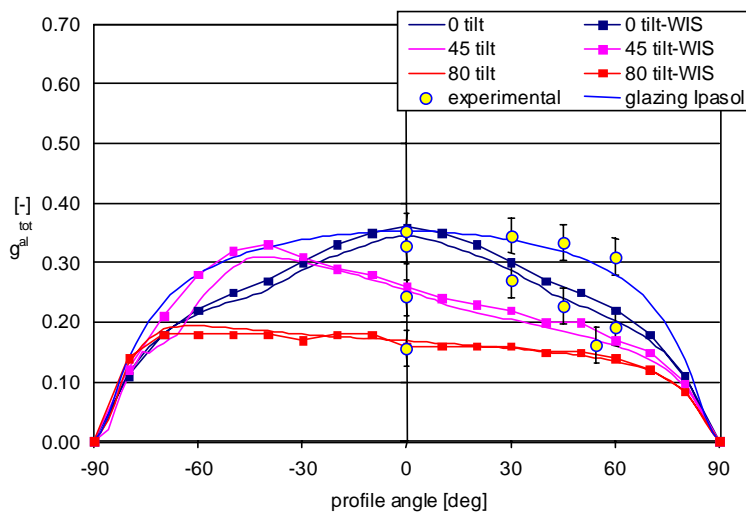


Figure 1-14: Experimental data for white interior Venetian blind solar protection glazing Ipasol 6634, compared with  
 a) WIS-Model (flat slats)  
 b) ISE-Model (curved slats)

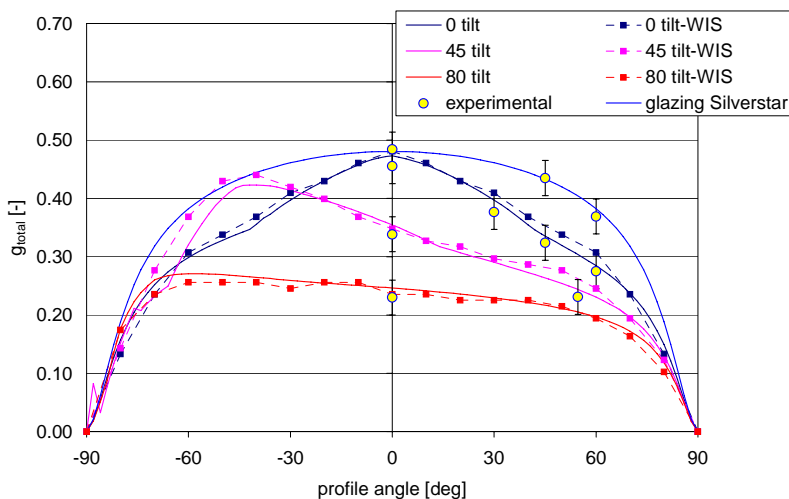


Figure 1-15: Experimental data for white interior Venetian blind solar protection glazing "Silverstar, compared with  
 a) WIS-Model (flat slats)  
 b) ISE-Model (curved slats)

### 3.4.1.3 Comparison with simplified model EN 13363-1

In addition to the models ISE (extended view factor) and WIS (EN 15099) the more simplified model EN 13363-1 was applied for two configurations by combining optical data of the shading device and g-/U-value of the glazing. It can be seen in Table 10 and Table 11 that the simplified calculation always overestimates the experimental results, which can be explained by the treatment of the secondary heat gain in EN 13363-1 as mentioned in paragraph 0.

Table 1-10: g-values from three models (ISE, WIS, EN) for interior white Venetian blind behind Silverstar sun protection glazing in comparison with experimental data (exp).

| Incidence angle | Tilt angle | exp  | ISE  | WIS  | EN   |
|-----------------|------------|------|------|------|------|
| 0               | 0          | 0.46 | 0.48 | 0.48 | 0.48 |
| 30              | 0          | 0.38 | 0.40 | 0.41 | 0.41 |
| 45              | 0          | 0.32 | 0.33 | 0.35 | 0.36 |
| 60              | 0          | 0.27 | 0.29 | 0.31 | 0.32 |
| 0               | 45         | 0.34 | 0.35 | 0.35 | 0.39 |
| 0               | 80         | 0.23 | 0.25 | 0.24 | 0.32 |

Table 1-11: g-values from three models (ISE, WIS, EN) for exterior white Venetian blind in front of Silverstar sun protection glazing in comparison with experimental data (exp).

| Incidence angle | Tilt angle | exp  | ISE  | WIS  | EN   |
|-----------------|------------|------|------|------|------|
| 0               | 0          | 0.43 | 0.42 | 0.51 | 0.49 |
| 45              | 0          | 0.10 | 0.12 | 0.15 | 0.14 |
| 60              | 0          | 0.07 | 0.07 | 0.12 | 0.08 |
| 0               | 45         | 0.15 | 0.19 | 0.18 | 0.21 |
| 45              | 45         | 0.04 | 0.05 | 0.06 | 0.05 |

### Comparison of outdoor testing results with other methods

A direct comparison of modelling, laboratory based and outdoor testing results can be made by collecting the results described before. From outdoor testing the result of the angle-dependent identification described in paragraph 0 is taken. The values for normal incidence ( $\varphi = 0$ ) are summarised in Table 12.

Table 1-12: Total solar energy transmittance of low- $\varepsilon$  glazing with horizontal white slats for normal incidence, determined by various methods.

| Method                     | Remarks   | $g_{direct} (\varphi = 0)$ |
|----------------------------|---|----------------------------|
| Measurement outdoor EMPA   | Identification result   | 0.44                       |
| Numerical model EMPA       | Glazing + shading model (cylindrical shape), solar band           | 0.43                       |
| Measurement laboratory ISE | Calorimetric broadband measurement with solar simulator           | 0.43                       |
| Numerical model ISE        | Glazing + shading model (cylindrical shape), spectral integration | 0.42                       |
| Simplified calculation     | EN 13363-1, $\tau_{blind} = 0.85$ , treated like a screen         | 0.48                       |

The agreement between the identified g-value and various other results for this example is good. As seen before the exact shape of the lamella is not critical in modelling even with the complex geometry of the investigated slat. Again the simplified calculation according to EN 13363-1 gives a too large value due to underestimation of the heat removal by the vented gap between shading and glazing.

In general comparison of outdoor measured and modelled average g-values is not simple because the directional distribution of the non-direct incident radiation is basically unknown. In the EMPA measurements the relatively high reflecting concrete slabs in front of the test façades turned out to be a dominant part of the hemispherical radiation on sunny days.

The assumption of a diffuse distribution of the non-beam fraction of the total irradiance is therefore not correct. Because this source is located vertically about  $-45^\circ$  to  $-50^\circ$  from the window normal, the result will be an overestimation of the solar gain in case of a horizontal slat position. If this localization of the non-direct radiation fraction is taken into account, the average g-value is in good agreement with the measured values for a weighting factor of three by one for a localized compared to a diffuse component respectively (Tabel 13).

Table 13: Comparison of measured and calculated weighted average g-values of an exterior shading device with a double pane IGU.

| Shading           | g-value               |                           |                 |
|-------------------|-----------------------|---------------------------|-----------------|
|                   | Calculation (diffuse) | Calculation (non-diffuse) | Outdoor testing |
| White, horizontal | 0.20                  | 0.17                      | 0.16            |
| Brown, horizontal | 0.12                  | 0.09                      | 0.10            |

Another comparison was made between the measurements on the interior Venetian blind and calculated average TSET values. The identified g-values together with weighted average calculation results are summarised in Table14. Good agreement can be observed in general. A somewhat lower experimental TSET, especially seen with the non-shaded

glazing, may come from a shading effect of the embrasures. The impact of a non-diffuse component in the hemispherical radiation distribution is less significant for this configuration, since the solar energy transmitted through the glazing is largely captured in the test cell.

The effect of blocked or free convection between shading gap and room can be identified from the data. The change of the g-value is about 0.02 in the measurement as well as in the calculation. Last but not least it should be noted that the measured g-values are above the recommended range even with closed shading and with the well highly lamella surface present in the actual measurements.

Table 1-14: Comparison of measured and calculated weighted average g-values of an interior shading device with a DGU "Silverstar".

| Shading condition                    | g-value         |             |
|--------------------------------------|-----------------|-------------|
|                                      | Outdoor testing | Calculation |
| Without shading                      | 0.39            | 0.41        |
| Horizontal                           | 0.32            | 0.33        |
| 45°                                  | 0.28            | 0.28        |
| Closed (ca. 20°), maximum convection | 0.25            | 0.26        |
| Closed (ca. 20°), blocked convection | 0.23            | 0.24        |

### 3.5 Requirements/recommendations

Many recommendations for optical and calorimetric measurements on complex components have been worked out in other projects like ALTSET (Angular Light- and Total Solar Energy Transmittance) [11] and REGES [12]. Here just some additional points are addressed that were recognised during the project.

#### 3.5.1 Calorimetric TSET-measurement

##### 3.5.1.1 General recommendations

If a highly anisotropic component such as a Venetian blind system is investigated it will be necessary to characterise it for different values of incidence and tilt angle in order to determine the system behaviour.

The basic values should cover the relevant range, but measurement uncertainty should still be at an acceptable level.

If the detector area is less than 10 times the inhomogeneity period of the specimen a series of measurements at different positions should be performed and averaged to get a representative property.

##### 3.5.1.2 Divergence of the solar simulator

With highly angle-selective components like a Venetian blind the influence of the direction of the incident radiation is more relevant than e.g. for standard glazing. If a large size

simulator or a simulator field is used – for instance to achieve averaging over an inhomogeneous surface – a distribution of incidence angles is applied. It can be shown that the problem occurs particularly at angles of a sharp bend of the transmission or reflection function as illustrated in Figure 16. With Venetian blinds this is typically the maximum (incidence parallel to slat) and the cut-off region.

To reduce those effects the simulator dimension should be kept small in the critical direction. For example a single simulator row parallel to the slat axis can be used instead of an extended two-dimensional simulator field.

Divergence effects have been studied in more detail in a German project [13].

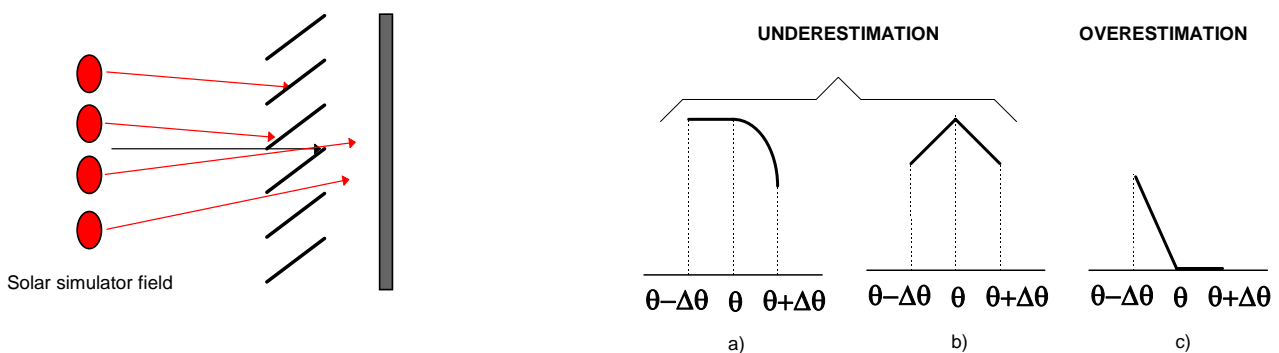


Figure 16: Influence of divergent simulator radiation at a so-called cut-off position of the shading device (left). Critical points for divergence errors on a transmission / reflection curve.

### 3.5.1.3 Component specific recommendation

To reduce measurement errors on large, inhomogeneous, angle selective components like shading devices the following recommendations can be given:

Integrating spheres should be used in optical measurements

- The aperture of the sphere should cover the inhomogeneities of the specimen
- The radiation field should be homogeneous at least in the range of one slat period
- The opening of the sphere should be a multiple of the vertical slat distance for proper averaging
- Multiple reflections in measurements with glazing and large incidence angle should be minimised

For measurements with the solar calorimeter the simulator divergence should be considered

- Minimisation of the divergence by optimisation of the simulator
- Measurement of g-values not for critical angles
- 2 measured values are sufficient in the quasi linear sections (exterior Venetian blinds)

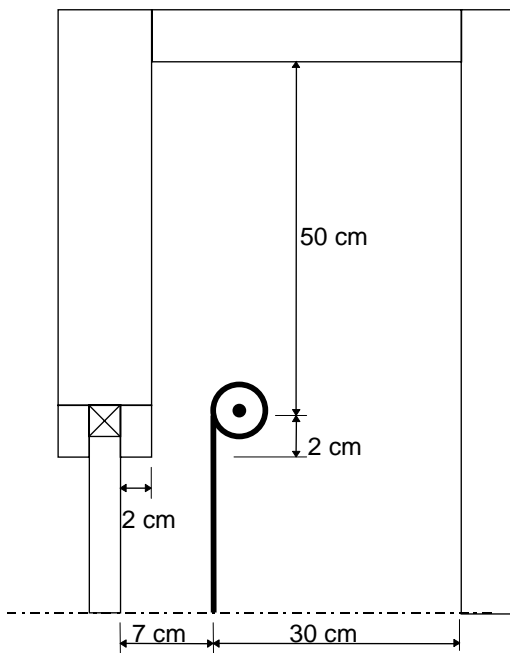
Edge effects should be avoided (e.g. exterior shading area should be larger than the glazing)

With interior shading convective heat transfer is important for the absorbed radiation. Free convection on both sides of the interior shading device is favourable (upper limit for g-value). To check for the lowest g-values ventilation gaps can be closed as far as possible.

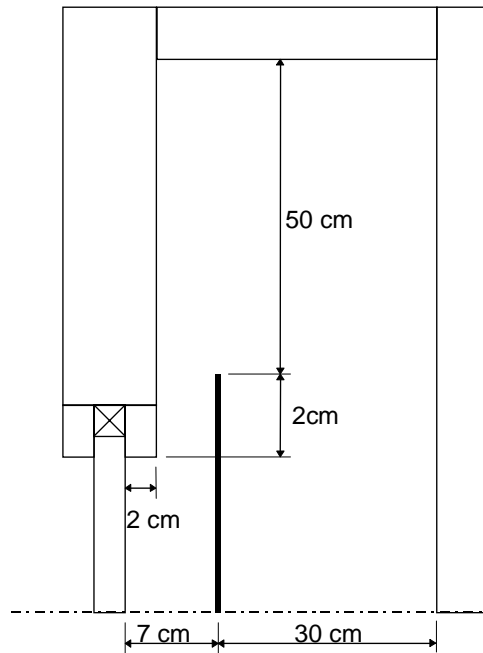
Recommended mounting details are shown in Figure 17 for test rooms / outdoor test facilities and calorimeters with little available space.

The distance between shading layer (pivot plane) and glazing should be indicated in all measurement reports.

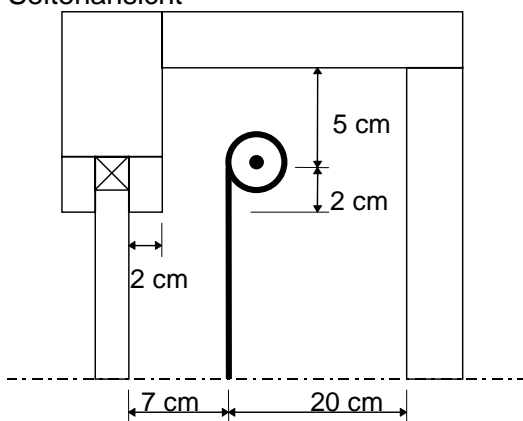
Seitenansicht



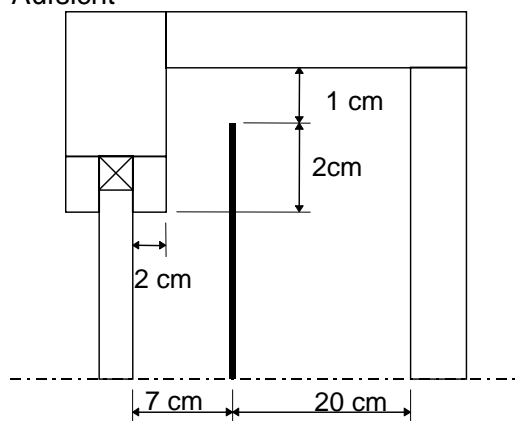
Aufsicht



Seitenansicht



Aufsicht



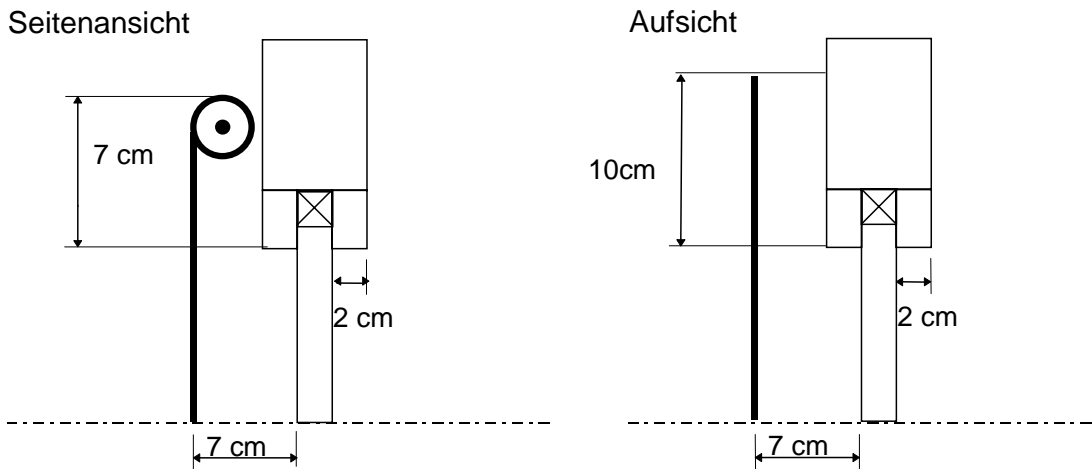


Figure 17: Mounting recommendations for interior shading devices in full size test cells (top) and for calorimeters with reduced space behind the glazing (middle). Recommended excess coverage of the glazing area by an exterior shading system (bottom).

### 3.5.2 Outdoor testing

A large number of reports and publications are available on measurements and identification of parameters in outdoor testing [14]. On the other hand it is obvious that outdoor tests are always unique to some extent: first because of the climate conditions that are neither constant nor repeatable, second because of different types of set-up and control of the testing environment, third because of a variety of options for the evaluation of component parameters. From this it is clear that outdoor testing is not a test method with a (quasi) standardised test procedure for the determination e.g. of standardised g- or U-values. Therefore, results from outdoor testing will never be comparable as lab determined values for well defined constant conditions. However, outdoor testing reflects the in-situ behaviour of a one-by-one scaled component under real conditions, and is therefore a valuable tool to evaluate the effective performance of complex components. Thus it is also useful to produce validation data for component models, which actually attempt to predict the in-situ behaviour.

The main uncertainty with angle-selective components like exterior Venetian blinds is the distribution of the radiation field. As described in paragraph 0 the assumption of a homogeneous radiation distribution apart from the direct component may significantly bias modelled results if ground reflection is the major source for “diffuse” (non-direct radiation) during a sunny period. This happens also with components installed in buildings, which means that a particular reflection environment around a building may significantly influence solar gains.

In short the following recommendations can be given:

- The radiation field should be measured as detailed as possible (direct, global and diffuse horizontal, global in façade plane, eventually global from below horizontal, infrared in façade plane).

- At least the Albedo of the environment should be determined or eventually reduced. It will change drastically upon snowfall...
- Further climate data should be recorded or monitored in detail (temperatures, wind speed, rain, snow)
- Measurements in winter should be made only with closed (or open) shading, unless the special situation is investigated intentionally

### 3.5.3 Modelling

From the comparisons between measurements and different modelling results it is concluded that the model in EN 13363-2 is not sufficiently accurate, as it is limited to flat slats and non-direct transmission. Just the latter aspect is critical, for instance if ground reflection has to be included for tilted slats.

Extended view factor calculation for spherically curved slats give good agreement with measured results, even for complex shaped slats. Flat slat models overestimate the transmission around parallel-to-slat incidence.

Heat transfer can be modelled reasonably well by a resistance approach for exterior and interior shading systems, while the simplified model EN 13363-1 overestimates the solar heat gain in most cases.

## 4 Shading devices and building performance

Highly glazed buildings are in advance worldwide, which means that solar control becomes a more and more crucial issue both for comfort and energy performance of buildings. However the interrelation between a variety of device characteristics plus control options and building performance is often not known, as heating, cooling, lighting and façade build a coupled system, which is more or less influenced by automatic or user control. Operative boundary limits for a building are given by thermal and visual comfort requirements and of course by limits of the energy demand that have to be respected. The following paragraphs deal with some of these aspects. First, thermal comfort aspects are addressed. Subsequently the impact of different shading configurations on cooling, heating and lighting energy demand is illustrated by an office room simulation.

### 4.1 Impact of solar shading on thermal comfort

Thermal comfort is a major issue in the indoor environment. The operative temperature is one of the main parameters that describe thermal comfort. The operative temperature is normally calculated as described in [15]. In common practice today the operative temperature is measured and calculated for a location in the shade. Short wave radiation on the body due to the sun is not included. Here a method is proposed to include direct solar radiation in the evaluation of thermal comfort. Details can be found in [16].

#### 4.1.1 Measured thermal comfort in an office

A south facing office located in Oslo was chosen for measurement of thermal comfort with different shading devices. The office was equipped for one person and a 100 W heater simulated the person. The work place in the office is shown in Figure 18. An operative temperature sensor is located at the desk in front of the PC. This location is close to where the person is located. In the back of the room where there is no sun we both measure the air and the operative temperature.



Figure 18: South facing office at SIEMENS Linderud. Measurement of operative temperature.

The office has 11 m<sup>2</sup> floor area and 3.6 m<sup>2</sup> glazing facing south. The window has clear double glazing with U-value 2.7 W/m<sup>2</sup>K, g-value 0.76 and light transmission 80%. An external and internal shading device was installed. Measurements were performed in the office on sunny days without shading, with internal and external shadings. It is electrically heated and mechanically ventilated. The operative temperature at the workplace and in the back of the room was measured together with outdoor air-, ventilation inlet air and room air temperature and outdoor solar radiation.

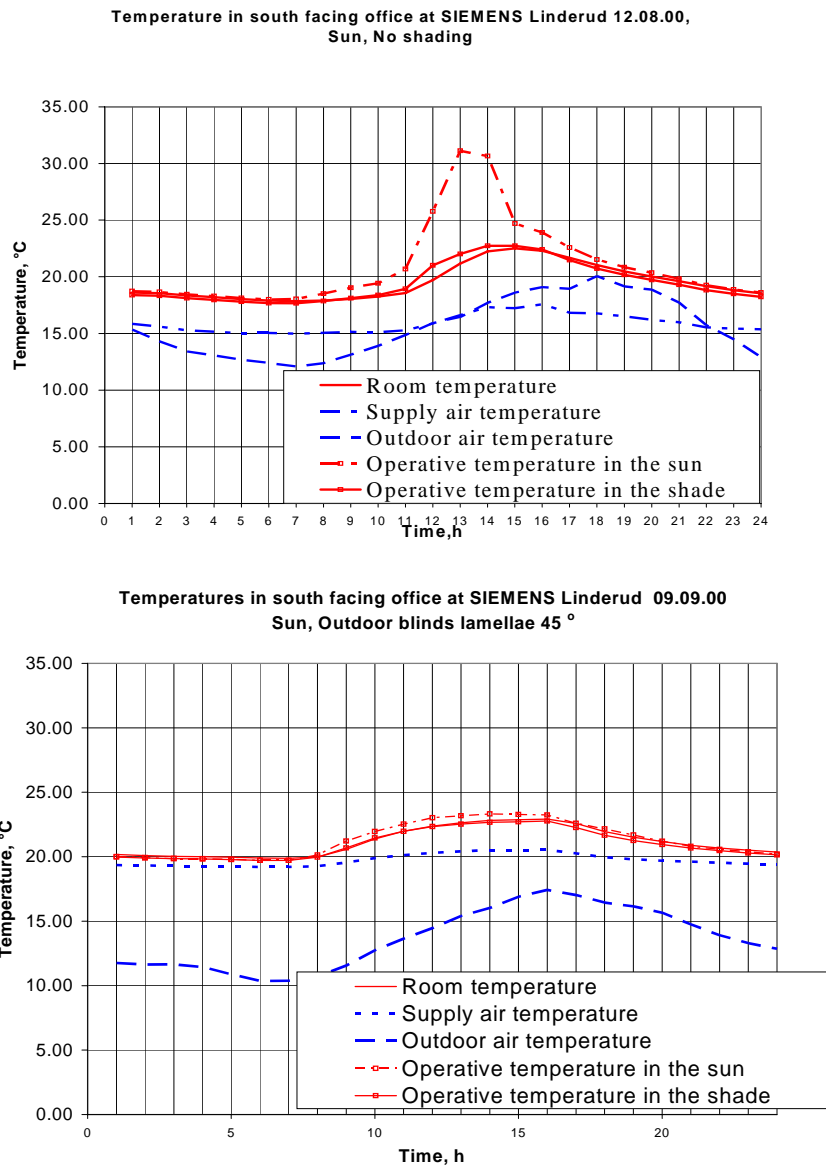


Figure 19: Temperatures in the office with (bottom) and without (top) shading.

The temperatures are measured in the office with no shading in the middle of August. As seen in Figure 19 the operative temperature at the workplace goes up to 31°C without shading. This will cause severe discomfort. At the same time the operative temperature in the shade is maximum 22.5°C and maximum air temperature is 22°C. When calculating thermal comfort only the operative temperatures in the shade is calculated in the existing calculation methods and simulation programs. By using common practice today the planners would calculate the operative temperature to be 22.5°C and the air temperature 22°C which mean it would be a very good indoor climate. In fact the operative temperature at the workplace is 8.5°C higher than would be calculated. This also shows that the common practice today often may lead to poor thermal comfort. By use of exterior shading

the operative temperature at the workplace was 23°C while the operative temperature in the shade and air was 22.5°C. The difference between the operative temperature at the workplace and in the back of the room is now only 0.5°C. The reason for this is the difference in direct solar radiation at the workplace for the two cases. A slightly higher difference was observed with interior shading.

#### 4.1.2 Calculation of the operative temperature in the sun

P.O. Fanger describes a calculation of the mean radiant temperature for a person who is affected by a high-intensity radiant source, which is the sun in this case. His equation was used to calculate the mean radiant temperature with influence of radiation:

$$T_{mrt} = \left( T_{umrt}^4 + \left( const \cdot f_p \cdot \alpha_{ir} \cdot q_{sun} \right) \right)^{0.25} \quad (6)$$

where,

$T_{mrt}$  – total mean radiation temperature included sun radiation [K]

$T_{umrt}$  – radiation temperature without sun contribution [K]

const –  $1/(0,97 \cdot \sigma)$

$\sigma$  –  $5,67 \cdot 10^{-8}$ , Stephan Boltzmanns constant [W/(m<sup>2</sup>K<sup>4</sup>)]

$f_p$  – projected area factor

$\alpha$  – Absorption factor

$q_{sun}$  can be found as:

$$q_{sun} = \frac{I_h}{\sin \theta} \alpha_k \quad (7)$$

where

$I_h$  – Global horizontal radiation [W/m<sup>2</sup>]

$\theta$  – Angel of incidence [°]

$\alpha_k$  – shade factor or direct solar transmittance

When the mean radiation temperature is found,  $t_{mrt}$  is used to calculate the operative temperature in the sun, by using this relation:

$$t_{optsun} = \frac{t_a + t_{mrt}}{2} \quad (8)$$

where  $t_a$  is the ambient air temperature [°C]

Equation (8) is valid when the air velocity is below 0.4 m/s and when the mean radiation temperature is below 50°C.

In the calculation of the mean radiant temperature equation (6) some assumptions were made. The projected area factor,  $f_p$ , is an area factor.

Fanger describes this factor with relation to a seated or standing person. In our case we have a globe, and an area factor for a globe will be  $f_p = A_s/A_k$ . Where

$A_s$  – area of a circle

$A_k$  – area of a globe

The equation that is valid for this case is

$$A_s = \frac{\pi}{4} d^2 \quad (9)$$

$$A_k = \pi d^2 \quad (10)$$

This results in an area factor for a globe at 0.25. If data from Fanger's diagram are used for a seated person, for an altitude at  $60^\circ$  and an azimuth at  $0^\circ$  we get a projected area factor at 0.26. We decided to use the area factor for a globe in our calculations, so we were nearest to our measurements. The absorption was set to 0.85, since a black globe was used to measure.

In our project we measured the global horizontal radiant,  $I_h$ , from the sun. The measurements were worked through 12.08.00. We measured  $I_h = 889 \text{ W/m}^2$  at 2:00 pm. When we calculated the theoretic sun we got  $I_h = 681 \text{ W/m}^2$ . The measured value here is over the theoretic possible value and we suspect that our measurements are too high. We assume the reason for this can be the placing of our instrument. It may have been exposed for considerable reflections, which lead to higher values of radiant than expected from the sun. For this reason we have used theoretic sun in our calculations.

$$f_p = 0,26$$

$$\alpha = 0,85$$

$$\alpha_i = 0,69 \text{ (direct solar transmission of glass)}$$

|         | $T_a$            | $T_{opt\_shad}$  | $I_h$          | $\theta$ | $q_{sun}$      | $T_{umrt}^{1)}$  | $T_{mrt} (6)$    | $T_{opt\_sun} (8)$ | $T_{opt\_sun}$   |
|---------|------------------|------------------|----------------|----------|----------------|------------------|------------------|--------------------|------------------|
|         | meas.            | meas.            | calc.          | calc.    | calc.          | calc.            | calc.            | calc.              | meas.            |
| Time    | $^\circ\text{C}$ | $^\circ\text{C}$ | $\text{W/m}^2$ | $^\circ$ | $\text{W/m}^2$ | $^\circ\text{C}$ | $^\circ\text{C}$ | $^\circ\text{C}$   | $^\circ\text{C}$ |
| 1.00 pm | 21,2             | 22,0             | 730            | 57       | 872            | 22,9             | 42,8             | 32,0               | 31,1             |
| 2.00 pm | 22,2             | 22,7             | 681            | 68       | 736            | 23,2             | 40,2             | 31,2               | 30,7             |

<sup>1)</sup>  $2 \cdot T_{opt\ shade} - T_a$ , c.f. (8)

At the hours 1:00 PM and 2:00 PM, when the weather was bright, the measurements and the theoretic calculations are quite similar. The measured temperature is slightly lower than the calculated. This may be caused by inexact direct solar transmission of the glass as the data used was taken from a catalogue. This leads us to believe that this method

---

can be used to calculate the operative temperature in the sun. It also shows that operative temperature in the shade is not a correct measure for thermal comfort.

To calculate the operative temperature in the sun we first calculate the operative temperature in the shade with a building simulation program where we use the g-value for the facade component. Then we calculate the operative temperature in the sun with the method described here where we also need the **direct solar transmission**. We therefore also need to know the direct solar radiation to compare to facade products.

We suggest that the method should be verified in laboratory tests where data on glazing is available and surroundings are controlled.

### 4.1.3 Conclusions

By using Fanger's theory about high-intensity radiant source we found a method to calculate the mean radiant temperature for persons exposed to high radiance. In our calculations we saw that the calculated and the measured operative temperature were similar. This shows that this method can be used for calculating the operative temperature in the sun. The results also show that operative temperature in the shade is insufficient to determine thermal comfort. We need also to calculate the operative temperature in the sun. The g-value is insufficient to describe the solar properties of a facade product. **Direct solar transmission** for the glazing and shading together is also necessary.

## 4.2 Impact of solar shading on heating – cooling – lighting energy demand

As mentioned earlier the impact of solar shading on comfort and energy performance of a building is complex. First of all, common Venetian blind shading has strongly directional dependent optical properties. This means that solar and visual transmittance through a shaded façade depend significantly on the façade orientation, the day time and the season in the year. In addition, shading is typically adjustable and / or (re)movable, saying that control is an important issue that may crucially influence the energy performance of a building.

Most building energy simulation tools use very simplified models to calculate the solar gain through a shaded façade or window. Often it is just switching between to numbers  $TSET_{clear}$  and  $TSET_{shaded}$ , independent of the actual transmittance characteristics at a preferred or fixed tilt angle of the shading slats. If at all, lighting is often treated vice versa, i.e. switching on a fixed lighting power if shading is activated.

Numerical models based on view factor calculation as described before allow calculating optical and thermal transmission properties correctly for example on an hourly basis normally used in building energy simulation.



location with a daylight factor TLQ = 4 % for an ideal visual transmittance 1 of the glazing.

Air exchange:  $0.5 \text{ h}^{-1}$  (from 20 h to 8 h if  $T_i > 23^\circ\text{C}$  and  $T_i > T_e$ )

Internal gains: 350 W in working hours, 50 W otherwise

Calculations were performed at an hourly basis applying the DRY climate data for Zurich (Switzerland) and for Rome (Italy), with the radiation characteristics in table 15.

Table 15: Solar irradiation on vertical planes for DRY Zurich and Rome.

| Location     | Global irradiation, kWh/m <sup>2</sup> |               |      |
|--------------|--|---------------|------|
|              | November – March                       | April – Sept. | Year |
| Zurich west  | 158                                    | 551           | 709  |
| Zurich south | 229                                    | 560           | 789  |
| Rome west    | 252                                    | 764           | 1016 |
| Rome south   | 422                                    | 691           | 1113 |

Variations are listed in Table 16. They were basically made with respect to orientation (south, west), shading position (exterior, integrated, interior), slat colour (white, grey) and tilt angle ( $0^\circ$  means closed), cut-off (adjust tilt angle for just no direct transmission, if necessary), and shading activation level (global irradiance on the façade plane in  $\text{W}/\text{m}^2$ ). A glare protection level was not considered.

In some cases a sun protection glass (Ipasol 53-39) was used as indicated. In configurations with integrated shading the state of natural ventilation (non-ventilated, ventilated) is indicated as well. Tabulated results are the annual energy demand per square meter floor area for cooling, heating and lighting ( $Q_{\text{cool}}$ ,  $Q_{\text{heat}}$ ,  $Q_{\text{light}}$ ). As a rough measure for the annual electricity consumption for cooling and lighting  $Q_{\text{elec}}$  was calculated assuming an annual performance factor 3 of the cooling system. Furthermore, the effective façade performance numbers  $g_g$  (global solar energy transmittance),  $q_i$  (secondary heat gain coefficient) and  $t_v$  (visual transmittance) are given for November – March and April – October.

The results are commented in the following paragraphs. It should be kept in mind that these findings apply for the examples and conditions described here. Other locations, room or building types as well as utilisation schemes and control strategies should be investigated to get more general results on the sensitivity to the large number of parameters.

Task 27 Solar Building Facade Components

Subtask A: Performance

Table 16: Calculation results for DRY Zurich and Rome (explanation see text).

| Configuration                           | #  | Q_cool | Q_heat | Q_light | Q_total | Q_elec | November - March |       |       | April - October |       |       |
|---|----|--------|--------|---------|---------|--------|------------------|-------|-------|-----------------|-------|-------|
|   |    | kWh/m2 | kWh/m2 | kWh/m2  | kWh/m2  | kWh/m2 | g_g              | q_i   | t_v   | g_g             | q_i   | t_v   |
| ZRH south ext grey18 150                | 1  | -13.9  | 16.3   | 20.3    | 50.4    | 24.9   | 0.147            | 0.029 | 0.095 | 0.122           | 0.024 | 0.054 |
| ZRH south ext grey45 150                | 2  | -18.0  | 14.5   | 16.6    | 49.1    | 22.6   | 0.179            | 0.035 | 0.115 | 0.166           | 0.033 | 0.082 |
| ZRH south ext grey90 150                | 3  | -22.0  | 8.4    | 8.0     | 38.4    | 15.4   | 0.329            | 0.061 | 0.234 | 0.213           | 0.042 | 0.115 |
| ZRH south ext grey90 cutoff 150         | 4  | -19.5  | 14.1   | 9.4     | 42.9    | 15.9   | 0.202            | 0.040 | 0.129 | 0.202           | 0.040 | 0.105 |
| ZRH south ext white18 150               | 5  | -16.2  | 15.3   | 20.3    | 51.8    | 25.7   | 0.162            | 0.031 | 0.106 | 0.139           | 0.027 | 0.067 |
| ZRH south ext white45 150               | 6  | -19.0  | 13.5   | 8.1     | 40.6    | 14.4   | 0.220            | 0.042 | 0.144 | 0.201           | 0.039 | 0.108 |
| ZRH south ext white90 150               | 7  | -32.9  | 7.3    | 7.4     | 47.6    | 18.3   | 0.379            | 0.070 | 0.266 | 0.267           | 0.052 | 0.155 |
| ZRH south ext white90 cutoff 150        | 8  | -29.0  | 11.8   | 7.5     | 48.3    | 17.2   | 0.265            | 0.051 | 0.171 | 0.257           | 0.050 | 0.145 |
| ZRH south integ grey45 150 nonv         | 9  | -31.0  | 6.7    | 20.9    | 58.7    | 31.3   | 0.218            | 0.099 | 0.098 | 0.202           | 0.093 | 0.068 |
| ZRH south integ grey45 150 vent         | 10 | -20.5  | 11.4   | 20.9    | 52.8    | 27.8   | 0.165            | 0.046 | 0.098 | 0.154           | 0.045 | 0.068 |
| ZRH south integ white45 150 nonv        | 11 | -25.5  | 6.9    | 11.0    | 43.4    | 19.5   | 0.233            | 0.080 | 0.128 | 0.211           | 0.073 | 0.095 |
| ZRH south integ white45 150 vent        | 12 | -19.6  | 10.4   | 11.0    | 41.0    | 17.5   | 0.204            | 0.051 | 0.128 | 0.185           | 0.047 | 0.095 |
| ZRH west ext grey18 150                 | 13 | -14.4  | 15.6   | 19.3    | 49.4    | 24.1   | 0.238            | 0.044 | 0.144 | 0.134           | 0.026 | 0.061 |
| ZRH west ext grey45 150                 | 14 | -19.6  | 14.4   | 15.2    | 49.2    | 21.7   | 0.276            | 0.051 | 0.171 | 0.185           | 0.036 | 0.090 |
| ZRH west ext grey90 150                 | 15 | -35.8  | 11.6   | 7.8     | 55.2    | 19.7   | 0.385            | 0.070 | 0.267 | 0.290           | 0.054 | 0.156 |
| ZRH west ext grey90 cutoff 150          | 16 | -20.6  | 14.5   | 9.5     | 44.6    | 16.3   | 0.283            | 0.053 | 0.174 | 0.213           | 0.042 | 0.110 |
| ZRH west ext white18 150                | 17 | -17.4  | 15.1   | 19.3    | 51.8    | 25.1   | 0.252            | 0.046 | 0.155 | 0.154           | 0.029 | 0.074 |
| ZRH west ext white45 150                | 18 | -22.5  | 14.0   | 7.9     | 44.4    | 15.4   | 0.309            | 0.057 | 0.196 | 0.227           | 0.044 | 0.118 |
| ZRH west ext white90 150                | 19 | -46.8  | 10.9   | 7.4     | 65.2    | 23.0   | 0.419            | 0.076 | 0.292 | 0.342           | 0.064 | 0.192 |
| ZRH west ext white90 cutoff 50          | 20 | -25.5  | 15.7   | 12.1    | 53.3    | 20.6   | 0.237            | 0.044 | 0.154 | 0.227           | 0.044 | 0.132 |
| ZRH west ext white90 cutoff 100         | 21 | -27.0  | 14.9   | 8.6     | 50.5    | 17.5   | 0.283            | 0.053 | 0.180 | 0.245           | 0.048 | 0.138 |
| ZRH west ext white90 cutoff 150         | 22 | -31.3  | 13.6   | 7.8     | 52.7    | 18.2   | 0.327            | 0.061 | 0.206 | 0.272           | 0.053 | 0.150 |
| ZRH west ext white90 cutoff 200         | 23 | -38.2  | 12.5   | 7.6     | 58.2    | 20.3   | 0.366            | 0.068 | 0.233 | 0.307           | 0.059 | 0.168 |
| ZRH west ext selective90 cutoff 150     | 24 | -20.1  | 15.1   | 7.8     | 43.0    | 14.5   | 0.283            | 0.053 | 0.206 | 0.213           | 0.042 | 0.150 |
| ZRH west ext twocolor90 cutoff 150      | 25 | -24.9  | 14.2   | 8.4     | 47.5    | 16.7   | 0.303            | 0.057 | 0.188 | 0.238           | 0.046 | 0.127 |
| ZRH west int white25 ipa53-39 150       | 26 | -41.9  | 12.1   | 24.3    | 78.3    | 38.3   | 0.281            | 0.170 | 0.085 | 0.256           | 0.180 | 0.046 |
| ZRH west int white45 ipa53-39 150       | 27 | -42.0  | 12.4   | 21.4    | 75.8    | 35.4   | 0.283            | 0.155 | 0.101 | 0.268           | 0.169 | 0.063 |
| ZRH west integ grey45 150 nonv          | 28 | -33.6  | 8.2    | 19.6    | 61.5    | 30.8   | 0.283            | 0.098 | 0.143 | 0.221           | 0.099 | 0.075 |
| ZRH west integ grey45 150 vent          | 29 | -22.4  | 11.7   | 19.6    | 53.8    | 27.1   | 0.243            | 0.059 | 0.143 | 0.171           | 0.049 | 0.075 |
| ZRH west integ grey45 ipa53-39 150 nonv | 30 | -19.8  | 11.2   | 26.3    | 57.2    | 32.9   | 0.156            | 0.065 | 0.071 | 0.125           | 0.065 | 0.037 |
| ZRH west integ grey45 ipa53-39 150 vent | 31 | -13.4  | 14.8   | 26.3    | 54.5    | 30.7   | 0.127            | 0.037 | 0.071 | 0.091           | 0.031 | 0.037 |
| ZRH west integ white45 150 nonv         | 32 | -29.3  | 8.3    | 10.7    | 48.2    | 20.4   | 0.297            | 0.086 | 0.168 | 0.236           | 0.079 | 0.104 |
| ZRH west integ white45 150 vent         | 33 | -22.7  | 11.3   | 10.7    | 44.7    | 18.2   | 0.273            | 0.062 | 0.168 | 0.209           | 0.052 | 0.104 |
| ROME south ext grey18 150               | 34 | -28.8  | 2.2    | 22.6    | 53.5    | 32.2   | 0.066            | 0.014 | 0.038 | 0.089           | 0.019 | 0.037 |
| ROME south ext grey45 050               | 35 | -28.7  | 2.0    | 19.5    | 50.2    | 29.0   | 0.071            | 0.015 | 0.044 | 0.102           | 0.022 | 0.054 |
| ROME south ext grey45 150               | 36 | -34.8  | 1.3    | 15.2    | 51.3    | 26.8   | 0.100            | 0.021 | 0.061 | 0.137           | 0.029 | 0.066 |
| ROME south ext grey90 150               | 37 | -57.4  | 0.3    | 5.1     | 62.8    | 24.2   | 0.273            | 0.052 | 0.205 | 0.189           | 0.039 | 0.104 |
| ROME south ext grey90 cutoff 150        | 38 | -40.0  | 0.9    | 6.8     | 47.8    | 20.1   | 0.132            | 0.027 | 0.082 | 0.175           | 0.036 | 0.091 |
| ROME south ext white18 150              | 39 | -33.0  | 1.6    | 22.6    | 57.2    | 33.6   | 0.084            | 0.017 | 0.052 | 0.107           | 0.022 | 0.050 |
| ROME south ext white45 050              | 40 | -34.2  | 1.2    | 9.4     | 44.8    | 20.8   | 0.122            | 0.025 | 0.082 | 0.144           | 0.029 | 0.085 |
| ROME south ext white45 150              | 41 | -39.5  | 0.8    | 5.3     | 45.7    | 18.5   | 0.148            | 0.030 | 0.096 | 0.174           | 0.035 | 0.095 |
| ROME south ext white90 150              | 42 | -80.5  | 0.2    | 4.3     | 85.0    | 31.1   | 0.335            | 0.063 | 0.249 | 0.247           | 0.050 | 0.147 |
| ROME south ext white90 cutoff 150       | 43 | -59.6  | 0.4    | 4.4     | 64.4    | 24.3   | 0.208            | 0.042 | 0.137 | 0.234           | 0.047 | 0.135 |
| ROME south integ grey45 150 nonv        | 44 | -59.4  | 0.1    | 19.7    | 79.2    | 39.5   | 0.166            | 0.098 | 0.053 | 0.183           | 0.095 | 0.056 |
| ROME south integ grey45 150 vent        | 45 | -39.0  | 0.6    | 19.7    | 59.3    | 32.7   | 0.103            | 0.035 | 0.053 | 0.131           | 0.042 | 0.056 |
| ROME south integ white45 150 nonv       | 46 | -52.3  | 0.1    | 7.4     | 59.8    | 24.9   | 0.180            | 0.073 | 0.091 | 0.191           | 0.072 | 0.084 |
| ROME south integ white45 150 vent       | 47 | -40.5  | 0.4    | 7.4     | 48.3    | 20.9   | 0.147            | 0.040 | 0.091 | 0.163           | 0.044 | 0.084 |
| ROME west ext grey18 050                | 48 | -21.2  | 3.3    | 26.9    | 51.4    | 33.9   | 0.156            | 0.031 | 0.090 | 0.084           | 0.018 | 0.036 |
| ROME west ext grey18 150                | 49 | -29.3  | 1.6    | 20.7    | 51.6    | 30.5   | 0.156            | 0.031 | 0.090 | 0.084           | 0.018 | 0.036 |
| ROME west ext grey45 150                | 50 | -37.2  | 1.1    | 11.6    | 49.9    | 24.0   | 0.200            | 0.039 | 0.121 | 0.138           | 0.028 | 0.068 |
| ROME west ext grey90 150                | 51 | -80.6  | 0.5    | 4.5     | 85.5    | 31.3   | 0.336            | 0.063 | 0.240 | 0.276           | 0.052 | 0.172 |
| ROME west ext grey90 cutoff 150         | 52 | -41.2  | 1.1    | 6.5     | 48.8    | 20.3   | 0.214            | 0.042 | 0.127 | 0.165           | 0.034 | 0.087 |
| ROME west ext white18 150               | 53 | -35.0  | 1.3    | 20.6    | 57.0    | 32.3   | 0.173            | 0.033 | 0.104 | 0.105           | 0.021 | 0.051 |
| ROME west ext white45 150               | 54 | -47.3  | 0.9    | 4.5     | 52.7    | 20.3   | 0.242            | 0.047 | 0.152 | 0.186           | 0.037 | 0.102 |
| ROME west ext white90 150               | 55 | -100.4 | 0.4    | 4.0     | 104.8   | 37.5   | 0.381            | 0.071 | 0.272 | 0.332           | 0.063 | 0.212 |
| ROME west ext white90 cutoff 150        | 56 | -62.0  | 0.7    | 4.4     | 67.1    | 25.1   | 0.270            | 0.053 | 0.169 | 0.231           | 0.046 | 0.135 |

### 4.2.1 Location

The two locations show a clearly different energy situation for the office room. Looking at the typical configurations #2 and #36 (exterior grey slats at 45° tilt angle) there is a heating (winter) and a cooling (summer) demand in Zurich, while in Rome heating is almost negligible (Figure 21). But the roughly doubled cooling demand increases the total yearly energy and more pronounced the electricity demand above the values in Zurich. The difference between the lighting energies is rather small with the grey coloured slats. This shows that the location plays an important role in the characteristics and requirements of shading.

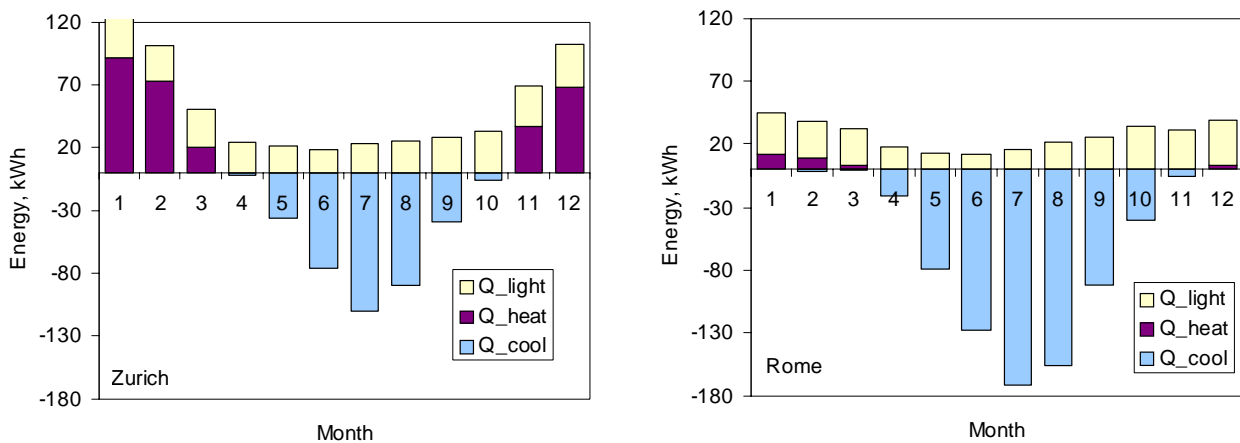


Figure 21: Energy demand in Zurich (left) and Rome (right) for the office room with south oriented façade and external grey blinds at 45°, activated for  $G_v > 150 \text{ W/m}^2$ .

### 4.2.2 Façade orientation

Since the profile angle of the sun as a function of time depends strongly on the façade orientation, the transmittance behaviour of a shading device with tilted slats is different for south and west orientation. The irradiation weighted monthly TSET and direct-hemispherical solar transmittance for configurations #6 and #18 (exterior white slats at 45° tilt angle) are shown in Figure 22. Although solar transmittance and TSET (particularly in winter) are higher in west orientation, the impact on the energy performance is not very big. This is mainly due to the higher irradiance on the south façade.

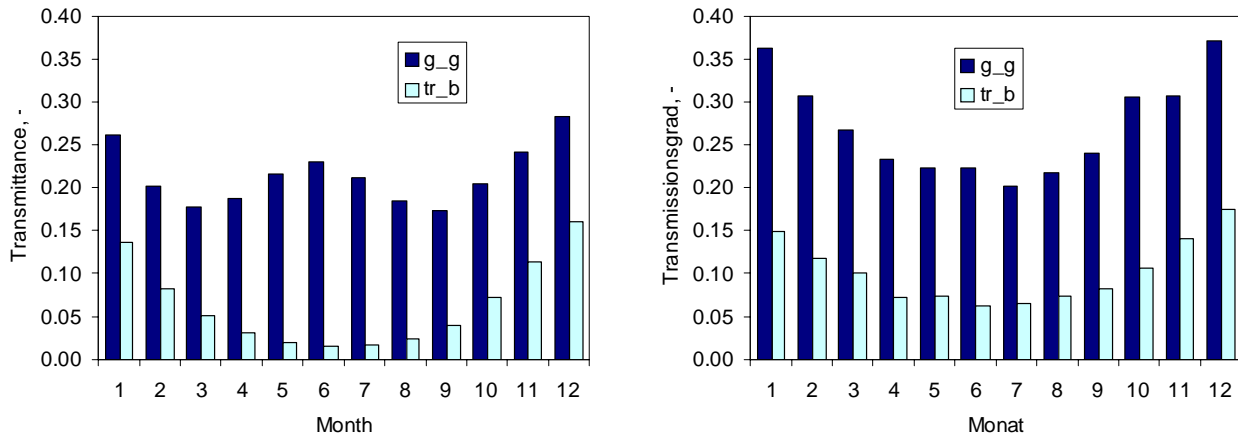


Figure 22: Weighted monthly values for TSET ( $g_g$ ) and direct-hemispherical solar transmittance ( $tr_b$ ) for the façade with white slats at  $45^\circ$  (Zurich), activated for  $G_v > 150 \text{ W/m}^2$ .

For Rome the situation is rather similar. In general the cooling energy demand is somewhat increased for west orientation, and the lighting demand slightly reduced. This applies also for the more absorbing grey slats. For horizontal slats the cooling loads are significantly higher in west orientation (#7 and #19), because direct transmission occurs in the later working hours of the day due to the low altitude of the sun.

#### 4.2.3 Optical properties and geometry

When comparing exterior shading configurations that differ only in colour (grey or white), the darker slats always give lower solar transmission and therefore reduced solar gain. On the other hand daylight supply is reduced, which has to be compensated by artificial lighting.

For the standard situations in Zurich (#2, #14, #6, #18) cooling loads are almost constant, however the lighting energy demand is almost doubled for the grey slats. In Rome (#36, #50, #41, #54) the situation is quite similar, with slightly reduced cooling loads but still increasing electricity demand with grey slats.

Looking at the daylight oriented  $90^\circ$  configurations (#3, #15, #7, #19) in Zurich, a clear improvement for daylight supply is seen with grey slats. For the white slats the lighting energy is not significantly lower. But the cooling energy, and therefore the electricity demand, is clearly higher. High cooling loads (and visual discomfort) appear for west orientation because of direct transmission. Best overall performance with fixed tilt angle is achieved with white slats at  $45^\circ$ , also with respect to daylight.

This is also valid for Rome. There the  $90^\circ$  fixed configurations (#51, #42, #51) are hardly acceptable due to huge cooling loads, except for grey slats and south orientation (#37). However the reduction of the lighting energy is rather small.

The other extreme, the most “closed” configuration #48 with low activation level gives indeed the lowest cooling energy, but the highest electricity demand (and presumably lowest acceptance) due to permanent artificial light and no visual contact with the environment.

The effect of optimized optical properties was checked in configurations #24 (selective surface  $\rho_e = 0.38$ ,  $\rho_v = 0.83$ , hypothetical) and #25 (bi-coloured white-grey) for Zurich west. In fact, the selective slat gives the best performance of all calculated cases, although #18 (white,  $45^\circ$ ) is not far behind. The bi-colour version shows no gain compared to white regarding energy, but might be beneficial with respect to glare prevention

#### 4.2.4 Shading position

Some configurations with integrated shading ( $45^\circ$ , activation level  $150 \text{ W/m}^2$ ) have been calculated. The double envelope was realised by adding a single glass pane on the outside of the shading device. The additional air gap was either closed or ventilated by free convection through openings at the bottom and top of the glazing (5 cm, full width). In all cases higher cooling loads and lighting energy demand result compared to the exterior shading. With non-ventilated clear glass (as partly realised in Switzerland), a high secondary heat gain, high glazing surface temperatures (Figure 23) and related cooling energy demand results (#9, #28). In Zurich (not in Rome), at little benefit is the reduction of the heating energy demand. Convective cooling of the gaps around the shading layer reduces cooling loads significantly, but also the (potentially useful) secondary heat gain in winter. Overall, a significant increase of electricity consumption remains, except for ventilated white slats (#12, #33). Replacement of the clear glass by a solar protection glass Ipasol 53/39 (#30, #31) reduces overheating problems, but – at least with grey slats – the electricity demand goes up because light is almost always on.

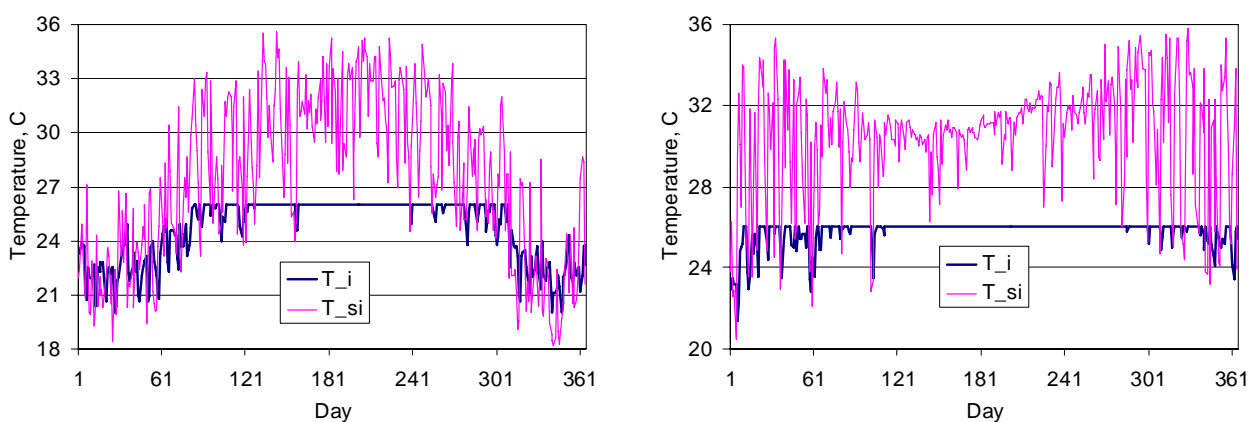


Figure 23: Daily maximum temperatures  $T_i$  (air) and  $T_{si}$  (glazing surface) for configurations #28 (left, Zurich west) and #44 (right, Rome south) with integrated shading.

For completeness two configurations with interior shading (#26, #27) were calculated for Zurich. The same solar protection glass as before was chosen as outer pane. Even so, solar gain and secondary heat gain are very high, and the daylight situation is poor with internal white slats that are frequently activated. At least the daylight aspect could be improved by a light-coloured glare protection screen with reasonable visual transmittance. However, using just a glare protection makes only sense in situations where solar gain is useful as heating energy.

#### 4.2.5 Control strategies

The investigation of control strategies really optimising conflicting requirements of inhabitants (thermal and visual comfort, air quality) and energy performance of a building is certainly an area for future research. Advanced control concepts should not only take user presence, user preferences, performance characteristics and “thermal history” of a building into account, but also seasonal adaptation and future (predicted) climate conditions in the range of the time constant of the building. For example, before or during a cold period solar gain (in an acceptable range) through the façade could have higher priority, especially with low occupation of the room/building (weekends) and discharged thermal mass. In high temperature periods, building control would have to optimise façades and other components for low solar plus internal gain.

At this stage stand-alone control of solar shading will not make sense anymore. However at present, if at all, only simple control patterns for shading are used. Even so, effects on energy performance are often not clear, in particular the trade-off between cooling and lighting energy. This matter could not be investigated in depth within this project. Just a few examples are given here for activation at a defined  $G_v$  threshold ( $150 \text{ W/m}^2$  if not stated otherwise) with fixed or variable (cut-off) slat tilt.

As mentioned before white slats at  $45^\circ$  tilt give best energy performance, for Zurich west, followed by the cut-off adjusted control (Figure 24) (#5 to #8). This is because of the clearly higher cooling energy demand with cut-off control. The same ranking is valid for south orientation (#17 to #19, #22). For cut-off control the dependence of the energy performance on the activation level was checked in configurations #20 to #23. As can be seen in Figure 25 there is a minimum between  $100$  and  $150 \text{ W/m}^2$ , showing that enhanced daylight input is energetically useful. With grey slats cut-off control is preferable in west orientation (#13 to #16), while in south orientation the  $90^\circ$  fixed tilt is slightly favourable (#1 to #4).

For Rome, the open positions with white slats, both  $90^\circ$  fixed and cut-off is not feasible due to large cooling loads (#42, #43, #55, #56).  $45^\circ$  fixed is also the best choice here (#41, #54). A very low activation level is unfavourable (#40). However with grey slats, cut-off control gives the best energy performance (#38, #52) as well as low lighting energy demand.

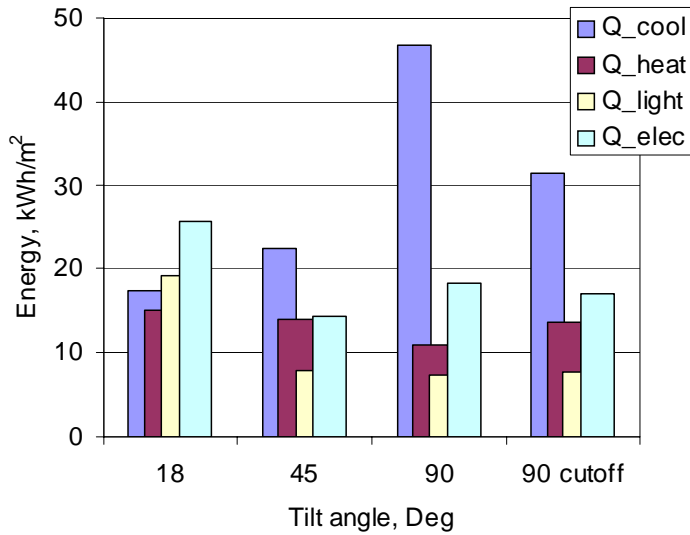


Figure 24: Energy performance for different shading configurations in Zurich west, exterior white slats, activated for  $G_v > 150 \text{ W/m}^2$ .

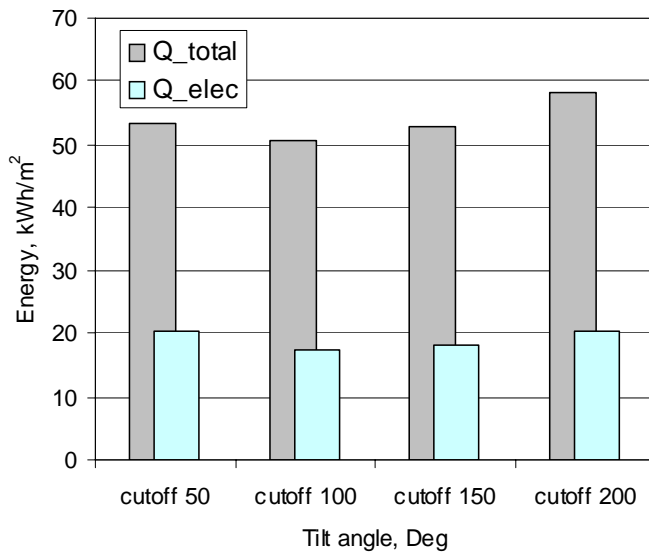


Figure 25: Energy performance for the activation levels 50, 100, 150, and 200  $\text{W/m}^2$  (Zurich west, exterior white slats, cut-off control).

Another simulation study [18] was performed on the influence of different control strategies on the energy consumption of a Norwegian office room (Figure 126).

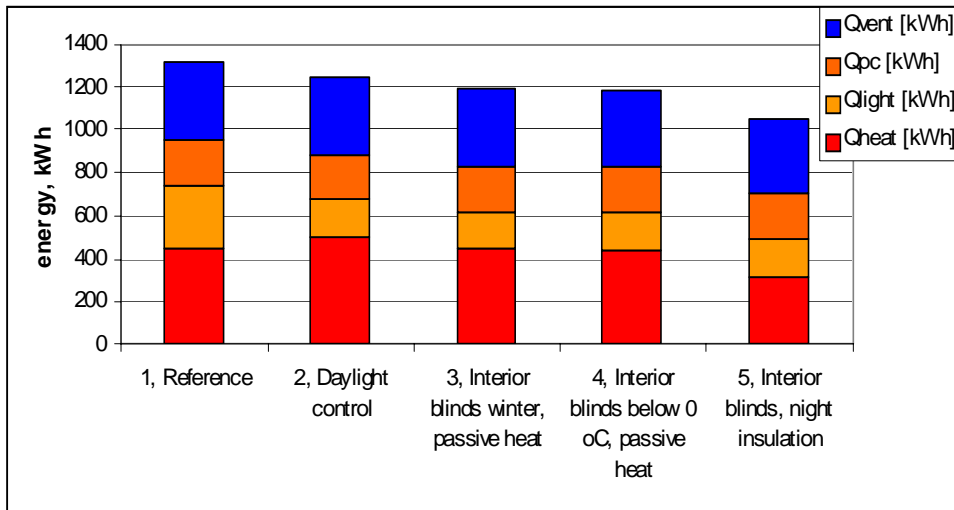


Figure 1: Energy consumption for different control strategies.

The reference (1) has standard outside shading and ordinary light. The energy consumption is 1310 kWh for the office. All the solutions have outdoor shading alone or in combination with interior shading. The first strategy (2) is to introduce daylight control. It reduces the energy consumption to about 1250 kWh. The heating energy use increase and the energy for light is reduced. The net reduction is 60 kWh electricity and increased energy flexibility. The next step is to use the outside shading only in the summer and the inside in the winter. This is calculated with a switch controlled by date (3) and by outdoor temperature (4). The result is the same, an energy consumption of 1190 kWh. This is 60 kWh saved heating by use of passive solar gain.

By introducing solar shading as night insulation (5) the final result is 1060 kWh which means a reduction on 20% or 26 kWh/m<sup>2</sup>. If refurbished this office would normally have local cooling. An introduction of local cooling would raise the energy consumption per office with 20-60 kWh/m<sup>2</sup> in addition. This shows that the potential of the solar shading technology is huge for energy saving. Demonstration and full scale projects would be useful for documentation of the real benefit of the technology.

## 5. Conclusions

As illustrated by the few non-representative examples the impact of shading on the energy (and comfort) performance of a building is rather complex. The large number of important parameters such as location, orientation and construction of the façade, optical and geometrical properties of the shading device, control strategies and user requirements, make a simple view impossible. This was also found in other studies (e.g. [19]).

Exterior Venetian blind shading with highly reflecting slats offers probably the widest range between solar protection and daylight utilisation. Solar-visually selective surfaces perform best, however the gain compared to standard bright white seems to be limited.

Shading integration into a multi-layer glass façade has to be carefully designed, as secondary heat gain and daylight supply may be in a critical range, in particular with low slat surface reflectance. Interior shading is good for glare protection, but the main part of the solar energy transmitted through the glazing remains inside. This can be useful in winter for heating dominated climate. Seasonal or conditional change of the shading system – interior if solar gain is useful, exterior if not – may be an energy efficient and still comfort achieving solution for countries in middle and north Europe. This requires the installation of two shading systems and suitable control.

Control strategies to date are rather simple and should be further investigated and developed. Cut-off control can improve daylight gain and acceptable solar gain with absorbing surfaces. Too high solar gain may occur with highly reflecting surfaces.

## 5 Shading data for building EPAM

### 5.1 Simplified performance indicators for EPAM

Due to the complex behaviour of shading systems including control with regard to building energy performance it is rather difficult to establish a simple method for energy performance assessment.

The usual approach of determining a simple performance value on the safe side is not applicable, since the impact on the building performance is ambiguous: If an overall g-value is too low it is a conservative choice with regard to heating energy, but may underestimate the cooling energy demand, and vice versa. If the façade state is assumed mainly “closed”, large lighting energy demand results, and cooling loads are again underestimated.

This makes clear that a single number is not sufficient. Monthly or at least summer / winter seasonal performance indicators are required for a realistic energy performance evaluation.

Performance indicators related to energy and comfort may be defined as

|                          |  |
|--------------------------|--|
| $g_{\text{total,eff}}^C$ | solar gain -> heating-cooling energy demand              |
| $\tau_{v,\text{eff}}^C$  | visual transmittance -> daylight, lighting energy demand |
| $q_{i,\text{eff}}^C$     | secondary heat gain -> thermal comfort                   |

which are effective monthly or seasonal values of the usual quantities. The problem is that these values not only depend on the façade orientation, but to a large extent also on the usage or control strategy C for the shading system, as shown in paragraph 0.

Actually this topic could not be investigated in more detail within this project. Just mentioned here is a German activity to evaluate options to determine the above indicators in a simple but realistic way.

One possible approach is to calculate the above performance indicators from the basic configurations:

- 1) glazing without shading
- 2) glazing with shading in cut-off position
- 3) glazing with shading fully closed
- 4) glazing with glare protection, if applicable

For these configurations simplified values can be measured or calculated as indicated in paragraph 2.4. For the four configurations effective values for  $x = g_{\text{total}}, \tau_v, q_i$  are evaluated. In the simplest approach the values are assumed constant (no seasonal / directional dependence), and are determined as follows:

$$\begin{aligned}
 x_{\text{eff}} &= 0.85 \cdot x \\
 x_{\text{eff,tot,cut-off}} &= 0.5 \cdot (x_{\text{tot,cut-off,dir}} + x_{\text{tot,cut-off,dif}}) \\
 x_{\text{eff,tot,closed}} &= 0.5 \cdot (x_{\text{tot,closed,dir}} + x_{\text{tot,closed,dif}}) \\
 x_{\text{eff,glare-prot}} &= 0.85 \cdot x_{\text{glare-prot,dir}}
 \end{aligned} \tag{11}$$

Finally the effective performance indicators are calculated by means of weighting factors  $a$  representing the occurrence of the configurations 1 – 4:

$$x_{\text{eff}}^C = a_1^{i,m} \cdot x_{\text{eff}} + a_2^{i,m} \cdot x_{\text{eff,tot,cut-off}} + a_3^{i,m} \cdot x_{\text{eff,tot,closed}} + a_4^{i,m} \cdot x_{\text{eff,glare-prot}} \tag{12}$$

The weighting factors  $a$  and thus the performance indicators depend on the month (season)  $m$  as well as on the orientation  $i$ . They depend also on local or regional climate conditions and must be determined statistically for a number of representative systems.

## 5.2 Shading concepts in building design

The previous chapters show that shading systems crucially influence the energy and comfort performance of buildings. Control of solar gains may help to save heating energy in colder periods, and to reduce cooling loads in other seasons. Daylight supply, visual comfort and lighting energy demand are largely influenced at the same time.

This makes clear that the degree of transparency and construction details of the building envelope as well as concepts for solar gain control must be carefully considered in an early stage of building design. Component and building models are now on a level that allows detailed analysis and at least iterative optimisation of coupled energy performance and comfort aspects.

In an early stage, before simulation tools are started, qualitative considerations on energy and comfort related requirements and subsequent consequences for building design are important. In the following some important aspects are briefly addressed. The information

is mainly condensed from a Swiss study on highly glazed buildings, which includes an extended simulation based parameter study with the DRY data for Zurich [20].

### 5.2.1 Energy and comfort related requirements

Acceptable the thermal comfort was defined - similar to respective regulations - as a PPD-level below 20%, which includes conditions on the room temperature variation, air temperature gradient ( $< 3$  K from 0.1 m to 1.1 m above floor, asymmetry of surface temperatures (cold walls  $< 10$  K, cold ceiling  $< 13$  K), and draft ( $< 0.2$  m/s). These numbers are valid in summer.

Normally thermal comfort improves with increasing distance from the glazed façade. It is proposed that comfort conditions should be fulfilled in an office room above 1 m distance from glazing surface, which corresponds to utilisation practise in actual office buildings.

Typical comfort problems have been identified as follows:

- Summer: Overheating, too high inside surface temperature on sunny days, but also too low temperatures in the morning are observed for glazing with  $U > 1.2$  W/(m<sup>2</sup> K) and forced ventilation for night cooling.
- Winter: Too low surface temperature of the glazed façade, cold air drop with room-high glazing elements (depending on U-value).
- Glare: Frequent glare problems in highly glazed buildings at work places close to the façade, reduced productivity at PC work places due to luminous reflections, reduced visual acuity caused by too large luminance differences.

### 5.2.2 Recommendations regarding building design

In the evaluation of the parameter study situations were found that turned out to be really uncritical or on the other hand that are critical.

No problems occurred with rooms with only one exterior wall, massive construction, maximum 30 % ratio of glazed to internal floor area, exterior solar shading device, and manually operable windows.

Not acceptable conditions were found for rooms with two glazed exterior walls with more than 50 % ratio of glazed to internal floor area and non-effective solar shading nor active cooling. Also unacceptable are permanent work places directly ( $< 1$  m) at the façade.

Other problem areas were identified:

- Small rooms: A 4 x 4 m<sup>2</sup> room with 2 work places has high specific internal gains. Gains are not redistributed among cooler walls in the room depth. At least one work place is close to the façade.
- High occupancy: In shared room with high occupancy and presence typically high internal gains result.

Low thermal mass: At least 350 kg per square meter floor area should be thermally active. Problems occur if the mass is decoupled from the air and with light-weight walls.

Control: Shading control is often done via a central horizontal illuminance sensor. Ventilation cooling is often not adjustable to internal loads in particular room. Comfort parameters are not monitored. Electric light is mostly manually operated.

Table 17: Recommendations for buildings with large glazing fraction.

| Component                       | Recommendation  |
|---------------------------------|---|
| Transparent area                | Detailed analysis of façade related questions required above 30 %, critical situations are likely above 50 % ratio of glazed to internal floor area.<br>Two-face glazed room should be avoided or specially handled.<br>Manual opening of windows should be possible.   |
| Façade properties               | Low g-value of the glazing (< 0.3) is unfavourable (heating dominated climate): missing solar gain in winter, low visual transmittance<br>Total U-value of façade < 0.9 W/(m <sup>2</sup> K)<br>TSET of glazing+shading < 0.1<br>q <sub>i</sub> < 0.08 (incl. shading)  |
| Shading system                  | Shading position preferably exterior, or max. 1 cover pane with free convection gap ventilation<br>Slat functions: up, down, turn, tilt angle<br>Resistance to wind loads: up to 40 km/h (1-h level), 60 km/h (1-min level), 75 km/h (1-sec level)<br>Control: automatic, façade oriented, set value G <sub>v</sub> (not illuminance) < 150 W/m <sup>2</sup> , active on weekends |
| Glare protection                | Separate interior glare protection is required for highly glazed buildings (particularly useful in winter)  |
| Lighting system, internal loads | Use of brightness and presence sensor for lighting, dimming function<br>Minimise other internal loads, use energy efficient information technology  |

Based on these points recommendations are given. It should be kept in mind that they were evaluated for the climatic conditions in Zurich. The situation should be rather similar for middle Europe north of the Alps, but may be different in northern or southern Europe or other global regions.

## 6 References

- [1] W.J. Platzer, Energy Performance Assessment Methodology, Final Report T27-A1-FRG-WJP-FPR IEA Task 27 (2006).
- [2] D. van Dijk (2001)] D. van Dijk, Matrix of products and thermal and solar properties Internal report IEA Task 27 (2001).
- [3] EN 410 (1998): Glass in building - Determination of luminous and solar characteristics of glazing.
- [4] EN 13363-1 (2003) / prEN 13363-2: Solar protection devices combined with glazing, Calculation of solar and light transmittance, Part 1: Simplified method / Part 2: Detailed calculation method.
- [5] EN 13363-2 (2005): Solar protection devices combined with glazing. Calculation of total solar energy transmittance and light transmittance. Part 2: Detailed calculation method
- [6] H. Simmler, B. Binder, R. Vonbank, Wärmelasten transparenter Bauteile und Sonnenschutzsysteme, Final Report (in German), EMPA/BFE (2000).
- [7] B. Binder, EMPA report 860'065, Work Package 3 / Round robin tests as feasibility study for standardisation, EN-Project No NNE5-1999-0511 (2003).
- [8] LORD 2.3, Developer O. Gutschker, Technical University Cottbus (2003).
- [9] EN ISO 15099 (2003): Thermal performance of windows, doors and shading devices - Detailed calculations.
- [10] Window Information System (WIS), actual version 3.0.1, TNO Building and Construction Research (2004).
- [11] W.J. Platzer, The ALTSET project, measurement of angular properties for complex glazing, Proc. 3<sup>rd</sup> Int. ISES-Europe Solar Congress, DK-Copenhagen (2000).
- [12] N. Sack et al., Entwicklung einer Referenzmethode zur kalorimetrischen Bestimmung des Gesamtenergiedurchlassgrades von transparenten und transluzenten Bauteilen REGES; Statusbericht BMBF "Solar optimiertes Bauen" (in German), D-Freiburg (1998).
- [13] IBIG – Integrale Bewertungsverfahren innovativer Gebäudehülle, Contact: Dr. W.J. Platzer, ISE Freiburg i.Br. (Germany).
- [14] PASLINK EEIG, c/o Belgian Building Research Institute (BBRI), Violetstraat 21-23, B-1000 Brussels (<http://www.paslink.org/>).
- [15] P.O. Fanger, Thermal comfort analysis and applications in environmental engineering, McGraw-Hill Book Company (1972).
- [16] I. Bryn, M. Smidsrød, Thermal comfort; Operative temperature in the sun, Internal report r-a1-eh-performance1 IEA Task 27 (2002).

- [17] H. Simmler, Sonnenschutz an Leichtbaufassaden: Messung und Berechnung der Solargewinne durch Glasfassaden mit Sonnenschutz, in German, Workshop „Innovative Fassaden - Planung und Umsetzung, EMPA (2004)
- [18] I. Bryn, M. Smidsrød, Control strategies, Internal report r-a1-eh-controlstrat1 IEA Task 27 (2002).
- [19] T.E. Kuhn et al., Evaluation of overheating protection with sun-shading systems, Solar Energy 69, pp. 59 – 74 (2000).
- [20] C.U. Brunner et al., Gebäude mit hohem Glasanteil – Behaglichkeit und Energieeffizienz (in German), Documentation SIA D0176, Swiss Society of Engineers and Architects, Zurich (2003).

---

## Case Study 2: Double Envelope Facades

Prepared by:

Ismo Heimonen, VTT Building and Transport, Espoo, FINLAND

### 1 Introduction

This document is a summary report of IEA TASK 27 Performance of solar facade components project A3: Solar building components and integrated assemblies, Case Study Double Envelope Facades. The double envelope façade is a wall or glazing façade, which is covered and protected with an extra glazing layer outside the normal wall structure. The extra layer outside the wall can be single glass, double glazed unit or PV-cell layer. The air gap in the structure can be ventilated and there can be solar protection or glare protection systems associated to the façade system. The motivation to build multi-functional glazed facades is, for example, architectural, aims to improve the utilisation of solar energy and daylight, improved sound insulation and ecological aspects. The glazed multi-functional facades have a large range of different practical applications with varying performance properties. The high level of expertise is needed in design, the structures are complex, there are high risks to have problems: overheating, glare, high energy consumption, condensation, maintenance, fire safety. The design practice needs lot of information on design and selecting. The simulation and modelling is needed in component level and in building level and new tools for design are needed. The long-term performance and service life planning are not well known in practice and more study is needed. The reality is that architects and owners want to have nice-looking, glazed buildings and glazing manufacturers want to sell glass as building material. The challenge of the engineering is to develop the knowledge to improve the quality of the applications.

The objective of IEA TASK 27 project A3: Solar building components and integrated assemblies Case Study Double Envelope Facades is

- Determine thermal performance and improve models of double envelope facades and their integration into building envelope assemblies or façade systems
- Develop recommendations for test and calculation procedures for the integrated thermal/solar/daylighting performance of double envelope facades

---

## 2 State-of-the-art of double envelope facades

The variety of the design options and proposals for classification of the systems are presented in (Magali Bodart. r-A3-B-1 UCL dbl envelope facades classification.doc - Proposition of climatic façades classification. March 16 2001) and (Dick van Dijk. r-A3-NL-4 TNO note on dble envelope facades, Note on active and double envelope facades). The positive and negative design aspects of typical double envelope facades has been evaluated (I. Heimonen. r-A3(2)-FIN-6 Summary of design aspects of double envelope facades, VTT Building and Transport). The evaluation of double envelope facades has been done from the point of view of rain protection, sound insulation, air tightness, thermal insulation and effect on the heating, solar control and effect on the cooling, ventilation and indoor air quality, daylighting and effect on lighting energy, moisture control and condensation and maintenance. Summary of requirements relevant to ventilated window and glazing facade design based on Finnish building codes and voluntary classification systems are presented in (Heimonen, I.& Hemmilä, K. r-A3(2)-FIN-5 Summary of requirements relevant to ventilated window and glazing facade design, Version 8.3.2001, VTT Building and Transport).

The importance of detailed design, potential and risk assessment in case of multifunctional ventilated facades is pointed out in ref (Ojanen, T.& Heimonen, I. Building integration of multi-functional glazed facades - Potential and risk assessment. Glass Processing Days Conference, June 2003, Tampere. p. 256 - 258.). The paper presents the general motivation to use multi-functional facades and evaluates the possible potentials and risks of the facades from different points of view. The main thermal performance parameters are presented ( $g$ ,  $g_{vent}$ ,  $U$ ,  $U_{vent}$ ). The case study results of PV-covered ventilated wall with supply air window were presented. An outdoor test cell PASLINK has been used for experimental study. The other case study is thermal, moisture and ventilation performance of Sibelius hall in Lahti, Finland. An innovative combination of wood, sand, thermal insulation and glazing has been used in ventilated facade of concert hall. The main focus in design was to optimize the acoustical performance of the wall. The glazing and ventilation design was optimized to avoid the moisture and overheating risks in the design. The numerical simulation model TCCC2D was used in the analysis.

An example of ventilated facade in smaller scale is the supply air window (Heimonen, I., Hemmilä K. Integration of windows and ventilation by smart supply air windows, Glass Processing Days Conference, June 2003, Tampere. 4 pages). In supply air window, the ventilation air flow is taken through the window structure. The air is preheating between the glazings due to heat losses and solar gains.

An example of exhaust ventilation facade is presented in (H. Manz & H. Simmler. Experimental and numerical study of a mechanically ventilated glass double envelope facade with integrated shading device. 2nd Int. Building Physics Conf., Leuven, Belgium, Sept. 2003. 8 pages). In this case study the facade included the shading screen in the inner air gap. The main focus in this case study was in total solar energy transmittance and cooling of the facade by the ventilation air. In the facade system, the air is directed to exhaust ventilation system.

The performance of double facades in dwellings is presented in (Ida Bryn, Jappe Hjelseth. Double facades in dwellings – lessons learned in Klosterenga, Oslo. ISES 2003, Gothenburg.). The facade type was separated from the balanced ventilation system. The manually operated external windows were used for venting the facades. The venetian blinds were manually operated.

### 3 Performance characterisation

The importance of detailed design, potential and risk assessment in case of multifunctional ventilated facades is pointed out in ref (Ojanen, T.& Heimonen, I. Building integration of multi-functional glazed facades - Potential and risk assessment. Glass Processing Days Conference, June 2003, Tampere. p. 256 - 258.). The aims and motivation for the system performance should be clearly set and the constraints, risks and potentials must be analysed. The thermal and solar characteristics of the components must be known and these can be determined by experimental study or using simulation programs.

The terms and definitions concerning heat flows in active and double envelope facades has been clarified (r-A3-2-NL-TNO Terms and definitions concerning heat flows in active and double envelope facades, TNO draft report). The main focus in IEA case study was in thermal and solar energy parameters.

An example of experimental characterisation of ventilated window is presented in (Heimonen, I., Hemmilä K. Integration of windows and ventilation by smart supply air windows, Glass Processing Days Conference, June 2003, Tampere. 4 pages.). The thermal performance of ventilated building envelope parts can be characterised by four main parameters, which are the thermal transmittance (U-value) and the solar energy transmittance (g-value). Both the U-value and g-value are separated to transmission and ventilation parts. The idea is to determine the effect of solar radiation on the transmission and ventilation energy transmitted through the wall component. The g-value represents the relative part of the solar radiation energy transmitted directly or by conduction or

convection. When solving the g-terms the reference case is without temperature difference and without solar radiation. The definitions for the four terms are:

- $g_{\text{vent}}$  Total solar energy fraction to ventilation air flow rate. The proportional amount of solar solar radiation energy transmitted to incoming air (heat flow through the wall due to temperature difference  $\Delta T$  omitted, only solar effect included).
- $g_{\text{trans}}$  Total solar energy transmittance fraction. The proportional amount of solar radiation energy transmitted by conduction inside the test cell and in case of window component, this is including direct transmittance (heat transmission through the wall due to temperature difference omitted, only solar effect included).
- $U$  Thermal transmittance of the component. Heat flow rate under steady state conditions divided by temperature difference, no solar radiation included, unit  $W/m^2K$ .
- $U_v$  The fraction of the thermal transmittance, which is transmitting to ventilation air flow rate, the amount  $U-U_v$  is transmitting outside (defined during no solar radiation), unit  $W/m^2K$ .

The results of characterisation of different facade systems by measurements and simulations are presented in the following sections.

## 4 Simulations and modelling of double envelope facades

The validity of CFD program FLOVENT in simulating the convective heat transfer in air or gas gaps of windows and facades was shown in reference (H. Manz, Numerical Simulation of Heat Transfer by Natural Convection in Cavities of Façade Elements, Energy and Buildings, Vol. 33, 2003, 305-311). The correlation of FLOVENT was compared to five different correlations found on literature. This study showed the applicability of FLOVENT on ventilated facade simulation. The simulation method combining GLAD, WINDOW and FLOVENT is presented in (H. Manz & H. Simmler. Experimental and numerical study of a mechanically ventilated glass double envelope facade with integrated shading device. 2nd Int. Building Physics Conf., Leuven, Belgium, Sept. 2003. 8 pages.). GLAD was used for calculation of the solar transmittance, reflectances and absorptances of the layers and the total values for the glazing. WINDOW was used to evaluate the angular dependency of these properties. The effective absorptances of the layers and measured climate data including temperature and solar radiation were taken as input values for FLOVENT

simulations. The analysis showed that the air flow pattern is much more complex than piston-flow assumption, which is used in most programs and standards (e.g. ISO/DIS 15099). The detailed analysis of air temperature distribution is only possible with CFD-calculations.

An simulation model CLIM2000 for evaluation of double glazed facade is described in (r-a3(2)-EDF-DC-DEF model (draft version).pdf - Documentation of the CLIM2000 Model, double envelope facade. EDF draft report. 14 pages, more in french version by J.Feburie). The facade model assumes one external glass and double glazed unit as internal glazing and possibility of using blind layer between in air gap. The general hypothesis and equations in the model are described in details.

The qualitative study of the thermal impact of a ventilated double envelope facade compared to a double glazed window is reported in (P.Aude. The qualitative study of the thermal impact of a ventilated double envelope facade compared to a double glazed window. EDF. September 2002. 25 pages). Simulation tool CLIM2000 was used for the analysis. Three different facades was compared: 1. traditional double glazed facade, 2. double envelope facade ventilated with air extracted from the room at room air temperature and 3. double envelope facade with tight inner facade and air gap ventilated from outside to outside. The performance of the facades and possibilities to improve the performance was studied. The influence of high performance solar control glazing, closing the gap in case of outdoor ventilated facade, solar control device (blinds) in facade system, control of blinds and forced ventilation of the facade during summer has been studied.

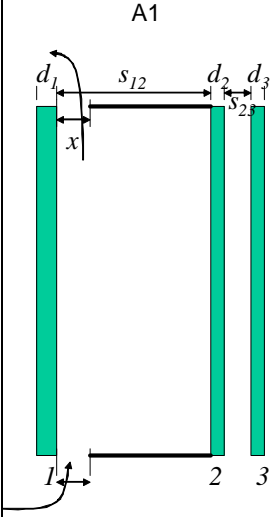
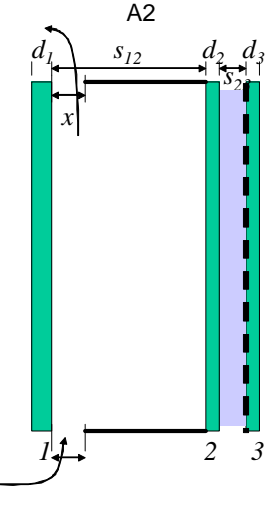
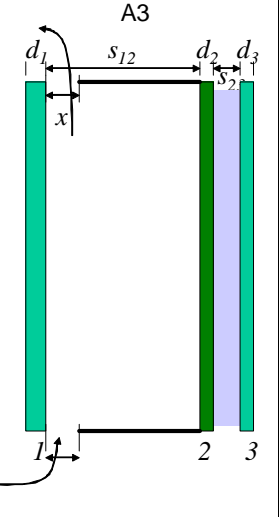
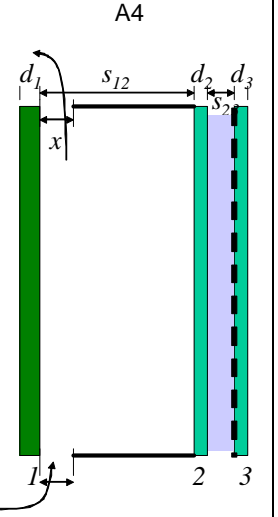
WIS simulation program is an example of the simple design tool, which can be used for evaluation of ventilated glazing structures. The algorithms used for ventilation are described in (WinDat-TNO-2002-04-29 WP3.2 WIS vent.algorithm.doc. Algorithms in WIS on ventilation in gaps. Dick van Dijk, Leo Bakker).

## 4.1 Case study - IEA Task 27 common simulation exercise

A common simulation exercise was performed in IEA Task 27 case study 'Double envelope facades'. The aim of the exercise was to define a common simulation exercise data set and performance parameters for the ventilated facades, compare methods and performance of the cases.

Transparent ventilated double envelope facades with 4 different glazing and opaque wall with external protective glass was described in details. The ventilation is natural (with selected ventilation gap width) or mechanically ventilated system with fixed air flow rate. The selected cases are presented in table 2-1.

Table 2-1. Compared cases in Task 27 simulation exercise.

| case            | A1   | A2   | A3   | A4   |
|-----------------|--|--|--|--|
|                 |                                   |                                     |    |   |
|                 | <b>A1</b><br>* 8 mm clear float<br>gap 800 mm air (*)<br>* 4 mm clear float<br>gap 12 mm air<br>* 4 mm clear float | <b>A2</b><br>* 8 mm clear float<br>gap 800 mm air (*)<br>* 4 mm clear float<br>gap 12 mm argon<br>* 4 mm low_e glass | <b>A3</b><br>* 8 mm clear float<br>gap 800 mm air (*)<br>* 6 mm solar control glass<br>gap 12 mm argon<br>* 4 mm clear float | <b>A4</b><br>* 6 mm solar control glass<br>gap 800 mm air (*)<br>* 4 mm clear float<br>gap 12 mm argon<br>* 4 mm low_e glass |
| ventilation     | natural or fixed 50 dm <sup>3</sup> /s/m   | natural or fixed 50 dm <sup>3</sup> /s/m   | natural or fixed 50 dm <sup>3</sup> /s/m   | natural or fixed 50 dm <sup>3</sup> /s/m   |
| gap             | 800/50 mm  | 800/50 mm  | 800/50 mm  | 800/50 mm  |
| height          | 20 m   | 20 m   | 20 m   | 20 m   |
| venetian blinds | no or white venetian blinds  | no or white venetian blinds  | no or white venetian blinds  | no or white venetian blinds  |

The main thermal and solar performance parameters were selected as compared values. Figures 1 and 2 present the calculated thermal transmittance (U-value) and total solar energy transmittance (g-value) for glazing case A1. The main reasons for differences in results are:

- difference in boundary conditions; different standards give different film coefficients for surfaces
- difference in ventilation approach; some participants selected the ventilation route from outside to inside, some from inside to inside
- difference in definition of U-value (differences in symbols)

- difference and possible errors in data input process

Table 2 shows the performance properties of ventilated facades in terms of U-and g-values in case of different glazing selection. The optimal selection depends on the climate and internal loads of the building. In general, low U-value is important in heating dominated climate and low g-value is important in cooling dominated climate.

Table 2-2. Characteristics of the ventilated facades. IEA Task 27 common exercise. VTT results.

| Case | U<br>W/m <sup>2</sup> K | U <sub>vent</sub><br>W/m <sup>2</sup> K | g <sub>trans</sub><br>(-) | g <sub>vent</sub><br>(-) | T <sub>sol</sub><br>(-) | T <sub>vis</sub><br>(-) | ε<br>(-) |
|------|-------------------------|---|---------------------------|--------------------------|-------------------------|-------------------------|----------|
| A1   | 2.020                   | 0.646                                   | 0.606                     | 0.038                    | 0.530                   | 0.710                   | 0.214    |
| A2   | 1.460                   | 0.469                                   | 0.525                     | 0.052                    | 0.446                   | 0.683                   | 0.156    |
| A3   | 1.920                   | 0.616                                   | 0.396                     | 0.097                    | 0.243                   | 0.440                   | 0.204    |
| A4   | 1.460                   | 0.468                                   | 0.286                     | 0.062                    | 0.226                   | 0.437                   | 0.155    |

This calculation exercise was mainly solved using WIS-program, which uses simple models to solve the performance of ventilated applications. Detailed analysis of air flow patterns, energy flows and temperature distribution is only possible to solve with CFD-tools (H. Manz & H. Simmler. Experimental and numerical study of a mechanically ventilated glass double envelope facade with integrated shading device. 2nd Int. Building Physics Conf., Leuven, Belgium, Sept. 2003. 8 pages.). Detailed simulation of double envelope facades requires use of spectral optical calculation tools (WIS, OPTICS, WINDOW etc.), utilizing CFD-tools and integration or importing of component level performance properties in building level simulation tools (TRNSYS, ESP, DOE etc.).

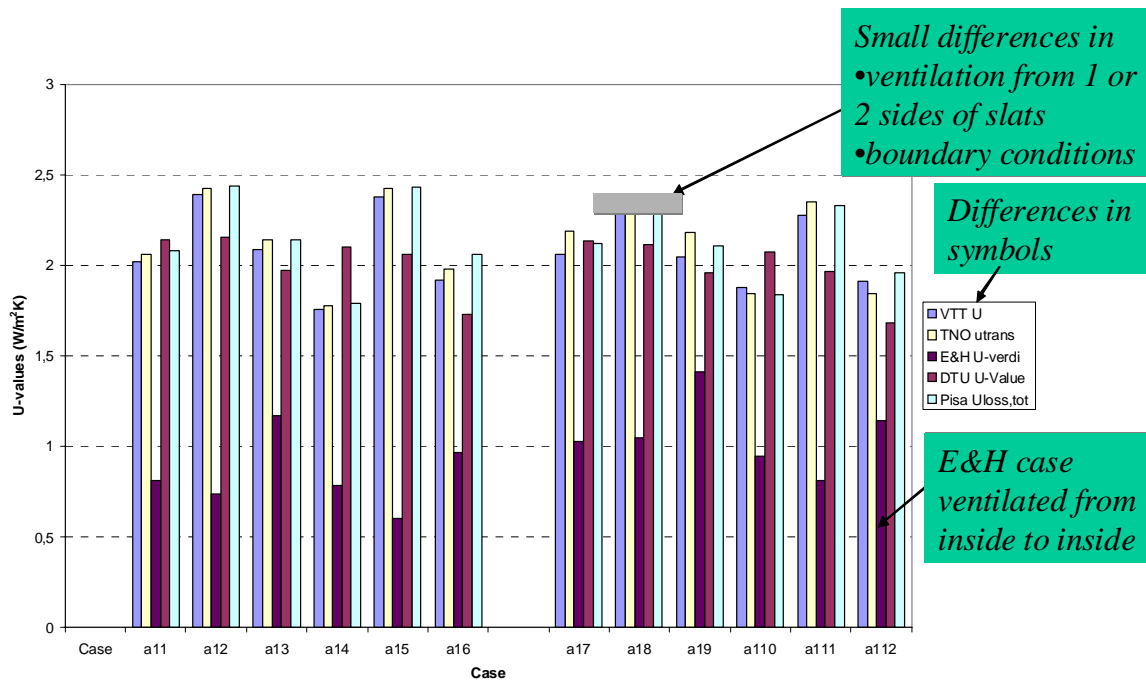


Figure 2-1. Comparison of calculated heat transmittance. 5 participants in the comparison. a11...a112 are different cases with same glazing structure A1.

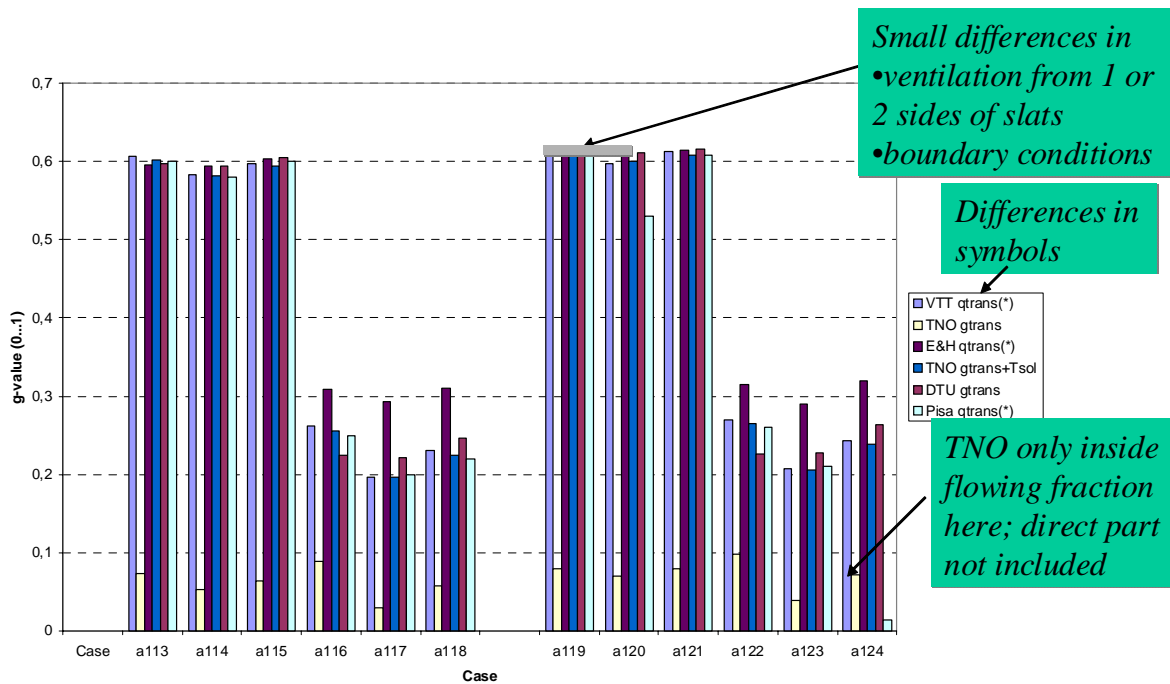


Figure 2-2. Comparison of calculated total solar energy transmittance. 5 participants in the comparison. a113...a124 are different cases with same glazing structure A1.

---

## 5 Evaluation of existing double envelope facades

The thermal and solar performance of **ventilated facade** prototype is presented in (H. Manz & H. Simmler. Experimental and numerical study of a mechanically ventilated glass double envelope facade with integrated shading device. 2nd Int. Building Physics Conf., Leuven, Belgium, Sept. 2003. 8 pages.). The facade is ventilated from inside to exhaust ventilation duct. The glazing is double glazed low-e coated solar control glazing combined with single glass inside and solar control screen between. The study shows the possibilities to control the total solar energy transmittance by varying the position of the shading screen. When using solar shading screen, the total solar energy transmittance into the room was 7 %. The fraction 18 % of the solar energy was transmitted by the exhaust ventilation. Without the solar shading screen, the direct solar transmittance increases significantly ( $T_s=28$  %).

The case study **building integration of ventilated window** is presented in (Heimonen, I., Hemmilä K. Integration of windows and ventilation by smart supply air windows, Glass Processing Days Conference, June 2003, Tampere. 4 pages). The principle of special supply air window used with mechanically ventilated room exhaust system is presented. The measurement for the window has been performed in PASLINK outdoor test cell. The compared window types were:

- (A) Finnish type MSE window (inwards opening, 2 sash, 1 + 2 glazing)
- (B) Finnish type MSE supply air window without venetian blinds
- (C) Finnish type MSE supply air window with venetian blinds totally closed

Smart ventilated window improves the total energy efficiency compared to tight window and different ventilation opening. The heat recovery efficiency  $\varepsilon$  in measured case was 32-36 %. The ventilation through the window increases U-value, but the net effect on energy consumption is positive. The heat recovery from heat losses is bigger than increase in heat losses. The net decrease in heat losses was 16-24 %. The results were measured for total air flow rate  $\sim 6,8 \text{ dm}^3/\text{s}$  and 20-22 Pa underpressure in room. The air preheating in the structure improves the thermal comfort during cold periods because of less draught problems. The venetian blinds in ventilated window increases the heat recovery effect and gives possibilities to control solar gains.

The case study **double facades in dwellings** presents the performance of the south oriented facade system in six floor residential building (Ida Bryn, Jappe Hjelseth. Double facades in dwellings – lessons learned in Klosterenga, Oslo. ISES 2003, Gothenburg). The control options are operable windows in external facade and solar control device (venetian

blinds) between the facades. The external facade is controlled by users. The performance of the facade system integrated in building was studied by experimental measurements. The thermal comfort was evaluated by temperature measurements. During the winter the facade worked as buffer for cold outdoor temperature. During the summer there exists a risk of overheating when using double envelope facade. The system worked quite well and there was no severe overheating in the flats. The air quality was evaluated by measurements of air humidity, CO<sub>2</sub> and ventilation rate. All these were in accepted level. The energy consumption was measured in two flats and it was slightly higher than expected. In the studied case, a balanced separate ventilation system was used. This made the design concept simple. The facade system was most of the year a passive layer improving the thermal insulation. The field study gave very positive results for double envelope facade in residential building.

The thermal, moisture and ventilation performance of Sibelius hall in Lahti, Finland has been evaluated by simulations and measurements (Ojanen, T & Heimonen, I. r-A3(2)-FIN-13 CaseSibeliushall\_T27\_a3\_2.ppt - Double envelope façade in Sibelius hall, Lahti, Finland (in Finnish: Sibeliustalon lasikatteisen seinärakenteen lämpö- ja kosteustekninen toimivuus seurantamittauksissa, Tuomo Ojanen, VTT, March 2002.)).

***An innovative combination of wood, sand, thermal insulation and glazing*** has been used in ventilated facade of concert hall. The main focus in design was to optimize the acoustical performance of the wall. The glazing and ventilation design was optimized to avoid the moisture and overheating risks in the design. The numerical simulation model TCCC2D was used in the analysis during the design phase. The field measurements for the temperature and relative humidity in air gap, temperature of external plywood, moisture conditions of plywood in both sides and thermal and moisture performance of insulation/wooden layer in middle has been performed. The measurements showed that the temperatures and moistures in the structure are in a safe level.

## 6 Development of the design tools and integration into existing design tools

WIS simulation program is an example of the simple design tool, which can be used for evaluation of ventilated glazing structures. The algorithms used for ventilation are described in (WinDat-TNO-2002-04-29 WP3.2 WIS vent.algorithm.doc. Algorithms in WIS on ventilation in gaps. Dick van Dijk, Leo Bakker). WIS program is under development and this is partly financed by WINDAT network project.

Detailed analysis of air flow patterns, energy flows and temperature distribution is only possible to solve with CFD-tools (H. Manz & H. Simmler. Experimental and numerical study of a mechanically ventilated glass double envelope facade with integrated shading device. 2nd Int. Building Physics Conf., Leuven, Belgium, Sept. 2003. 8 pages.). Detailed simulation of double envelope facades requires use of spectral optical calculation tools (WIS, OPTICS, WINDOW etc.), utilizing CFD-tools and integration or importing of component level performance properties in building level simulation tools (TRNSYS, ESP, DOE etc.).

## 7 Publications

- [1] Ida Bryn, Jappe Hjelseth. Double facades in dwellings – lessons learned in Klosterenga, Oslo. ISES 2003, Gothenburg.
- [2] H. Manz, Numerical Simulation of Heat Transfer by Natural Convection in Cavities of Façade Elements, Energy and Buildings, Vol. 33, 2003, 305-311
- [3] H. Manz & H. Simmler. Experimental and numerical study of a mechanically ventilated glass double envelope facade with integrated shading device. 2nd Int. Building Physics Conf., Leuven, Belgium, Sept. 2003. 8 pages.
- [4] H. Manz, A. Schaelin, H. Simmler, Airflow patterns and thermal behaviour of mechanically ventilated glass double façades, Building and Environment (submitted)
- [5] Heimonen, I., Hemmilä K. Integration of windows and ventilation by smart supply air windows, Glass Processing Days Conference, June 2003, Tampere. 4 pages.
- [6] Ojanen, T. & Heimonen, I. Building integration of multi-functional glazed facades - Potential and risk assessment. Glass Processing Days Conference, June 2003, Tampere. p. 256 - 258.

(Planned: H. Manz et al., Experimental and numerical investigation of a glass double façade with free convection)

## 8 Working documents

r-A3-B-1 UCL dbl envelope facades classification.doc - Proposition of climatic façades classification. March 16 2001

i-a3(2)-ULC-MB-first results on belgium double envelope building - april 2002.doc

r-A3(2)-FIN-1 General workplan Case Study Double Envelope Facade, VTT

r-A3(2)-FIN-2 Questionnaire Double envelope Facades, VTT

r-A3(2)-FIN-3 STATE-OF-THE-ART OF DOUBLE ENVELOPE FACADES - 1st RESULTS OF THE QUESTIONNAIRE (Draft 8.10.2000), VTT

r-A3(2)-FIN-4, Status Report & Actions, 9.10.2000, VTT

r-A3(2)-FIN-5 SUMMARY OF REQUIREMENTS RELEVANT TO VENTILATED WINDOW AND GLAZING FACADE DESIGN, Version 8.3.2001, VTT Building and Transport

r-A3(2)-FIN-6 SUMMARY OF DESIGN ASPECTS OF DOUBLE ENVELOPE FACADES, VTT Building and Transport

r-A3(2)-FIN-7 PROGRESS REPORT, March 2001, VTT

r-A3(2)-FIN-8 Proposal for common simulation exercise.

r-A3(2)-FIN-9 PROGRESS REPORT, October 2001, VTT

al-A3(2)-FIN-10 Actionlist\_Progress\_Rome.doc, STATUS REPORT & ACTION LIST ROME MEETING, October 2001

r-A3(2)-FIN-11 Common simulation exercise.ppt

r-A3(2)-FIN-12 FirstResultsCommon simulation exercise.ppt,

r-A3(2)-FIN-13 CaseSibeliushall\_T27\_a3\_2.ppt - Double envelope façade in Sibelius hall, Lahti, Finland (in Finnish: Sibeliustalon lasikatteisen seinärakenteen lämpö- ja kosteustekninen toimivuus seurantamittauksissa, Tuomo Ojanen, VTT, March 2002.)

r-A3(2)-FIN-14 ResultsCommon simulation exercise.ppt

r-A3(2)-FIN-15 Thermal\_Perf\_Ventilated\_Window.ppt - Evaluating the thermal performance of ventilated window, April 2003.

r-A3-NL-4 TNO note on dble envelope facades, Note on active and double envelope facades (rough draft, for discussion), TNO

r-A3-NL-5 TNO definitions shading and dble facades; Note on definition of main thermal parameters in case of solar shading devices and/or active or double skin facades, TNO

r-A3-2-NL-TNO terms definitions heat flows dble facades.doc - Terms and definitions concerning heat flows in active and double envelope facades, TNO draft report

WinDat-TNO-2002-04-29 WP3.2 WIS vent.algorithm.doc. Algorithms in WIS on ventilation in gaps. Dick van Dijk, Leo Bakker.

p-a3(1)-ch1 Modelling of Air Flows in Double Facades with Shading Devices:Goal, First Steps and Outlook, EMPA

r-a3(2)-EMPA-HS-2.pdf – Experimental and numerical study of a double envelope façade. Status report. September 2002.

r-a3(2)-EDF-DC-DEF model (draft version).pdf - Documentation of the CLIM2000 Model, double envelope facade. EDF draft report.

r-a3(2)-EDF-DC-Double Envelope Building (translated).pdf - P.Aude. The qualitative study of the thermal impact of a ventilated double envelope facade compared to a double glazed window. EDF. September 2002. 25 pages.

E&H\_report\_N-v-002.doc - KLOSTERENGA ØKOLOGIBOLIGER, Klima- og energilogginger, RESULTATER OG KONKLUSJONER ENERGIBRUK. December 2001.

## Case study 3: Performance of TI façades

Prepared by:

Hans Simmler

EMPA Laboratory for Applied Physics in Building, Switzerland

### 1 Introduction

Within this case study in IEA-SHC Task 27, performance characteristics of transparent insulation façade assemblies (TIF) were investigated. This summary is not a collection of product data but an overview of properties and performance indicators, which are relevant mainly with respect to the solar and thermal performance. It should be emphasised that due to limited resources just a few spots in the broad area of “transparent insulation” concepts and systems could be examined in more detail. For similar reasons no substantial collaboration among different labs could be established within this case study. The main focus is given on effects of assembling and integration into the building envelope, which are often not taken into account. Within this case study only TI systems attached on an opaque external wall are considered. Thermal comfort aspects are just briefly mentioned, as well as durability issues, which were not further investigated in this case study.

After an introduction of the building envelope assembly “TI façade”, the concept of performance indicators as defined in IEA-SHC Task 27 project A1 is summarised in short. Performance indicators of TI assemblies are described in more detail, and standard quantities for the characterisation of components are listed quickly. Then the calculation of solar heat gains with regard to the energy performance of buildings is summarised and demonstrated. Based on measurements of a “model” system in an outdoor test facility integration effects are discussed which could cause differences between the real climate performance and performance indicators determined by standard laboratory procedures (Simmler, 2001-2003). In the last section some recommendations on performance assessment of TI systems under development are given.

## 2 TI façade systems

### 2.1 What is “transparent insulation”?

The term “transparent insulation” (TI) is basically used for a material, structure or assembly that acts as a thermal insulation in the building envelope and similarly allows for a non-negligible transmission of solar radiation. The most common example is insulating glazing, which is typically used in windows because of its view through and daylighting properties. Normally other types of geometric TI materials are used in front of an opaque external wall, mainly insulation “boards” built of transparent polymeric tube or honeycomb structures with one or double-side covering glass pane(s). Translucent insulating glazing units with geometric or silica aerogel filling are available as well.

### 2.2 Principles and examples

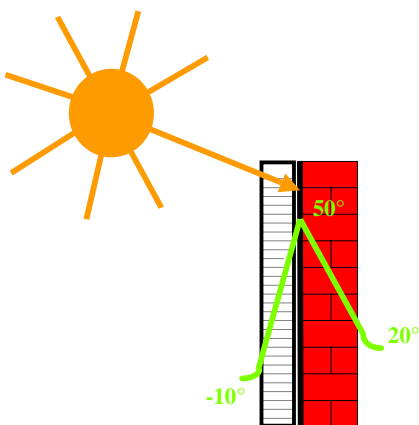


Fig. 3-1: Basic types of TI systems: Direct gain or light wall (top), and solar wall (bottom). Bottom left:

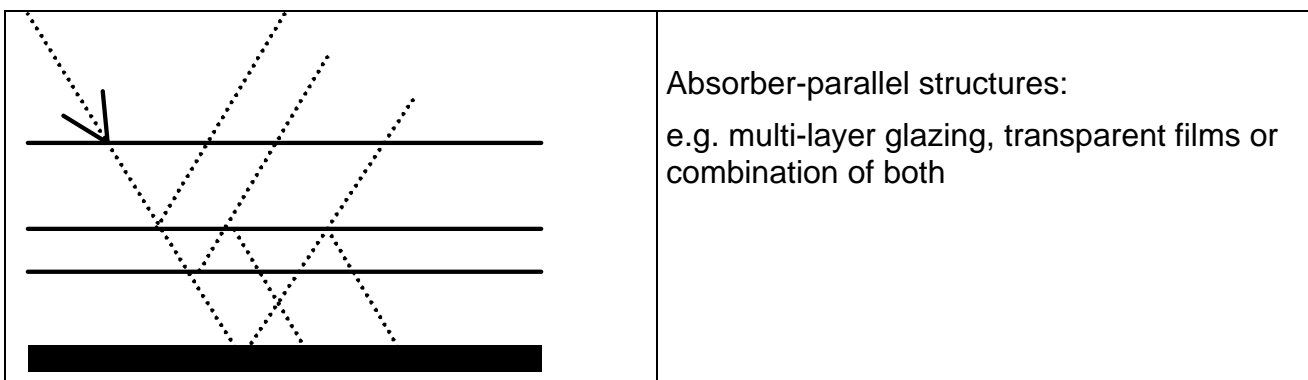
principle of a solar wall, bottom right: building with a solar wall in the lower part of the façade

As indicated above, TI components are basically used in two different ways. If the TI component replaces (partially) the external wall, solar radiation propagates directly to the inside area of a building and is converted to heat on the internal surfaces. The efficiency of this *direct gain* or *light wall* is quite high. The daylight transmittance is also advantageous. However, due to the immediate impact on the room temperature, overheating problems often occur or must be prevented by shading, i.e. blocking of the incident radiation. Heat storage and release cannot be influenced. In the *solar wall* configuration, transparent insulation instead of a conventional thermal insulation is attached on an opaque external wall. The transmitted solar radiation is absorbed and heats up the outside surface of the massive wall, which acts as a heat storage element (Fig. 1). TI assemblies with an integrated absorber plate have been developed also, hence becoming a special opaque cladding element in this version.

Depending on the thermal properties of the wall heat is released at the inside surface with a time lag of several hours and moderate surface temperatures. In many applications a shading system is installed anyhow to avoid uncomfortable indoor surface temperatures in the warmer periods of the year. A lot of information and examples can be found e.g. in Kerschberger (1997).

More complex systems have been set up, i.e. with controllable natural or mechanical ventilation of the air gap between TI and wall. The system design also can be similar to an air collector which is connected to an active storage/heating system. The following sections are focused on the classic solar wall situation.

## 2.3 Typical layout of structures



|  |   |
|--|---|
|  | <p>Absorber - perpendicular structures ("classic" Transparent Insulation): e.g. transparent polymeric or glass tubes, honeycombs, transparent films. At least one side of the structure is to be covered with a (transparent) layer</p> |
|  | <p>Transparent polymeric cavity structures</p>  |
|  | <p>Translucent bulk structure:<br/>e.g. silica aerogel</p>  |

Fig. 3-2: Classification of different types of transparent insulation.

TI structures can be classified in 4 groups (Platzer, 1988) that are indicated the Fig. 2. Mainly used polymeric materials are acrylic (PMMA) and polycarbonat (PC) films, which have a high transmittance and little degradation. Also produced are thin glass tubes assembled as TI double glazing.

## 2.4 Estimation of performance

Besides the component performance the energy performance of a solar wall is strongly dependent on the climatic conditions and the wall orientation. A rough estimate is given in the following example. A more detailed performance calculation method is described later.

In a steady state approximation the solar heat gain can be estimated as  $Q_S = \gamma G_x \tau$ , where  $G_x = \Sigma G_{xi} \Delta t_i / \tau$  is the mean global solar energy input on the wall of orientation  $x$  during the time interval  $\tau = \Sigma \Delta t_i$ . The efficiency of a solar wall is approximately  $\gamma = g_{TI} U / U_{TI}$ , that is the total solar energy transmittance  $g_{TI}$  times the ratio of the thermal transmittances  $U$  (total) and  $U_{TI}$ .

Heating relevant transmission losses are estimated by  $Q_T = U \Delta T \tau$ , where  $\Delta T = \Sigma \Delta T_i \Delta t_i / \tau$  is the mean indoor-outdoor temperature difference above a certain threshold level.

Then the ratio between average solar heat gain and thermal transmission loss is

$$Q_S / Q_T = \frac{g_{TI}}{U_{TI}} \frac{G_x}{\Delta T} \quad (1)$$

To illustrate the range, data for Switzerland (latitude ca. 47° north) are shown in Tab. 1 for an indoor air temperature  $T_i = 20^\circ\text{C}$  and the heating period defined by the days with  $T_{e,\max}$  below  $12^\circ\text{C}$ . Assumed TI performance is  $g_{TI} / U_{TI} = 0.5 \text{ m}^2\text{K/W}$ , which is not too ambitious. Best achievable  $g_{TI} / U_{TI}$  values (centre) are around  $0.8 \text{ m}^2\text{K/W}$ .

It can be seen that except of the north orientation all walls act as heat suppliers. For a north wall the heat losses are approximately compensated by the solar gain. For a total solar wall U-value of  $0.6 \text{ Wm}^{-2}\text{K}^{-1}$  the estimated net heat gain is roughly between 100 and 200 kWh/m<sup>2</sup> for a south wall in the different climates.

Tab. 3-1: Average temperature difference, solar irradiance, gain to loss ratio, and net heat gain of a solar wall in the heating period. Climate data are typical for the alpine region (cold, sunny) and for the most populated area in the midlands (less cold, lower solar irradiance) of Switzerland.

| Location              | $\Delta T_{12/20}$<br>(K) | Orient. | $G_{x,12}$<br>(W/m <sup>2</sup> ) | $Q_S / Q_T$<br>(1) | Net gain<br>(MJ/m <sup>2</sup> ) |
|-----------------------|---------------------------|---------|-----------------------------------|--------------------|----------------------------------|
| Bever (alpine region) | 19.9                      | S       | 126                               | 3.2                | 758                              |
|                       |                           | W       | 84                                | 2.1                | 384                              |
|                       |                           | E       | 81                                | 2.0                | 357                              |
|                       |                           | N       | 39                                | 1.0                | -4                               |
| Zurich (midlands)     | 16.2                      | S       | 86                                | 2.7                | 320                              |
|                       |                           | W       | 51                                | 1.6                | 112                              |
|                       |                           | E       | 49                                | 1.5                | 97                               |
|                       |                           | N       | 24                                | 0.7                | -50                              |

---

## 3 Concept of performance indicators

### 3.1 Layer model

For the general assessment of the energy performance of a special building envelope component a large number of data and model relations are needed. The energy performance assessment methodology (EPAM) is relating the measured physical data to the performance of the component installed in a building and climatic environment. The performance of a building is characterised by a number of aspects, namely heating, cooling, lighting and comfort (visual, thermal, and air quality). More details on the methodology and relevant indicators are given by Platzer (2001). There are a number of elements needed in the performance assessment which have to be linked together. The task therefore is of considerable complexity.

### 3.2 Detailed and simplified indicators

The first part is a consistent set of component performance indicators (CPI) characterising quantitatively the building component physically. The most prominent parameters are the U-value of the component, the total solar energy transmittance  $g$ , the visual transmittance  $\tau_v$ . The degree of sophistication is of course dependent on the level needed for building energy calculation. For example, in simplified tools only single number values are needed for this characterisation, but for building energy simulation tools like ESP-r angular dependent data of  $g$  and  $\tau_v$  are favourable, and the tool itself for this purpose needs angular optical properties and thermal properties of the glazing layers. Even more advanced models one may perceive in future would probably use even spectral data. Information on frame and edge seal design is needed to input a linear thermal conductance PSI.

The second part connected to the experimental data therefore is the component model within the simulation routine, which may be a part of the EPAM. The simplest so-called trivial component model is just the instruction "Feed in the measured parameter, e.g. U into the calculation". A more sophisticated model would be the calculation of effective parameters derived from measured data to be fed into the building model. An example is the determination of frame U-value and PSI-value from frame design according to EN ISO 10077 in order to feed these data in to a simulation tool requiring these parameters. Or an optical glazing calculation tool can be used to calculate effective solar transmittance and absorptance for input to, say, the TRNSYS library from measured optical spectral data using an empirical formula to derive angular optical data from normal incidence measurements.

The third part would be the integration and description of components like windows integrated into the building model. Questions of window-wall connections and shading by window apertures will be treated here. Even if in many cases a so-called trivial model again is employed in many current energy performance calculations, one should be aware

that even in very simplified tools empirical coefficients (e.g. relating TSET g and solar irradiation for solar gain calculation) are implicit integration models.

In the following section, performance indicators are listed and briefly commented for the various levels bottom-up (from materials to building). Information on measurement and calculation methods and standards was collected by D. van Dijk (2001).

## 4 Performance indicators

### 4.1 Basic materials

Optical properties of the TI materials - e.g. transparent films, tubes or sheets - are the basis for the properties of TI structures formed with it. Normally, specular data are sufficient. For scattering bulk media such as silica aerogel, direct-hemispherical data will be necessary. Spectral or integral properties are used in modelling of structures. Relevant properties are listed in Tab. 2.

For many TI products these basic data are not known. In this case simulation is often not possible, but is usually replaced by measurements of the TI structure or assembly.

Angular dependence is generally not determined. For uncoated films or sheets angular dependence of transmittance / reflectance can be calculated analytically. For bulk scattering materials however, the angular dependence of optical properties normally has to be determined experimentally.

Tab. 3-2: Properties for characterisation of basic TI materials.

| Parameter                            | Symbol, details   | Relevance, comments   |
|--------------------------------------|---|---|
| IR-emissivity                        | $\varepsilon(\lambda, \text{far IR}), \varepsilon$ (integral, far IR) | radiative heat exchange in the structure (thermal transmittance)  |
| ev. IR-transmittance                 | $\tau(\lambda, \text{far IR}), \tau$ (integral, far IR)               | normally integral values used in modelling  |
| solar transmittance                  | $\tau(\lambda, \text{solar band})$ or $\tau_e$ (solar)                | solar radiation propagation through TI structure  |
| solar reflectance                    | $\rho(\lambda, \text{solar band})$ or $\rho_e$ (solar)                | reflectance/absorptance also for absorber and frame surface   |
| solar absorptance                    |   | modelling: spectral (integral)  |
| visual transmittance                 | $\tau_v$ (visual)   | used for modelling of daylight properties, important for light walls                                      |
| visual reflectance                   | $\rho_v$ (visual)   |   |
| thermal conductivity                 | $\lambda(T)$  | may be relevant for modelling of polymeric structures<br>not important for thin polymeric films and glass |
| thermal conductivity of the absorber | $\lambda(T)$ along the plate normal                                   | if an absorber plate is integrated in a TI assembly   |

## 4.2 TI structures

For TI structures (including possible glass covers) the parameters listed in Tab. 3 are needed for further performance assessment. In principle, the properties can be calculated from geometry and basic materials data. In practise, the properties are mainly determined by spectral or broadband calorimetric measurements of the whole structure (Platzer, 2000) since standardised procedures and calculation tools exist only for specular multiple glazing.

Tab. 3-3: Performance data to characterise the energy performance of TI structures.

| Parameter  | Symbol, details  | Relevance, comments   |
|--|--|---|
| solar transmittance (direct-hemispherical)                   | $\tau_{dh}(\lambda, \text{solar band})$ or $\tau_{dh}(\text{solar})$<br>incl. angular dependence | angular dependence is needed to calculate the transmittance for diffuse irradiation                           |
| solar transmittance (normal incidence)                       | $\tau_n(\text{solar})$   | near vertical incidence: key parameter for solar heat gain calculation  |
| solar transmittance (diffuse irradiation)                    | $\tau_h(\text{solar})$   | hemispherical irradiation: key parameter for solar heat gain calculation<br>often calculated from $\tau_{dh}$ |
| solar reflectance (diffuse irradiation)                      | $\rho_h(\text{solar, backward})$   | used to calculate multiple reflection effects between absorber and TI, often not determined ( $< 0.1$ )       |
| total solar energy transmittance TSET (direct-hemispherical) | $g_{dh}$<br>incl. angular dependence   | angular dependence is needed to calculate the TSET for diffuse irradiation                                    |
| total solar energy transmittance (normal incidence)          | $g_{t,n}$  | near vertical incidence: key parameter for solar heat gain calculation  |
| total solar energy transmittance (diffuse irradiation)       | $g_{t,h}$  | hemispherical irradiation: key parameter for solar heat gain calculation<br>often calculated from $g_{dh}$    |
| thermal resistance of the TI (including absorber)            | $R_t = U_t^{-1}$   | measurement or calculation (multiple glazing)   |

### 4.3 TI façade element with integrated absorber

If a TI façade element is prefabricated with an integrated absorber, the TSET values above may be calculated from the solar transmission data of the TI structure, the solar absorptance and the thermal resistance of the absorber plate. The calculation follows the procedure described in the next section. However, the solar transmission properties of the TI structure may not be known. In this case, the TSET values described above are determined directly by calorimetric measurements (including solar absorptance and thermal resistance of the absorber).

Also the central thermal resistance of the whole element shall be determined, either calculated from component data according to calculation standards or measured on the whole assembly (temperature dependence!).

### 4.4 Combination of TI-façade and wall

Upon attachment of the TI structure (element) to an external wall the following properties (Tab. 4) are needed to calculate the thermal performance.

Tab. 3-4: Performance parameters needed to calculate the efficiency of a solar wall.

| Parameter  | Symbol, details                                     | Relevance, comments   |
|--|---|---|
| solar absorptance of the wall                    | $\alpha = 1 - \rho_{h,Wall}$ (solar)                | used to calculate the g-value of TI without integrated absorber<br><br>not used if absorber is integrated |
| thermal resistance of the air gap absorber-wall  | $R_{al}$  | used to calculate the correct efficiency (c.f. EN ISO 6946 / EN 673)                                      |
| thermal resistance of the wall                   | $R_i$   | wall resistance between the inside and outside surface  |
| thermal resistance of internal, external surface | $R_{si}, R_{se}$                                    | standard values are: 0.13 m <sup>2</sup> K/W, 0.04 m <sup>2</sup> K/W                                     |
| total wall resistance                            | $R = R_{si} + R_i + R_{al} + R_t + R_{se} = U^{-1}$ | c.f. EN ISO 6946  |

The calculation procedure for the total solar gains of a solar wall, based on work of Platzer (1999), is integrated in the actual prEN ISO 13790. The assumption is that the monthly average solar gain of a TI façade can be calculated in the form

$$g_{t,j,m} = \alpha (g_{t,h} - c_{j,m} g_{t,n}) \quad (2)$$

for systems without absorber, or

$$g_{t,j,m} = \frac{R_{se} + R_t}{R_{se} + R_t + R_{al}} (g_{t,h} - c_{j,m} g_{t,n}) \quad (3)$$

for systems with integrated absorber.

Optimized coefficients  $c_{j,m}$  were determined by means of measured directional properties of several products and tested for a number of local climates in Germany. It could be shown that “constant” values independent from location and product type can be used with reasonable accuracy. Those values, also given in prEN 13790, are summarized in Tab. 5.

Tab. 3-5: Coefficients  $c_{j,m}$  dependent on the orientation  $j$  and month  $m$ .

|           | S      | SW/SE  | W/E    | NW/NE | N     |
|-----------|--------|--------|--------|-------|-------|
| October   | -0.054 | -0.025 | 0.024  | 0.014 | 0.000 |
| November  | -0.093 | -0.034 | 0.049  | 0.004 | 0.000 |
| December  | -0.105 | -0.026 | 0.052  | 0.000 | 0.000 |
| January   | -0.105 | -0.034 | 0.054  | 0.002 | 0.000 |
| February  | -0.067 | -0.027 | 0.033  | 0.008 | 0.000 |
| March     | -0.023 | -0.010 | 0.016  | 0.016 | 0.000 |
| April     | 0.042  | 0.002  | -0.012 | 0.030 | 0.011 |
| May       | 0.073  | 0.022  | -0.005 | 0.018 | 0.021 |
| June      | 0.089  | 0.037  | -0.002 | 0.013 | 0.031 |
| July      | 0.094  | 0.036  | -0.012 | 0.013 | 0.042 |
| August    | 0.062  | 0.013  | -0.007 | 0.024 | 0.012 |
| September | 0.005  | -0.015 | -0.001 | 0.033 | 0.000 |

Then for a given climate, an effective collecting area for orientation  $j$  and month  $m$

$$A_{s,j,m} = A F_s F_F g_{t,j,m} U / U_t \quad (4)$$

is calculated and treated similarly to other direct gains.

Therefore, heat gains of a solar wall are decreased by the same utilization factor in prEN ISO 13790 as other direct solar heat gains such as from windows. The storage effect of the massive wall is not taken into account, which leads to a considerable underestimation of the heat gains of solar walls in the actual standard.

Further simplifications aiming at a constant TSET e.g. for the entire heating season have been proposed. In Platzer (1999), orientation dependent correction factors for the hemispherical TSET

$$g_{t,j} = g_{t,h} \cdot Z_j \quad (5)$$

are given as shown in the following table:

Tab. 3-6: Orientation dependent seasonal factors  $Z_j$  (Platzer, 1999).

| Orientation j | S    | SW/SE | W/E  | NW/NE | N    |
|---------------|------|-------|------|-------|------|
| $Z_j$         | 1.04 | 1.02  | 0.98 | 0.99  | 1.00 |

In Ochs (2001) irradiation weighted seasonal values were calculated from the monthly correction factors (Tab. 5):

$$c_j = \frac{\sum_m c_{j,m} G_{j,m}}{\sum_m G_{j,m}} \tag{6}$$

In the same paper a comparison of the different calculation schemes for various heating period lengths was made for 4 climate stations in Switzerland: Zurich-SMA (midland, 596 m altitude,  $T_{e,av,y} = 9.0 \text{ }^\circ\text{C}$ ,  $G_{s,h,y} = 3906 \text{ MJ/m}^2$ ), Basel-Binningen (northwest, 317 m alt.,  $T_{e,av,y} = 10.0 \text{ }^\circ\text{C}$ ,  $I_{s,h,y} = 3938 \text{ MJ/m}^2$ ), Davos (alpine, 1590 m alt.,  $T_{e,av,y} = 3.3 \text{ }^\circ\text{C}$ ,  $I_{s,h,y} = 4967 \text{ MJ/m}^2$ ), and Lugano (south of the alps, 276 m alt.,  $T_{e,av,y} = 12.0 \text{ }^\circ\text{C}$ ,  $I_{s,h,y} = 4064 \text{ MJ/m}^2$ ). The results for south orientation are shown in Fig. 3. The differences between the 4 stations as well as between the stations and the averaged coefficients are small. For the different heating periods the coefficients  $c_j$  vary between -0.09 for a short heating period and -0.05 for a long heating period. The average of  $c_j$  over the 4 heating periods is about -0.07. Considering that  $g_{t,n}$  is typically around 20 % higher than  $g_{t,h}$  this leads to an error of less than 3 %. The results for the coefficients averaged over the 4 heating periods for the 4 climate stations and all orientations are given in Tab. 7. Assuming  $g_{t,n}$  being e. g. 20 % higher than  $g_{t,h}$ , the irradiation weighted g-value is 8 % higher than the  $g_{t,h}$ , while the orientation corrected hemispherical value is 4 % higher than  $g_{t,h}$ . The various results for the south orientation are illustrated in Fig. 4.

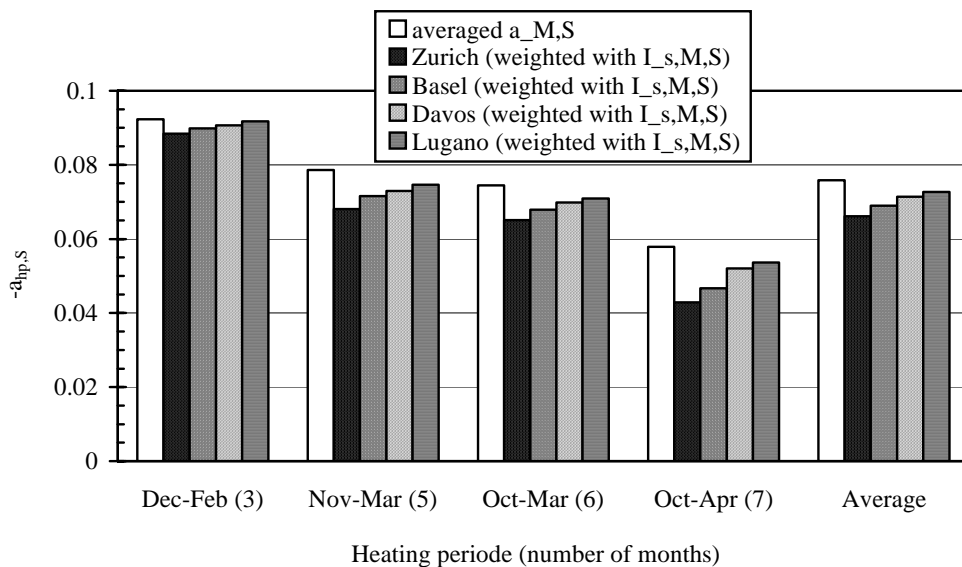


Fig. 3-3: Coefficients  $-a_{hp,S} = -c_j$  for south orientation and different lengths of heating periods and

different climate stations.

To summarize, the suggested way to calculate an irradiation weighted constant g-value for the TI system over the heating period takes the angular selectivity and the climate conditions explicitly into account. For the south orientation the resulting g-values are slightly higher than the orientation corrected hemispherical values without the input of irradiation data. For the other orientations the two results are quite similar. The differences will be higher for TI elements with especially high differences between  $g_{t,n}$  and  $g_{t,h}$ .

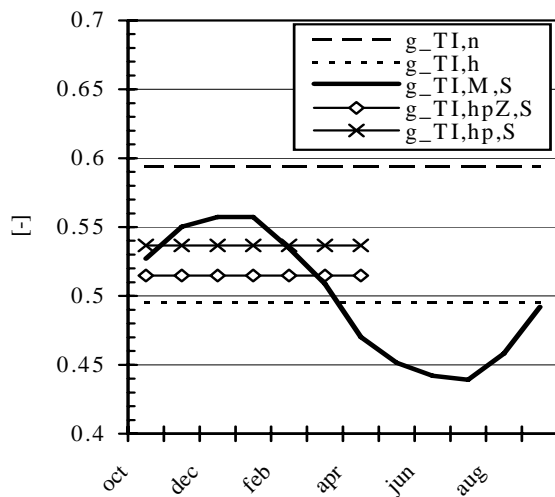


Fig. 3-4: g-values for a south orientated TI element without integrated absorber with characteristic values  $g_{n,B} = 0.55$ ,  $g_{n,B} = 0.66$ , and  $\alpha_s = 0.9$ .  $g_{TI,M,S}$  is the time dependent value  $g_{j,m}$ ,  $g_{TI,hp,S}$  is the average over the heating period.

Tab. 3-7: Time period averaged coefficients  $c_j$  in dependence of orientation  $j$ .

|                                 | <b>S</b>     | <b>SW/SE</b> | <b>W/E</b>  | <b>NW/NE</b> | <b>N</b>    |
|---------------------------------|--------------|--------------|-------------|--------------|-------------|
| Zurich-SMA                      | -0.066       | -0.023       | 0.033       | 0.010        | 0.001       |
| Basel-Binningen                 | -0.069       | -0.024       | 0.033       | 0.009        | 0.001       |
| Davos                           | -0.071       | -0.024       | 0.034       | 0.009        | 0.001       |
| Lugano                          | -0.073       | -0.025       | 0.035       | 0.009        | 0.000       |
| <b>Average <math>c_j</math></b> | <b>-0.07</b> | <b>-0.02</b> | <b>0.03</b> | <b>0.01</b>  | <b>0.00</b> |

In order to get an estimate of the accuracy of the simplified methods, the g-values of two solar wall assemblies were compared with results obtained by the dynamic building energy simulation tool HELIOS, c.f. Frank et al. (1992). The program performs an hourly energy

balance in a single zone based on a response factor method. The net solar heat gain was determined as the difference of the total energy input in a control volume at 20 °C with and without solar absorption by the exposed solar wall, normalized with the total incident solar energy during the calculation period.

The properties of the TI materials were taken into account in the following way: For the direct-hemispherical TSET measured angular dependent values are used. For the remaining fraction of the global solar radiation a constant value is assumed. The temperature dependence of the thermal conductivity is modelled by a second order polynomial. In the dynamic calculations, a 120-mm PMMA capillary material with an external 4-mm float glass cover including an air gap of 10 mm was used. The solar absorptance of the wall was set to 0.95. Value used in the static calculation are:  $g_{t,n} = 0.759$ ,  $g_{t,h} = 0.498$ ,  $R_{se}+R_t+R_{al} = R_e = 0.984 \text{ m}^2\text{K/W}$ .

The climatic data of the Swiss town Interlaken were applied in a period from October until April (average outdoor temperature  $T_e = 2.4^\circ\text{C}$ , total incident solar energy  $G_{\text{south}} = 1923 \text{ MJ/m}^2$ ,  $G_{\text{south-west}} = 1586 \text{ MJ/m}^2$ ). The results are shown in Tab. 8.

Tab. 3-8: Comparison of static and dynamic calculation of TSET.

| Description  | System 1                      | System 2                    |
|--|-------------------------------|-----------------------------|
| Wall type  | 24 cm Brick wall (fired clay) | 20 cm Light-weight concrete |
| $1/U$ $\text{m}^2\text{K/W}$                         | 1.693                         | 1.309                       |
| $U/U_t$ -  | 0.581                         | 0.752                       |
| $g_{t,\text{south}}$ -                               | 0.551                         | 0.551                       |
| $g_{\text{wall},\text{south}}$ -                     | 0.320                         | 0.414                       |
| $g_{\text{wall},\text{south},\text{dynamic}}$ -      | 0.316                         | 0.381                       |
| $g_{t,\text{south-west}}$ -                          | 0.513                         | 0.513                       |
| $g_{\text{wall},\text{south-west}}$ -                | 0.298                         | 0.386                       |
| $g_{\text{wall},\text{south-west},\text{dynamic}}$ - | 0.309                         | 0.372                       |

In general, the agreement between the simplified method and the dynamic calculation is good. The deviation for the south oriented concrete wall is somewhat larger.

## 5 Building integration effects

A possible deviation between lab determined and in-use performance was investigated by outdoor measurements on a pre-fabricated TI façade element with a 14 cm layer of PMMA tubes and integrated absorber have been performed [r-a3(3)-ch-2.doc]. Two elements ( $w \times h = 1.41 \times 0.94 \text{ m}^2$ , transparent area ca.  $2.36 \text{ m}^2$ ) were fixed on a 19 mm wood fibre board ( $w \times h = 1.5 \times 2.0 \text{ m}^2$ ) which was placed in an insulating test frame of the outdoor test site (Fig. 5).

The following “real climate” results were evaluated from the outdoor measurements by means of a dynamic system identification procedure:

| Property                    | Unit            | Real climate | Lab value |
|-----------------------------|-----------------|--------------|-----------|
| $g_{TI}$ , transparent area | -               | 0.49         | 0.55      |
| $U_{TI}$ , with frame       | $Wm^{-2}K^{-1}$ | 0.96         | 0.80      |

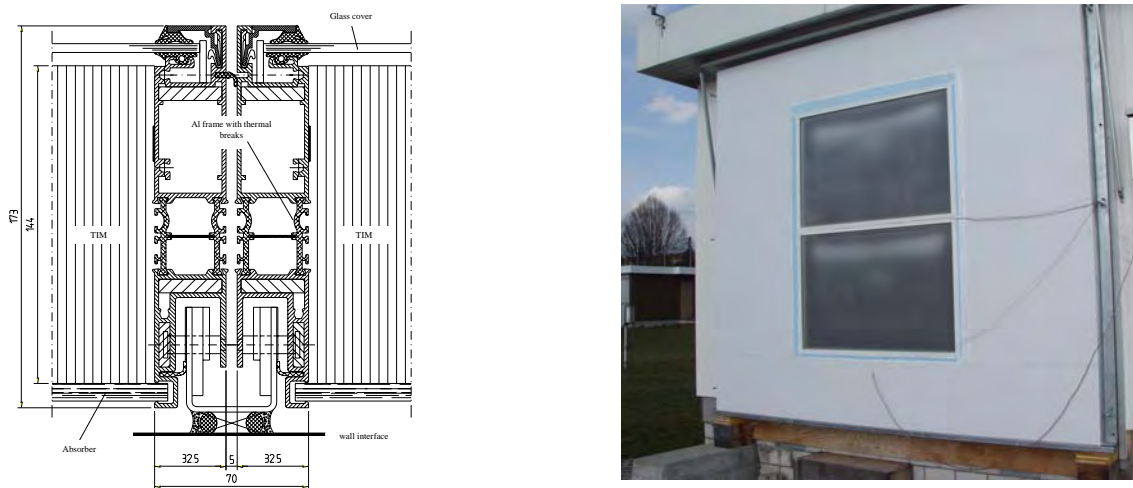


Fig. 3-5: Cross section of the pre-fabricated TI element (left) and experimental setup of two TI façade elements for outdoor testing (right). Internal condensation on the glass cover can be observed in the upper part of each element.

Compared to an estimated value  $g_h \approx 0.55$  for the transparent area, derived from measured optical data for TI and absorber, the outdoor  $g$ -value is about 10% lower. The thermal transmittance in the dark state according to the standard hot box measurement ISO 8990 including frame is approximately 17% lower than measured under real climate conditions.

In the following paragraphs possible reasons for the lower “real” performance are discussed. The reduction may be related e.g. to thermal losses (framing, internal convection, moisture effects), and shading effects by the frame.

## 5.1 Heat loss through the frame

A possible reason for additional heat loss in the illuminated state has been further investigated: heat absorbed in the tubes and on the integrated absorber may be lost through the frame to the exterior. The effect was estimated by a 2-dimensional heat

transfer calculation. To simulate a volumetric absorption in the structure, 4 equal planar heat source layers were placed, with the absorber plane as the first layer (40 mm distance between each source layer). Assuming a linear edge heat loss

$$Q_{\text{lin}} = gG\ell\Psi_{\text{lin}} \quad (7)$$

the edge corrected g-value is

$$g_{2D} = g\left(1 - \frac{\ell}{A}\Psi_{\text{lin}}\right) \quad (8)$$

where

|                     |   |
|---------------------|---|
| G                   | Global solar radiation ( $\text{Wm}^{-2}$ ) |
| $\ell$              | length of the edge (m)                      |
| A                   | Transparent area ( $\text{m}^2$ )           |
| $\Psi_{\text{lin}}$ | edge transmittance (m)                      |

The edge transmittance is determined by comparison of the 1- and the 2-dimensional heat flow:

$$\Psi_{\text{lin}} = b(1 - f_{2D} / f_{1D}), \quad (9)$$

where

|   |  |
|---|--|
| f | $Q_{\text{in}} / Q_{\text{source}}$ ratio of inward / source heat flow |
| b | width of the edge zone (m)   |

From the calculation  $\Psi_{\text{lin}} = 0.0044$  m was determined (Fig. 4). With a ratio  $\ell / A = 3.8$  m-1 the relative change of the TSET is 1.7 %. The conclusion is that – even with unfavourable assumptions – a loop back heat flow through the frame is not an important gain loss mechanism. This is valid also for constructions with absorption on the wall.

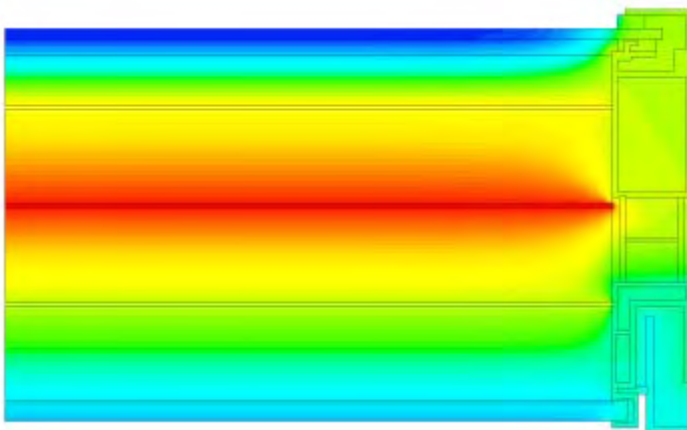


Fig. 3-6: Heat flow calculation next to the edge of an aluminium-framed TI façade element with 4 planar heat source layers. The exterior glass pane is on top.

## 5.2 Heat loss through internal convection

The thermal transmittance measured under real climate conditions is substantially larger compared to a standard hot box measurement. Possible reasons are i) increased internal heat transfer caused by high temperatures in the illuminated state, ii) increased exterior surface transfer coefficient, iii) increased ventilation losses (wind loads).

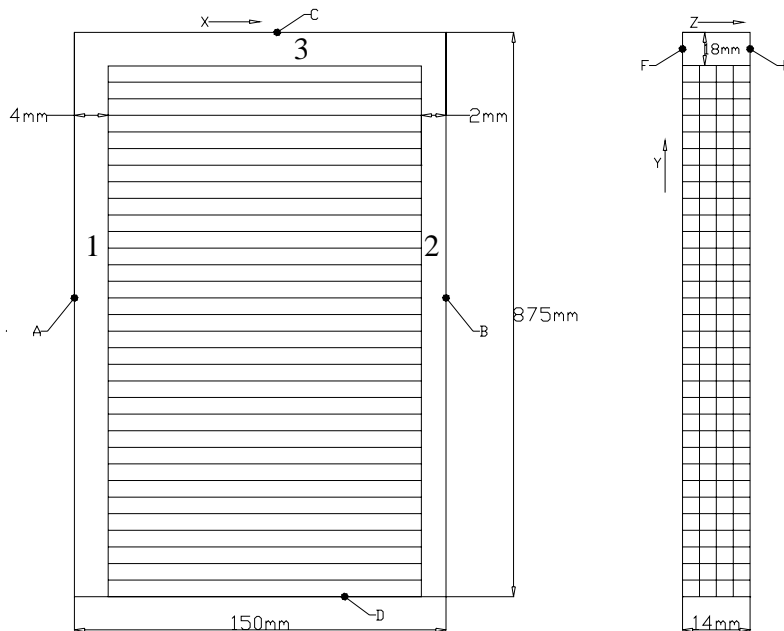


Fig. 3-7: Schematic CFD representation a TI structure in an air cavity. Gaps are on the left (gap 1 between TI and glass pane A at 0°C), on the right (gap 2 between TI and absorber B at 20 °C) and on top (gap 3, settlement of the TI structure). On surfaces C and D adiabatic boundaries were set.

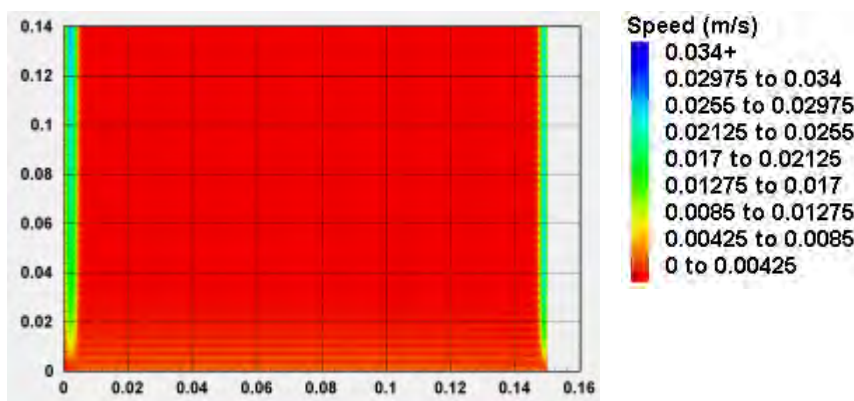


Fig. 3-8: Image of the calculated airflow speed distribution in the lower part of the TI structure (vertical plane through the centre of the cells).

Since internal convection is indicated by the moisture condensation pattern seen on the glass pane (Fig. 5) in the outdoor measurements the effect of different gap situations was analysed by means of 3-dimensional CFD modelling. Due to the large number of cells in the vertical direction a width section of four (square) cells was used (Fig. 7). Heat conduction in the cell walls and radiative heat transfer were not taken into account. An example of the calculated flow fields is visualized in Fig. 8.

The configurations and calculated Nusselt numbers (convective heat transfer coefficient relative to static air) are summarised in Tab. 9. In the undisturbed case almost no convection occurs. Little impact is also seen if there is just a gap on top. The Nusselt number is increased by more than 50 % if gap 2 between TI and absorber is opened. An additional gap 3 on top has almost no influence. It can be concluded that the U-value can be strongly increased if not at least one side of the TI structure has an airtight cover. In laboratory measurements a displacement of the absorber plate towards the TI structure on irradiation was observed. Therefore a potential gap should be less severe for the g-value of the investigated component. But by virtue of repeated absorber motion and high temperatures in the outdoor climate there could certainly emerge a gap situation causing a substantial increase of the U-value.

Accordingly direct air exchange between the "hot side" of a TI façade and the environment, e.g. through a leaking air gap between the massive wall and the TI component could also reduce the performance considerably.

Tab. 3-9: Calculated Nusselt numbers for an air cavity with horizontal TI structure (see text). Gap 3 on top has little influence, but gap 2 with a width of 2 mm increases the Nusselt number by almost 50 %.

| Configuration                         | Gap 1 | Gap 2 | Gap 3 | Nusselt number |
|---------------------------------------|-------|-------|-------|----------------|
| Ideal case, one intended gap          | 6 mm  | 0 mm  | 0 mm  | 1.038          |
| Settlement                            | 6 mm  | 0 mm  | 8 mm  | 1.062          |
| Displacement of absorber              | 4 mm  | 2 mm  | 0 mm  | 1.531          |
| Settlement & displacement of absorber | 4 mm  | 2 mm  | 8 mm  | 1.531          |

In particular in conjunction with internal convection additional heat loss could arise from latent heat transport in condensation-evaporation cycles, as indicated in Fig. 3. Within this project no work was done to quantify such effects.

It should be noted that the displacement of the absorber at high temperatures also causes a breathing effect of the non-sealed TI element. However, this should be a minor effect regarding heat exchange since the volume exchange rate is estimated to be well below  $0.1 \text{ h}^{-1}$ , for which the U-value increases less than  $0.005 \text{ Wm}^{-2}\text{K}^{-1}$ .

### 5.3 Shading effects, solar absorption by the frame

As can be easily observed, a direct beam entering at a certain incidence angle  $\phi$  propagates through the TIM approximately like a cone with a similar opening angle, due to multiple transmission and reflection (Fig. 9). The top of the cone is at the entry point of the beam. If the cone is not disturbed by the (absorbing) frame, the hemispherical transmittance will be equal to the value measured in the lab. However, if the beam entry point is closer to the frame than  $d \cdot \tan(\phi)$ , the propagation is disturbed, i.e. the transmittance will be lowered by edge absorption.

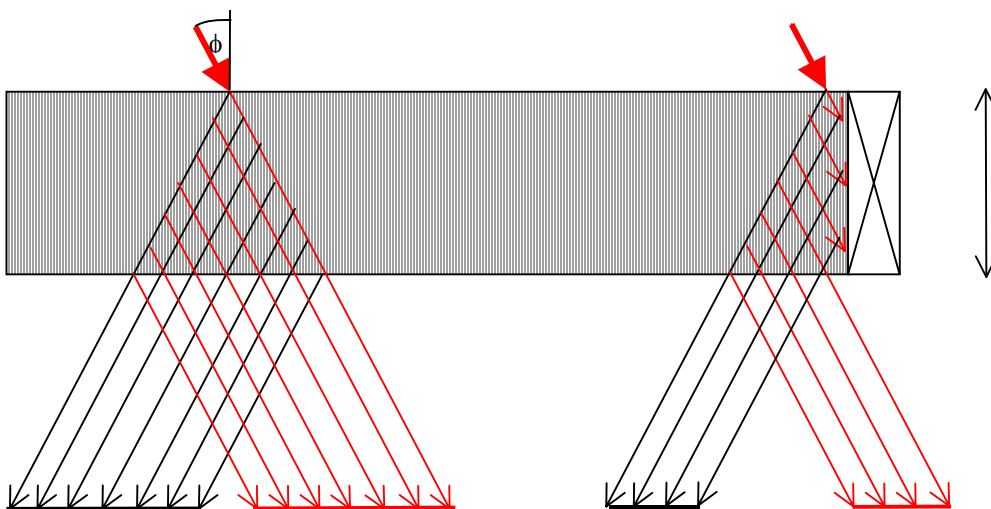


Fig. 3-9: Heat flow calculation next to the edge of an aluminium-framed TI façade element with 4 planar heat source layers. The exterior glass pane is on top.

Assuming an incidence angle  $\phi = 30$  degrees,  $d = 140$  mm and a TIM area of  $1.345 \times 0.875 \text{ m}^2$  (similar to the outdoor measurements), the width of the edge zone is about 80 mm. 28 % of the TIM area is in this edge zone where the transmittance is more or less reduced. To get an order of magnitude of the impact on the TSET, the transmission through a two-dimensional thin film TIM-structure as indicated in Fig. 9 was modelled. If scattering is not taken into account, the propagation is given by a "tree" of transmission / reflection paths. It is well known that, without edge effects, the total transmittance is  $\tau_{\text{TIM}} = (\tau + \rho)^N$ , where N is the number of intersections between the direct beam and the layer structure. The escaping radiation is described by a binomial (symmetric) distribution. Near the edge, the symmetry is broken. Therefore, the propagation was calculated numerically. The distribution of the transmitted beam is shown in Fig. 10 (top) for  $N = 25$  (corresponding to  $\phi = 30^\circ$ ,  $d = 140$  mm) and for various distances between beam entry point and edge. The other parameters are  $\tau = 0.8$ ,  $\rho = 0.18$ ,  $\rho_{\text{edge}} = 0.3$ .

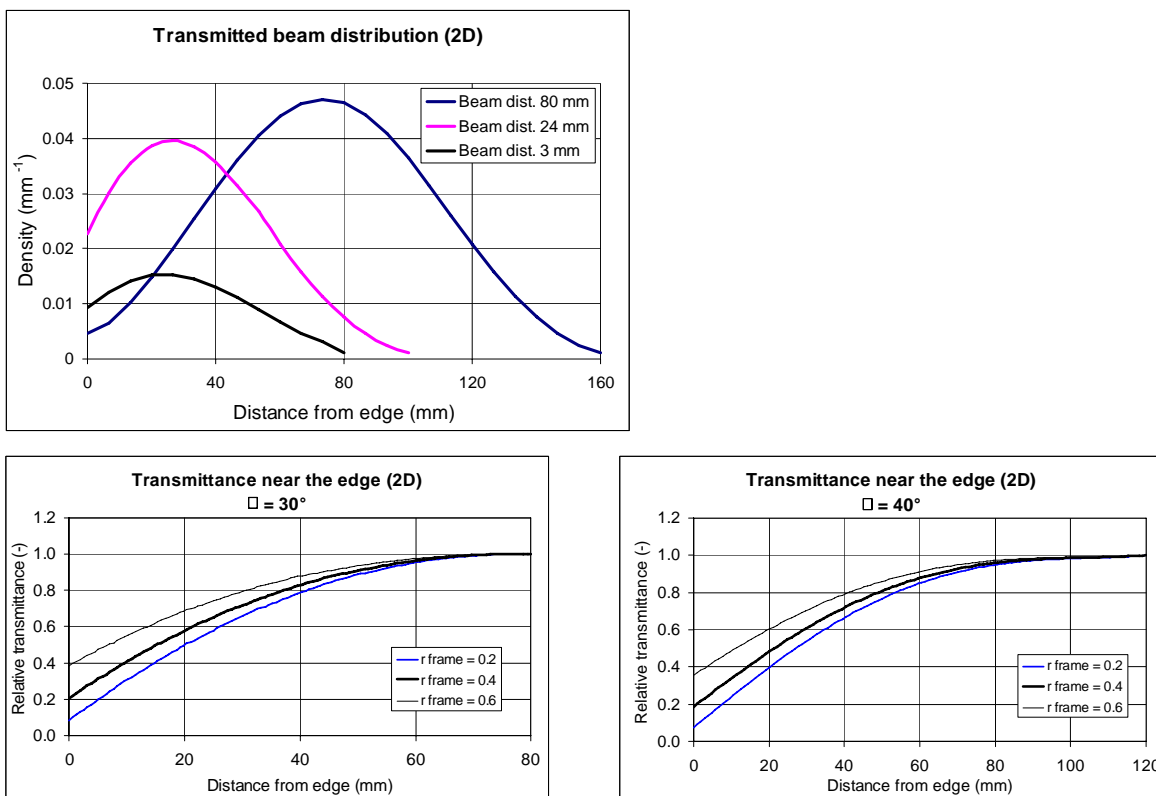


Fig. 3-10: Distribution of solar radiation transmitted through a 2D TI-structure for various distances between beam entrance and edge (top) and decrease of the transmittance near the frame for two different incidence angles (bottom).

The relative transmittance in the edge zone is displayed in Fig. 10 (bottom) for the incidence angles  $\phi = 30$  degree and  $\phi = 40$  degree.

It can be concluded from the investigated examples that for beam-parallel structures the solar transmittance  $\tau_h$  is reduced in an edge area with the width  $d \cdot \tan(\phi)$ . Depending on the average incidence angle and the solar reflectance of the frame surface ( $\rho_{\text{frame}} = 0.2 \dots 0.6$ ), the ratio of the integrated values  $r = \tau_{\text{edge}} / \tau_h$  in the edge zone is roughly between 0.7 - 0.8.

Therefore the effective transmittance can be described as

$$\tau_{TIF} = \tau_h \left( 1 - \frac{L}{A} d \tan(\phi) (1 - r) \right) \quad (10)$$

For an estimated  $\phi_{\text{average}} = 40^\circ$  (direct plus diffuse solar radiation) in the outdoor measurement, the reduction is about  $\tau_{TIF} / \tau_h = 91\%$ , which is in the range of the missing performance.

Summarising this study of integration effects in TI façades, significant performance lowering effects have been identified. It was shown that internal convection through the TI structure could reduce the thermal and solar performance significantly if an open horizontal TI structure is not tightly covered at least on one side. Hence it is crucial to address this point carefully in the system design. Accordingly direct air exchange between the "hot side" of a TI façade and the environment, e.g. through permeable joints between façade elements or leakage of the air gap between wall and TI component, could also reduce the performance considerably. A forced thermal stack effect is induced by the large temperature difference between gap and environment under irradiation. The thermal stack effect in the gap may be limited by horizontal air flow barriers, which shorten the height of the vertical "duct" between TI façade and underlying wall.

Shading effects by frame absorption of the beam-cone in beam-parallel structures are less severe, but still a transmittance reduction in the order of up to 10 % may occur depending on thickness, ratio between frame circumference and area, and frame absorptance. In any case "large" and square shaped areas are favourable. If a small area or a bad circumference-to-area ratio is unavoidable for constructional reasons, TI thickness and frame surface reflectance should be optimised in order to minimise the transmittance loss.

## 5.4 Thermal comfort, overheating

It is obvious that large TI areas have a big influence on the indoor climate in adjacent rooms. At this point just some remarks are made on the links between performance indicators of a TI façade and thermal comfort.

Due to their attenuated and time shifted heat dissipation solar walls are generally less critical with respect to comfort problems compared to glazing or light walls. Nevertheless, depending on climate conditions, orientation and thermal properties of the massive wall and shading options solar heat gain and thermal transmittance of the TI assembly have to be designed properly in order to prevent thermal discomfort such as large temperature

---

fluctuations and building up of unacceptable operative temperatures, which mainly occurs in transitional periods and in summertime.

Questions on thermal comfort are closely related to the whole solar wall as well as the building system including shading, ventilation, control strategies etc. Therefore comfort related performance assessment is useful only on the building level (IEA Task 27 project A1). Some results on comfort in TI buildings can be found e.g. in Maiwald, (2000).

With low or medium performing systems in buildings with reasonable thermal mass adjustable shading facilities can often be omitted. However, overheating protection will be unavoidable with large scale high performance TIF.

## 5.5 Durability

Durability aspects were not investigated within this project. Therefore just some general hints are given here.

On the materials level general knowledge on durability and degradation of polymeric materials is available. Some information on typical materials used for TI structures is available from IEA Task 18. Under the temperature, humidity and UV conditions present in typical TI façades reasonable service life should be reached with the polymeric materials used in recent products. More information on aging of polymeric glazing materials will be available from durability testing in subtask B of IEA Task 27 (case study B3, c.f. respective publications).

On the assembly level, settlement and deformation of polymeric TI structures have been identified earlier in laboratory experiments as potential problems (Simmler, 1997). Similar deformation effects have been observed in applications, so that TI structures had to be replaced after a rather short service life. A not perfectly solved problem is a durable planar join of the TI structure and either the outside glass pane or the inside glass or absorber surface. Both adhesive and mechanical fixing may reduce the solar performance and cause other problems. Dimensional stability problems may be avoided to a large extent if the TI structure is caught between two glass panes or integrated in a sealed glazing unit. This is however a performance lowering and costly alternative if daylight transmittance is not asked for.

In a non-sealed assembly penetration of dust, moisture or driving rain should be avoided as far as possible to prevent both moisture related aging and performance reduction due to dust accumulation. Yet it is often difficult to completely eliminate condensation on the inside of the outer cover glazing. Condensation is normally related with the day-night temperature cycle and frequently occurs due to radiant cooling under clear sky conditions at night. Up to now this seems to be rather an aesthetic than a degradation problem. It is also assumed that there is no strong impact of moisture on the energy efficiency of a TI façade, as no "one-way" heat pipe effect is apparent in these systems. However, these questions should be further investigated.

---

On building integration driving rain tightness as well as a low air permeability are the most important functions of a TI façade, similar to other façade constructions. It should be emphasized that these requirements are even more important in the case of a TI façade since they not only ensure the longevity of the building structure but also directly affect the energy performance of the building envelope.

## 5.6 Further aspects

There are further aspects which were not addressed in this project, i.e. mechanical stability, fire safety, and noise protection. At this point just some general remarks can be given.

The requirements for mechanical stability are similar to other façade constructions. Accordingly TI façades have to comply with the respective standards and / or regulations. As one of the major load factors wind driven forces have to be taken into account properly in the design of thickness and fixation of a covering glass pane as well as of the load-bearing frame system. As the specific weight of a TI construction is rather low compared to other types of façades, no particular problems should arise with the self-weight of a TI façade, provided the underlying masonry is not deteriorated as could occur with an old building under renovation.

The situation with fire safety is quite difficult, since many national regulations exist. For low-rise buildings no critical restrictions on materials exist for instance in Germany and Switzerland. In taller buildings more stringent requirements apply for materials as well as to limit spreading of fire and smoke in the building structure. One concern is fire propagation across several floors through a façade cladding containing air cavities and even combustible materials. In this case – which is not typical for TI application – separation of the air gaps between floors could possibly be upgraded to act as horizontal fire barriers in order to fulfil fire safety regulations.

Regarding noise protection standard measurement procedures similar to other wall construction can be applied. As TI façades by nature are light-weight constructions no substantial sound insulation capability is expected e.g. for single glazed systems without an extra absorber plate. That is, the sound insulation properties are mostly determined by the massive (masonry) wall. A more significant airborne sound reduction is achieved with multiple glazing and / or an integrated absorber plate.

## 6 Performance assessment recommendations

### 6.1 Solar / thermal performance

A minimal set of solar and thermal performance data must be determined and declared by manufacturers in order to properly calculate monthly or yearly solar heat gain and heat loss of a solar wall in a building performance calculation scheme i.e. as described in prEN ISO 13790. A more detailed performance evaluation guideline for a light wall as well as solar

wall (TI in front of an opaque wall) was developed by the German FVTWD (1999). In agreement with the performance indicators described before the following data is essential:

- Normal-hemispherical solar transmittance  $\tau_{t,n}$  or total solar energy transmittance  $g_{t,n}$  (if absorber integrated). The values may be calculated from spectral optical data.
- Hemispherical solar transmittance  $\tau_{t,h}$  or total solar energy transmittance  $g_{t,h}$  (if absorber integrated). These values may be calculated from directional-hemispherical data, also from spectral optical data for  $\tau_{e,h}$ .
- Thermal resistance of the TI component  $R_t$  including absorber (if integrated)
- For the evaluation of the total performance of the solar wall the following data shall be given by the system supplier:
- Mounting air gap resistance  $R_{al}$  (where applicable, e.g. with integrated absorber)
- Solar absorptance  $\alpha$  of the wall surface with the appropriate painting (without integrated absorber)
- Total U-value of the wall including frame and other thermal bridges
- Total area  $A$  and ratio of transparent to total area  $F_F$

## 6.2 Durability

The following recommendations on durability are based on problems observed in application. Respective testing may show weak-points of materials and / or system design and is intended as "initial type testing", that is not on the basis of a permanent production control.

On the materials level it is evident that expected thermal, hygric or UV stress in service should be taken into account with regard to degradation. Limitations shall be determined and declared by the respective material manufacturer.

To ensure long-term dimensional stability of the assembly and the TI structure in particular, behaviour under cyclic solar and thermal load shall be performed to check for settlement or other kinds of deformation of the TI structure such as bending, as well as proper fixation to at least one covering layer. Possible tests are shown by Simmler (1997). Since system layouts widely vary, no fixed assessment procedure can be given, but tests and monitored properties should be tailored to the system under assessment.

In addition more standardized façade testing is suggested. Among the most important tests are driving rain tightness and air permeability of the TI system.

## 7 References

D. van Dijk, *Matrix of products and thermal and solar properties*, Working Document, IEA/SHC Task 27 (2001)

EN 673 Glass in building - Determination of the thermal transmittance (U-value) - Calculation method (1997)

EN ISO 6946, Building components and building elements – Thermal resistance and thermal transmittance – Calculation method (1996)

Th. Frank, K. Mathis, J. Heierli, Benutzerhandbuch HELIOS - PC (Version 1.0), EMPA Bauphysik, CH-Dübendorf (1992)

FVTWD (Fachverband TWD), *Bestimmung des solaren Energiegewinns durch Massivwände mit transparenter Wärmedämmung* (Guideline in German), author W.J. Platzer, D-Gundelfingen (2000), see also [www.fvtwd.de](http://www.fvtwd.de)

Kerschberger, W. Platzer, B. Weidlich, *Transparente Wärmedämmung*, Bauverlag Wiesbaden+Berlin, ISBN 3-7625-3444-6 (1997)

R. Maiwald, Die transparente Wärmedämmung im Spannungsfeld Komfort-Energie und Leistungstest an einer transparenten Wärmedämmung, Dissertation Universität Karlsruhe, D-Karlsruhe (2000)

M. Ochs, A. Haller, H. Simmler, *A simple method to calculate the heat gains of solar wall heating with TI*, Proceedings EuroSun 2000, 3rd ISES-Europe Solar Congress, DK-Copenhagen (2000)

W.J. Platzer, Solare Transmission und Wärmetransportmechanismen bei transparenten Wärmedämmmaterialien, Dissertation Albert-Ludwigs-Universität, D-Freiburg (1988)

W.J. Platzer, *Energetische Bewertung von Transparenter Wärmedämmung*, Bauphysik, Band 21 Heft 2, pp. 67-76 (1999)

W.J. Platzer, *The ALTSET Project: Angular Properties of Complex Glazings Through Solar Calorimetry*, Proceedings EuroSun 2000, 3rd ISES-Europe Solar Congress, DK-Copenhagen (2000)

W.J. Platzer, Building Performance Indicators for a Energy Performance Assessment Methodology, Working Document, IEA/SHC Task 27, and General Energy Performance Assessment Methodology, Draft Report, IEA/SHC Task 27 (2001)

prEN ISO 13790, Thermal performance of buildings - Calculation of energy use for space heating (2003)

H. Simmler, Hygro-thermal properties of a TIM façade element under laboratory conditions, Final project report EMPA, IEA/SHC Task 18 (1997)

H. Simmler, Progress reports on TI façade investigation: r-a3(3)-ch-2.pdf, r-a3(3)-ch-3.pdf, r-a3(3)-EMPA-HS-4.pdf, r-a3(3)-EMPA-HS-5.pdf, IEA/SHC Task 27 (2001-2003)

## Case Study 4: Daylighting elements

### From optical performances characterization of a redirecting daylight material to daylighting simulations

Prepared by:

Richard Mitanchey

l'École des Travaux Publics de l'Etat, ENTPE, France

#### 1 Optical performance characterization: principle of virtual goniophotometry

Efforts were made to characterize the optical performances of daylighting components in order to perform daylighting component performance analysis as well as daylighting simulation using usual daylighting software. Usual optical performance characterization involves experimental goniophotometry with the measurement of bi-directional distribution functions of reflectance and transmittance.

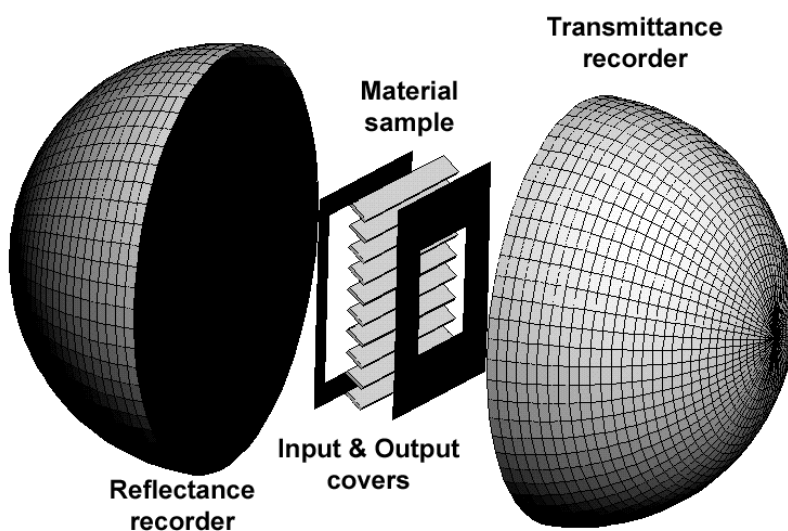


Fig. 4-1: Virtual goniophotometer components

Our aim was to characterize the response of the daylighting component to a given illumination condition also including outdoor conditions (ground, site surroundings like buildings and or vegetation) (Fig. 2). From indoor point of view, such a response of the

system to outdoor illumination can be seen as a new source-like equivalent illumination condition at the interface between indoor and outdoor.

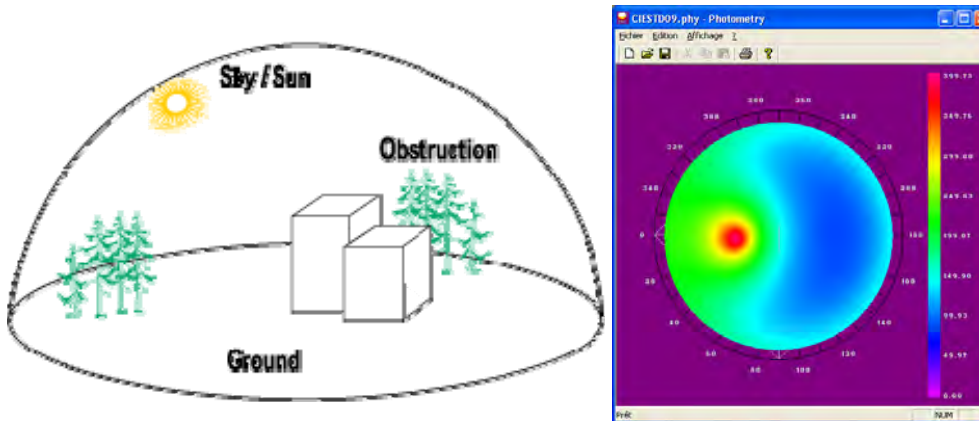


Fig. 4-2: Outdoor components of equivalent light source input (left), and visualization of CIE Standard sky N° 09 (right).

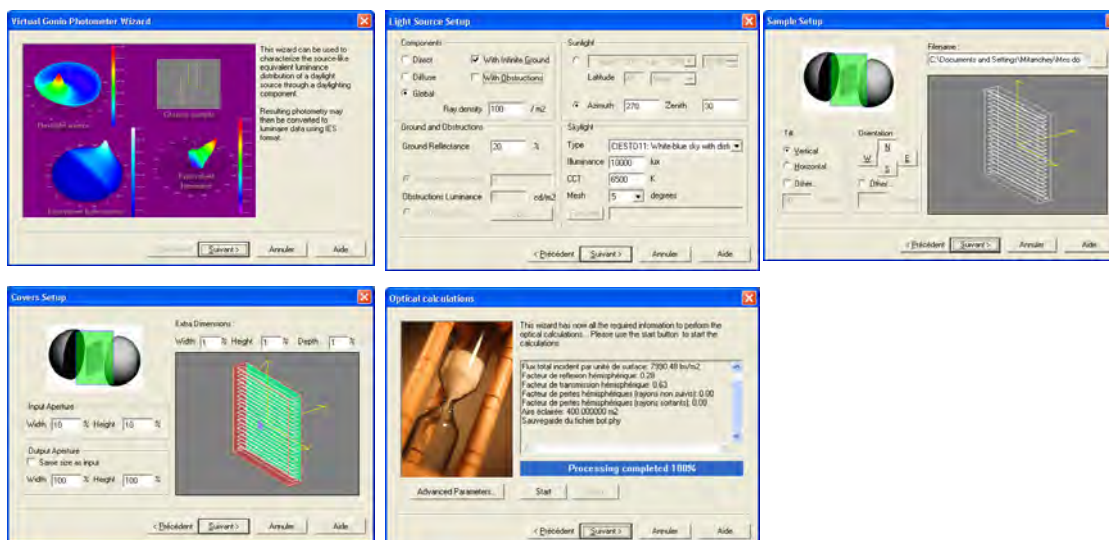


Fig. 4-3: Wizard panels of the virtual goniophotometer ray-tracing software. Panels include (from left to right, and top to bottom) a) introduction, b) light source description, c) sample description, d) apertures description and e) final calculations

This can be described by mean of virtual goniophotometry ray-tracing software (Fig. 1), were the geometry of system is described by mean of CAD input, and the photometry by reference of either materials library or physical laws implementation. In order to avoid boundary effects, input and output covers might be necessary to restrict the illuminated area of the system. Optical rays are generated from outdoor illumination source (either direct or indirect) to the system, and collected over two perfect absorbers, one for reflection and one for transmission, and recording each impact. Depending on the

continuity property, raw-collected data may then be interpolated or not, and described using IEA SHC Task 21 Raw data format for bi-directional quantities.

According to this principle, software components have been developed, and assembled together into a virtual goniophotometry application software. Input data and parameters are prepared by mean of a wizard including outdoor description, sample and covers description, recorders, and finally simulation control (Fig. 3).

## 2 Redirecting daylight material description

Because it offers at the same time view through the window, and ceiling illumination by sky (Fig. 4), the interesting Serraglaze product has been chosen as the redirecting daylight material sample. A Serraglaze (SG) window is typically a mosaic made of 2 x 2 x 250 mm square SG panel array glazed between two panes of 3 mm glass.



Fig. 4-4: Operating principle of the Serraglaze product (left), and view through the window (right).

The SG panel edges are cut clean and square and butted together (Fig. 5), and the autoclave lamination process is using PU laminating film.

The profile of the Serraglaze product has been modelled using CAD software, as an input to virtual goniophotometer raytracing software. In order to avoid boundary effects, several SG edges (a total of 20) have been described within the model (Fig. 6).

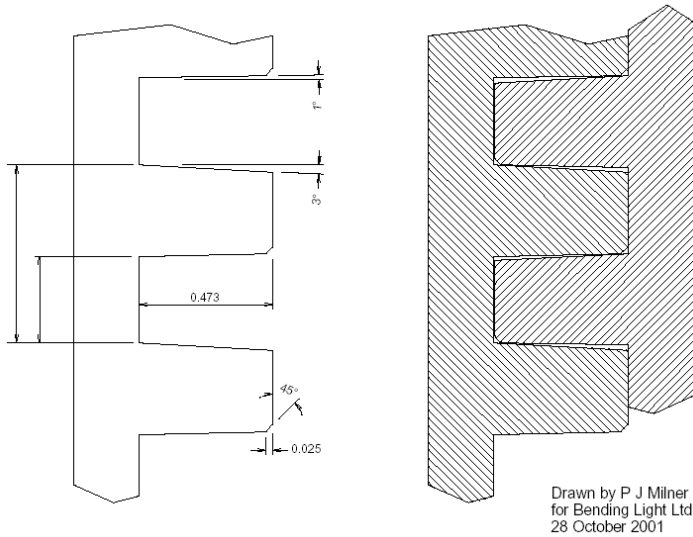


Fig.: 4-5: Profile and assembly principle of the Serraglaze product

### 3 Characterization results: light source equivalent distributions

The Serraglaze product has been tested in virtual goniophotometry, and compared with simple glazing as reference case (Fig. 6). The configuration was using a vertical sample, with no ground and no outdoor obstruction. Several illumination conditions have been tested, with one case for each CIE Standard Sky, thus leading to a total of 15 skies.

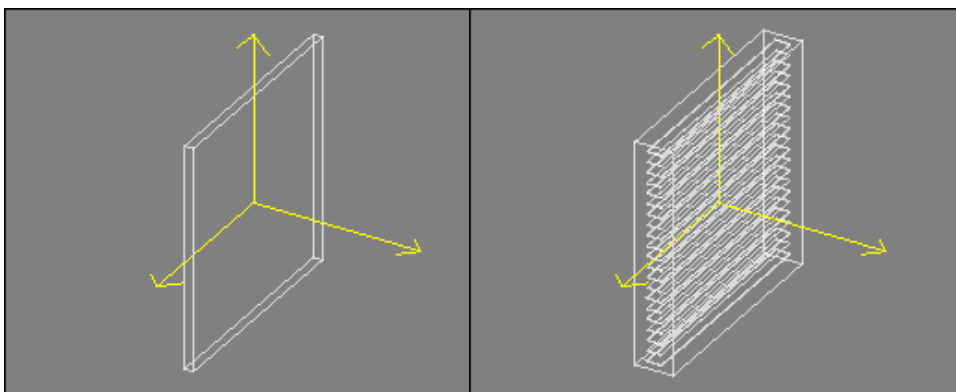


Fig. 4-6: Sample geometrical description (CAD input), with simple glazing reference case (left) and Serraglaze (right).

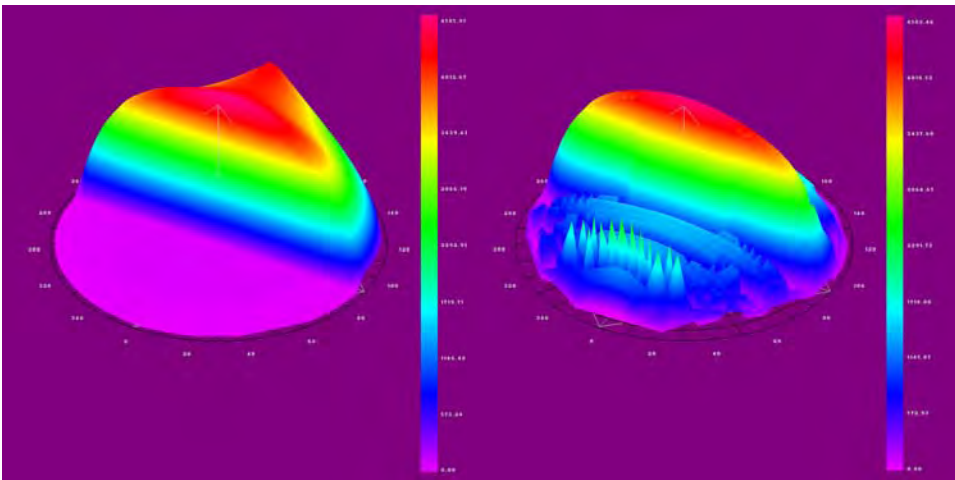


Fig. 4- 7: Light source equivalent distribution of intensities of simple glazing (left) and Serraglaze (right) under CIE Standard Sky N° 09 illumination.

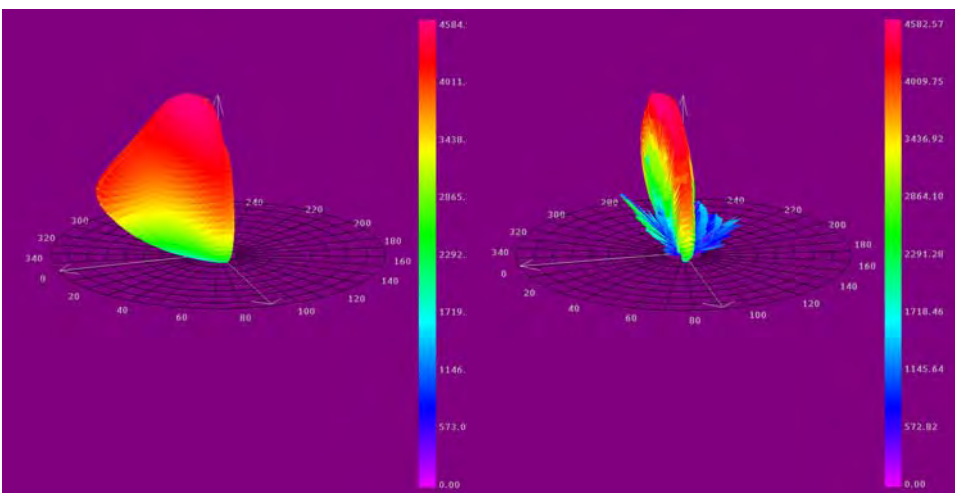


Fig.4- 8: Luminaire equivalent IES distribution of intensities of simple glazing (left) and Serraglaze (right) under CIE Standard Sky N° 09 illumination.

Characterization results were expressed as photometries using bi-directional raw format data of IEA SHC Task 21 (Fig. 7), and also expressed as luminaire data using standard IES format (Fig. 8). Visualization and other Input/Output software may be obtained from IEA SHC Task 27.

From Fig. 7 & 8 analysis, it is obvious that the Serraglaze product redirects the light coming from zenith parts of the sky toward the ceiling, while the light coming from the horizon part of the sky remains globally unchanged.

## 4 Daylighting simulations

In order to use virtual goniophotometry results as input to daylighting simulation, an office test room has been proposed (Fig. 9), with two occupants within the room, and variable length. The window system is an assembly of two tiltable parts, with lower part consisting of simple glazing, while upper part consists of either simple glazing (left pictures) or Serraglaze (right pictures).

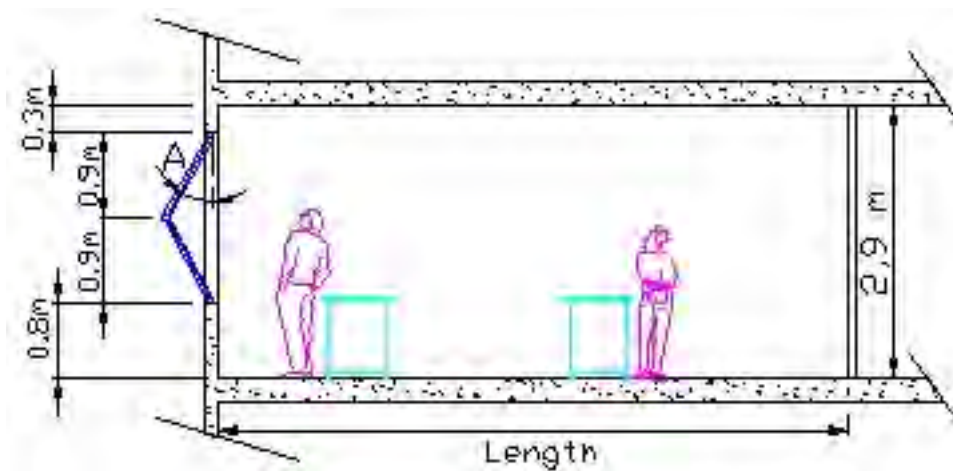


Fig. 4-9: Geometry of the test room

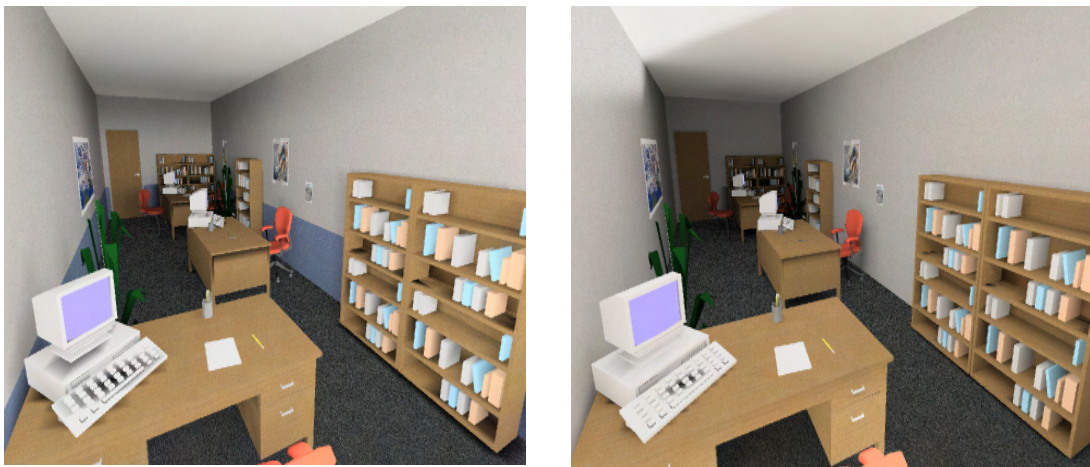


Fig. 4-10: Daylighting simulation of simple glazing (left) and Serraglaze (right) – Views from the window



Fig. 11: Daylighting simulation of simple glazing (left) and Serraglaze (right) – Opposite views.

Lightscape simulation software was also adapted in order to consider input from virtual goniophotometry. Several parameters were checked, either depending on outdoor illumination and conditions (15 CIE Standard Skies, ground or not, obstructions or not), or depending on the room itself (Length, and inclination of the tiltable panels). The pictures below (Fig. 10 & 11) show only a very small part of such results, were for example illuminance levels deep inside the room are increased by a factor of almost 3 (Fig. 12).

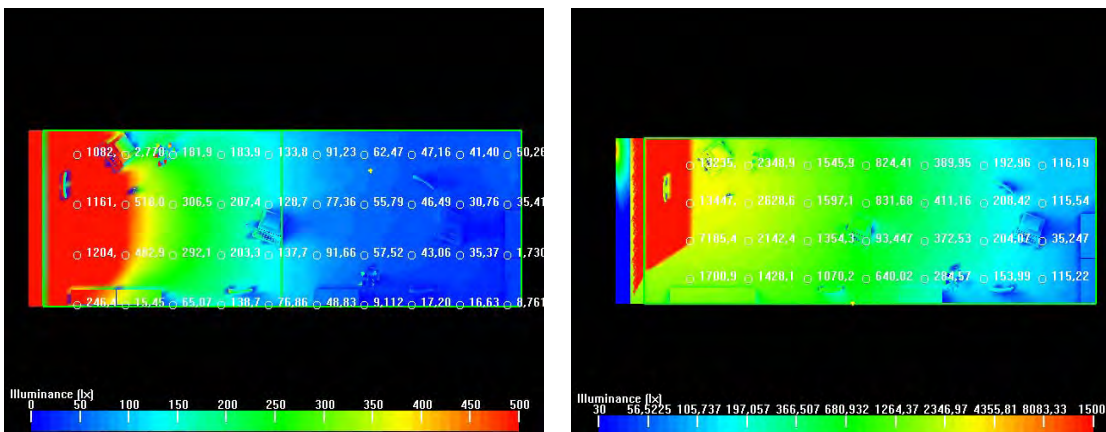


Fig. 4-12: Daylighting simulation of simple glazing (left) and Serraglaze (right) – Illuminance levels

## 5 Real case study setup : daylighting within the Twincells

In order to validate simulation results, a real case study has just started, and based on full 1:1 scale experiment within the TwinCells (IEA SHC Task 21), where the left room is equipped with tiltable Serraglaze product, and compared with the right reference room (Fig. 13).



Fig. 4-13: Real 1:1 scale experiment within the TwinCells (right). Left Room is equipped with tiltable Serraglaze window (left).

Observed quantities include outdoor and indoor luminances and illuminances, with input from calibrated digital photography and cells measuring illuminance levels. Luminance field of view study should also lead to glare parameters analysis.

Unfortunately, due to the early stage of the experimental setup, no results are yet available. However, in order to compare simulation with experimental results, we also now need to change the geometry of the test room to the geometry of the TwinCells.

## 6 Conclusion

It is now possible to characterize and analyse the daylighting performance of daylighting components, either in situation with adapted daylighting simulation, or globally, by mean of source-like equivalent distribution that can be obtained by mean of virtual goniophotometry. However, such an approach and associated software components and applications still need to be validated by mean of real full-scale experiments. On the other hand, it is clear that experimentally measured photometries have also a big role to play within the virtual goniophotometry approach, were the system response needs to be characterized prior any daylighting simulation. This would also be the challenge of future works.

## Case study 5: Window – Wall/Roof Assembly

Prepared by:

Toke Rammer Nielsen

Technical University of Denmark, Department of Civil Engineering

The following participants have been involved in the work presented in this report: Technical University of Denmark, University of Massachusetts, National Research Council of Canada, Fraunhofer Institute for Solar Energy Systems, Velux, VTT Building and Transport, Netherlands Organisation for Applied Scientific Research, Eidgenössische Materialprüfungs- und Forschungsanstalt and Institut für Fenstertechnik.

### 1 Introduction

In this study, effects of building integration on the thermal and total solar energy transmittance of windows are investigated. Methods for characterizing the assembly of typical window products and typical wall/roof constructions will be evaluated and tested by comparative calculations on reference cases.

The thermal transmittance of the complete window-wall/roof assembly can be characterized by 1-dimensional heat transfer coefficients and linear thermal transmittance values arising from the assembly. The heat transfer coefficients and linear thermal transmittances can be evaluated based on calculations with detailed 2-dimensional calculation tools and the calculated values can be checked by hot box measurements. This work presents existing methods to characterize the impact of the assembly on the heat loss and proposes a new method that simplifies the characterization. The impact of the assembly is shown for a number of typical window-wall/roof assemblies used in the participating countries.

The total solar energy transmittance (the g-value) of a window is a function of the solar incidence angle and shading effects from the surrounding environment. Shades may have significant influence on the resulting g-value. Shades arising from the integration of a window in a wall construction can be characterized and included in the resulting g-value of the window/wall assembly. The resulting g-value can in many cases be found from calculations and to some extent checked by calorimetric measurements. This work presents a method that characterizes the effect of the assembly on the total solar energy transmittance of the window.

## 2 Thermal transmittance for window - wall/roof assembly

The linear thermal loss that is introduced by the window - wall/roof assembly is mainly due to the two-dimensional heat transfer that occurs when a slim window is attached to a thick wall construction. The linear loss depends partly on the thermal break at the window rebate and partly on the window design – especially the location of the glazing with respect to the insulation in the window rebate. A location straight in front of the insulation is advantageous from a thermal point of view whereas a dislocation to one or the other side results in an increased geometrical thermal bridge and an increased linear thermal loss.

### 2.1 Characterization according to standards

Calculation of the thermal transmittance of the frame and the linear thermal transmittance in the frame-glazing assembly are described in prEN ISO 10077-2. The thermal transmittance of the frame is calculated in a situation where the glazing is replaced by an insulating panel.

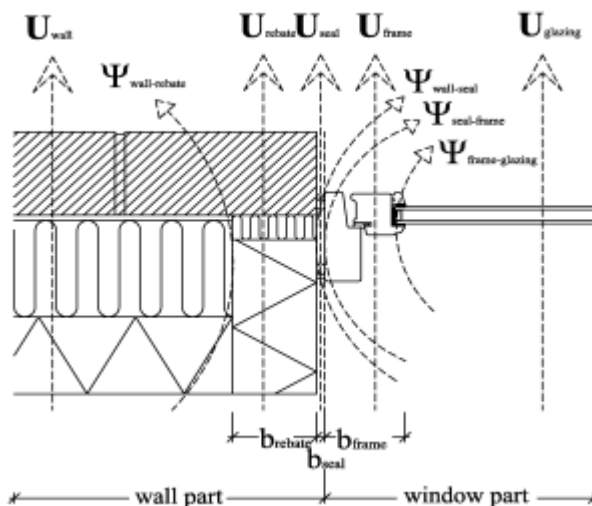


Fig. 5-1: Heat transfer coefficients and linear thermal transmittances for window-wall assemblies.

Calculation of linear thermal transmittances in general building constructions is described in prEN ISO 10211-2 where a linear thermal bridge is defined as a "Thermal bridge with a uniform cross-section along one of the three orthogonal axes". If this is taken literally a division of the window-wall assembly as shown in Fig. 5- 1 applies and a linear thermal transmittance must be calculated for all the connections: wall/rebate, rebate/seal, seal/frame and frame/glazing and U-values must be found for the wall, rebate, seal, frame

and window. But some window-wall assemblies e.g. as shown in Fig. 5- 2 are more complex and the definition of linear thermal bridges as given in prEN 10211-2 does not apply to such cases.

## 2.2 The expanded linear thermal transmittance

The ideal situation (at least from a thermal point of view) is an assembly of the glazing and the wall/roof (without the rebate and frame) through which only one-dimensional heat transfer occurs. In the real world two-dimensional heat transfer occurs in the assembly leading to an increased heat loss. The extra heat loss that arises from a real world assembly between the glazing and the wall/roof can be characterized by an expanded linear thermal transmittance denoted  $L$  that includes all the extra thermal losses arising from the rebate, the sealant between frame and wall, the window frame and the joints between the different elements as illustrated in Fig. 5- 3.

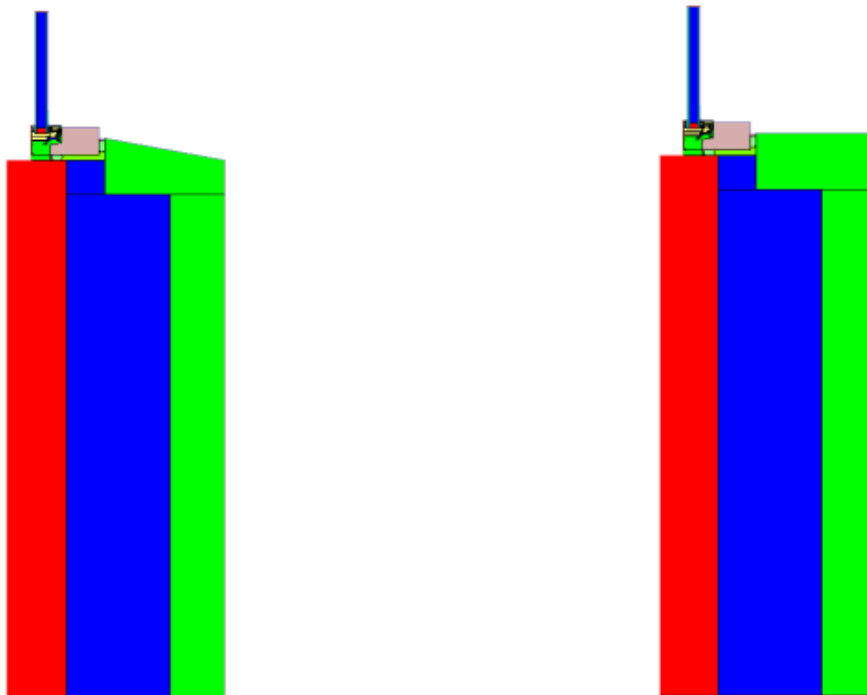


Fig. 5-2: Cases where linear thermal bridges in window/wall assembly are difficult to define in accordance with prEN ISO 10211-2.

The expanded linear thermal transmittance includes contributions from the four linear thermal transmittances occurring at the rebate ( $\Psi_{\text{wall-rebate}}$ ), at the windows assembly with the wall/roof ( $\Psi_{\text{wall-seal}}$  and  $\Psi_{\text{seal-frame}}$ ) and at the frame/glazing assembly ( $\Psi_{\text{frame-glazing}}$ ) and

the one-dimensional thermal transmittances of the rebate, the sealing and the frame shown in Fig. 5- 1.

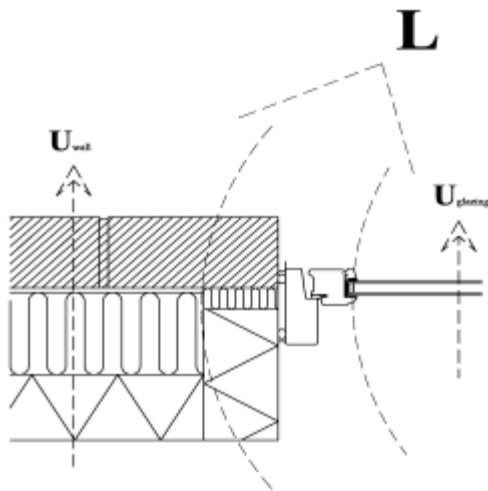


Fig. 5-3: The expanded linear thermal transmittance.

Calculating the linear thermal transmittances and one-dimensional thermal transmittances of the window-wall assembly shown in Fig. 5- 1 includes a large number of calculation steps.

The expanded linear thermal transmittance can be calculated in three steps:

Calculate the total two-dimensional heat transfer,  $\Phi_{2\text{-dim}}$ , through the assembly plus 0.2 m of the glazing and minimum 1.0 m of the wall and sealing construction. See Fig. 5- 4

Subtract the corresponding one-dimensional heat flows,  $\Phi_{1\text{-dim}}$ , through the wall construction (without the rebate) and the glazing calculated with the dimensions indicated in Fig. 5- 5.

Divide the result by the difference between inside and outside temperatures ( $\theta_i - \theta_o$ ).

The expression has the following form:

$$L = \frac{\Phi_{2\text{-dim}} - \Phi_{1\text{-dim}}}{\theta_i - \theta_o} \quad (1)$$

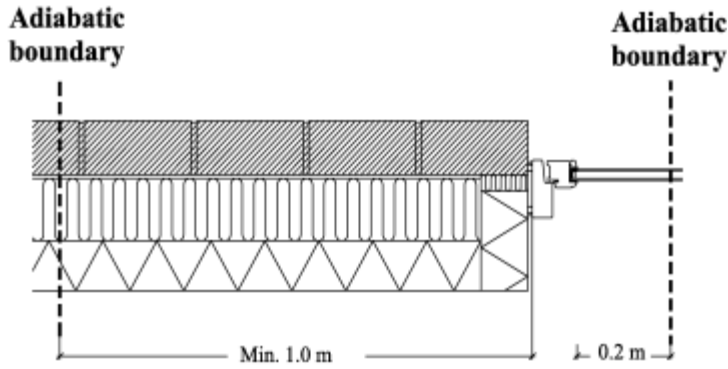


Fig. 5- 4. Calculation of two-dimensional heat flows,  $\Phi_{2\text{-dim}}$ , through wall and glazing.

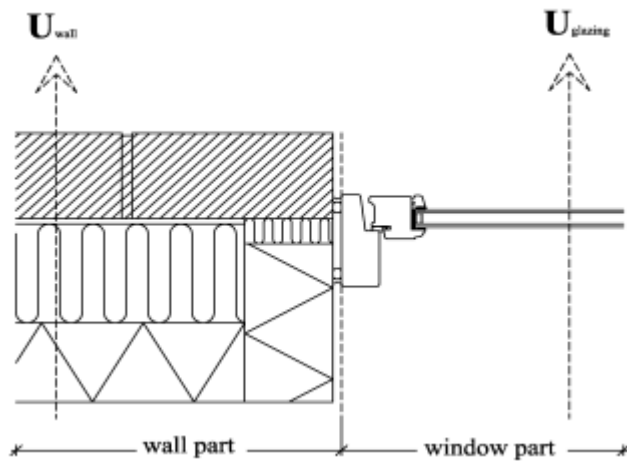


Fig. 5- 5: Calculation of one-dimensional heat flows,  $\Phi_{1\text{-dim}}$ , through wall and glazing.

where the one-dimensional heat flows are calculated from:

$$\Phi_{1\text{-dim}} = (U_{\text{wall}} \cdot b_{\text{wallpart}} + U_{\text{glazing}} \cdot b_{\text{windowpart}})(\theta_i - \theta_o) \quad (2)$$

In terms of the one-dimensional thermal transmittances and linear thermal transmittances shown in Fig. 5- 27 the expanded linear thermal transmittance, L, can be expressed as:

$$L = b_{\text{rebate}}(U_{\text{rebate}} - U_{\text{wall}}) + \Psi_{\text{wall-rebate}} + b_{\text{seal}}(U_{\text{seal}} - U_{\text{wall}}) + \Psi_{\text{wall-seal}} + \Psi_{\text{seal-frame}} + b_{\text{frame}}(U_{\text{frame}} - U_{\text{glazing}}) + \Psi_{\text{frame-glazing}} \quad (3)$$

## 2.3 Thermal transmittance case study

The purpose of this case study is to compare calculations of linear thermal transmittances according to the procedures described in the existing standards and the expanded linear thermal transmittance for a reference window-wall assembly and to show that different institutes can arrive at the same results.

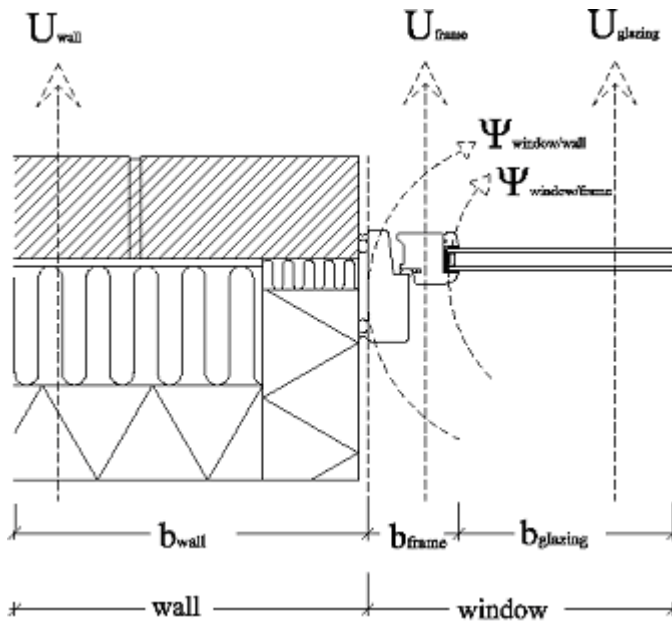


Fig. 5-6: Division of wall/window-assembly used in the case study.

In this case study the division of the window-wall assembly is simplified compared to the division shown in Fig. 5- 1. Only one linear thermal transmittance is used to describe the window-wall assembly and the window-wall assembly is divided as shown in Fig. 5- 6. Therefore, the linear thermal transmittance  $\Psi_{\text{window/wall}}$  include all the thermal effects of the rebate and the wall/rebate, the rebate/seal and the seal/frame assemblies.

The total heat loss,  $\Phi_{2\text{-dim}}$ , through the window and the wall shown in Fig. 5- 6 may be expressed by:

$$\Phi_{2\text{-dim}} = (U_{\text{wall}} \cdot b_{\text{wall}} + \Psi_{\text{window/wall}} + U_{\text{frame}} \cdot b_{\text{frame}} + \Psi_{\text{window/frame}} + U_{\text{glazing}} \cdot b_{\text{glazing}}) \cdot d \cdot \Delta T \quad (4)$$

or

$$\Phi_{2\text{-dim}} = (U_{\text{wall}} \cdot b_{\text{wall}} + U_{\text{glazing}} \cdot (b_{\text{glazing}} + b_{\text{frame}}) + L) \cdot d \cdot \Delta T \quad (5)$$

To calculate the linear thermal transmittances and the expanded linear thermal transmittance a two-dimensional simulation tool is used to find the following heat flows:

$\Phi_{2\text{-dim}}$  two dimensional heat loss of window and wall (prEN ISO 10211-2) [W]

$\Phi_{\text{frame+panel}}$  two dimensional heat loss of frame with insulation panel  
(prEN ISO 10077-2)[W]

$\Phi_{\text{frame+glazing}}$  two dimensional heat loss of frame with glazing (prEN ISO 10077-2) [W]

The following values must also be known:

$U_{\text{panel}}$  1-dim. U-value of panel [W/m<sup>2</sup>K]

$U_{\text{glazing}}$  Center U-value of glazing [W/m<sup>2</sup>K]

$U_{\text{wall}}$  1-dim. U-value of wall [W/m<sup>2</sup>K]

$b_{\text{wall}}$  Length of wall section including rebate and sealing [m]

$b_{\text{frame}}$  Length of frame section [m]

$b_{\text{glazing}}$  Length of glazing section [m]

$d$  Length in 3. dimension (perpendicular to the paper plane) Normally 1m. [m]

$\Delta T$  Temperature difference [K]

The desired values can be calculated using the following formulae:

$$U_{\text{frame}} = \frac{\frac{\Phi_{\text{frame+panel}}}{d \cdot \Delta T} - U_{\text{panel}} \cdot b_{\text{glazing}}}{b_{\text{frame}}} \quad (6)$$

$$\Psi_{\text{frame/glazing}} = \frac{\Phi_{\text{frame+glazing}}}{\Delta T \cdot d} - U_{\text{frame}} \cdot b_{\text{frame}} - U_{\text{glazing}} \cdot b_{\text{glazing}} \quad (7)$$

$$\Psi_{\text{window/wall}} = \frac{\Phi_{2\text{-dim}}}{\Delta T \cdot d} - U_{\text{wall}} \cdot b_{\text{wall}} - U_{\text{frame}} \cdot b_{\text{frame}} - U_{\text{glazing}} \cdot b_{\text{glazing}} - \Psi_{\text{frame/glazing}} \quad (8)$$

$$L = \frac{\Phi_{2\text{-dim}}}{d \cdot \Delta T} - U_{\text{glazing}} \cdot (b_{\text{frame}} + b_{\text{glazing}}) - U_{\text{wall}} \cdot b_{\text{wall}} \quad (9)$$

### 2.3.1 Geometry and thermal properties of the reference window-wall assembly

The reference window-wall assembly is typical for Danish conditions. The window is made of a low-e glazing mounted in wooden frame. The wall construction is from the outside made of brick, insulation and lightweight concrete. In the window rebate the thickness of the lightweight concrete is increased so the window can be fastened and sealed. To avoid a large linear thermal loss in the rebate, 32mm of insulation is inserted between the brick and the lightweight concrete. The window geometry is shown in Fig 7. The thermal properties and the geometry of the window-wall assembly are shown in Fig. 5- 8 and the thermal properties of the window are given in Fig. 5- 9.

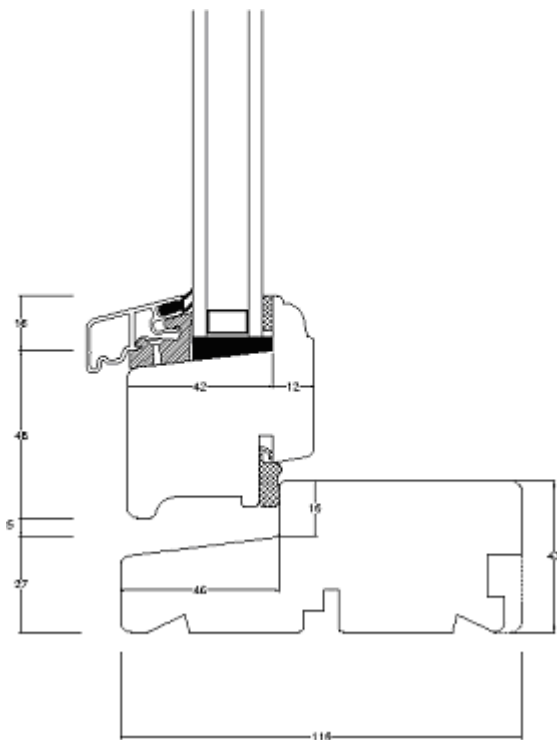


Fig. 5-7: Geometry of window (not in scale).

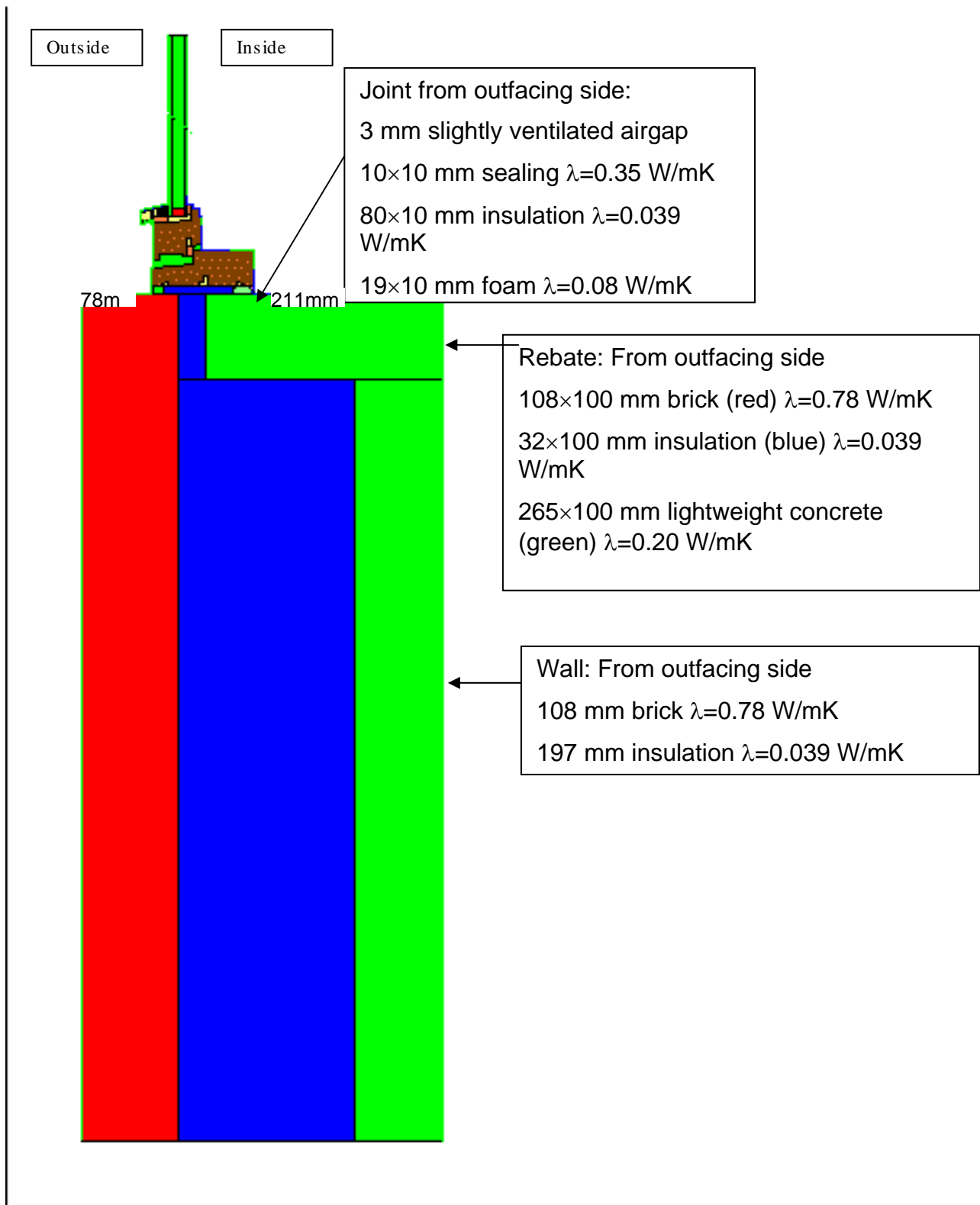


Fig. 5- 8: Thermal properties of window mounted on wall (not in scale).

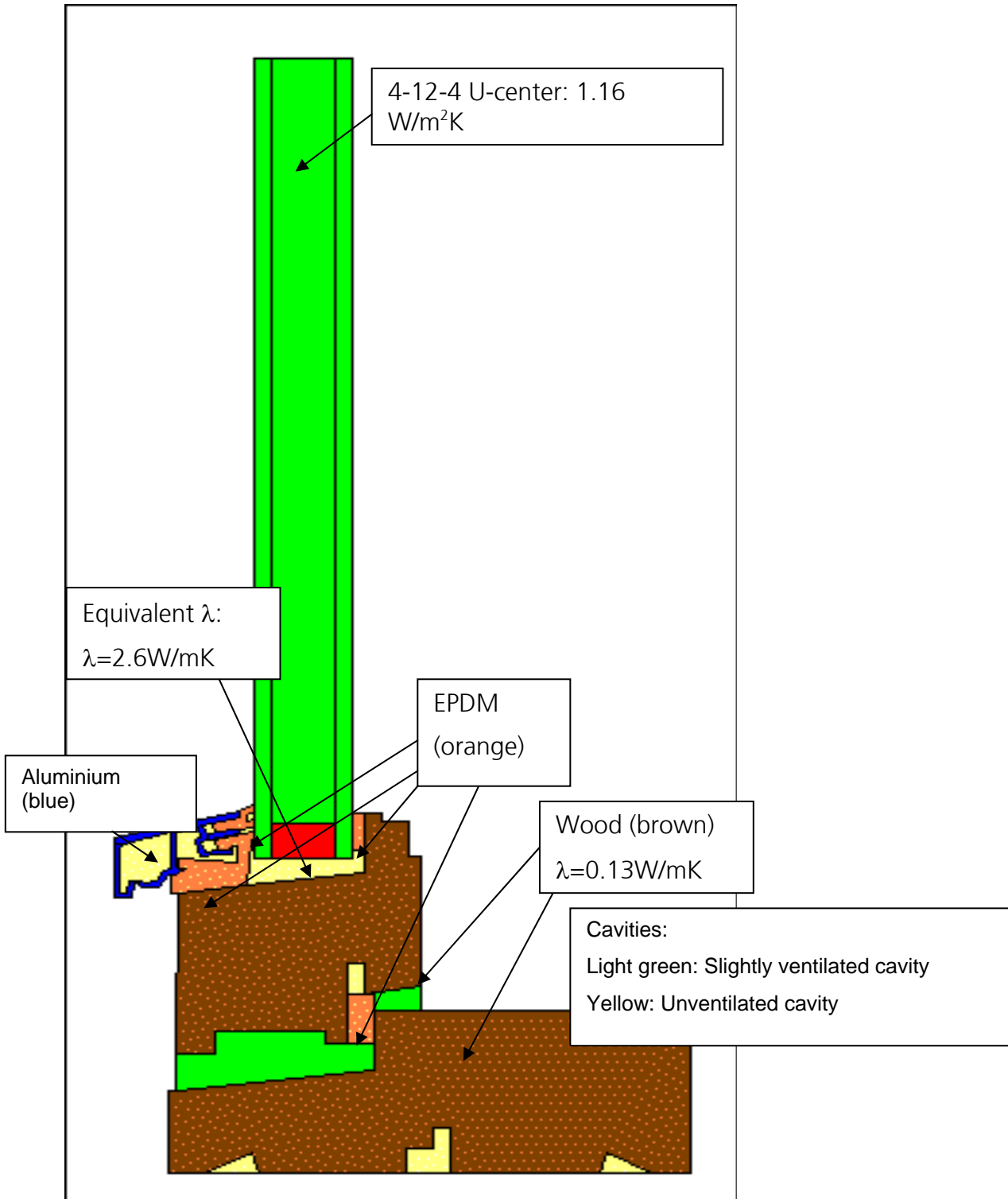


Fig. 5-9: Thermal properties of window (not in scale).

### 2.3.2 Results

In Table 1 the results reported by the different participants are given. An unclarity in the case study description led to calculations with two different air gap thicknesses in the glazing. The results derived from the detailed two-dimensional calculations are the thermal transmittance of the frame,  $U_{\text{frame}}$ , the linear thermal transmittance in the assembly between the frame and the glazing,  $\Psi_{\text{frame/glazing}}$ , the linear thermal transmittance between the window and wall,  $\Psi_{\text{window/wall}}$ , and the extended linear thermal transmittance,  $L$ .

Table 5-1: Results from case study.

| Air gap thickness                                      | 14mm   | 14mm   | 14mm   | 12mm   | 12mm    | 12mm   |
|--|--------|--------|--------|--------|---------|--------|
| Institute  | TNO    | FRG    | DTU    | DTU    | EMPA    | VELUX  |
| Calculation program                                    | Trisco | Therm  | Therm  | Therm  | Bisco   | WinIso |
| $b_{\text{wall}}$ [m]                                  | 1.010  | 1.000  | 1.010  | 1.010  | 1.0066  | 1.01   |
| $b_{\text{frame}}$ [m]                                 | 0.096  | 0.095  | 0.0953 | 0.0953 | 0.096   | 0.095  |
| $b_{\text{glazing}}$ [m]                               | 0.2    | 0.2    | 0.2    | 0.2    | 0.2012  | 0.2    |
| $d$ (normally 1m) [m]                                  | 1      | 1      | 1      | 1      | 1       | 1      |
| $\Phi_{2\text{-dim}}$ [W]                              | 14.15  | 14.156 | 14.138 | 14.138 | 14.0175 | 13.959 |
| $\Phi_{\text{frame+panel}}$ [W]                        | 8.10   | 7.629  | 7.980  | 8.394  | 8.4789  | 8.410  |
| $\Phi_{\text{frame+glazing}}$ [W]                      | 9.42   | 9.284  | 9.440  | 9.446  | 9.2932  | 9.398  |
| $U_{\text{panel}}$ [ $\text{W}/\text{m}^2\text{K}$ ]   | 1.252  | 1.195  | 1.2522 | 1.3487 | 1.3487  | 1.349  |
| $U_{\text{glazing}}$ [ $\text{W}/\text{m}^2\text{K}$ ] | 1.160  | 1.162  | 1.1615 | 1.1577 | 1.16    | 1.160  |
| $U_{\text{wall}}$ [ $\text{W}/\text{m}^2\text{K}$ ]    | 0.1707 | 0.171  | 0.1707 | 0.1707 | 0.1707  | 0.171  |
| $\Delta T$ [K]   | 20     | 20     | 20     | 20     | 20      | 20     |
| $U_{\text{frame}}$ [ $\text{W}/\text{m}^2\text{K}$ ]   | 1.6104 | 1.494  | 1.5587 | 1.5734 | 1.5894  | 1.586  |
| $\Psi_{\text{frame/glazing}}$ [ $\text{W}/\text{mK}$ ] | 0.0844 | 0.089  | 0.0911 | 0.0908 | 0.0787  | 0.0872 |
| $\Psi_{\text{window/wall}}$ [ $\text{W}/\text{mK}$ ]   | 0.0641 | 0.073  | 0.0625 | 0.0622 | 0.0642  | 0.0554 |
| $L$ [ $\text{W}/\text{mK}$ ]                           | 0.1917 | 0.194  | 0.1915 | 0.1926 | 0.185   | 0.1830 |

The specific heat loss through the window and assembly is calculated for two window sizes based on the calculated values for the thermal transmittance of the frame,  $U_{\text{frame}}$ , the linear thermal transmittance in the assembly between the frame and the glazing,  $\Psi_{\text{frame/glazing}}$ , the linear thermal transmittance between the window and wall,  $\Psi_{\text{window/wall}}$ , and the extended linear thermal transmittance,  $L$ . The heat loss  $Q_1$  is calculated using the standard method and the heat loss  $Q_2$  is calculated using the extended linear thermal transmittance.

$$Q_1 = \Psi_{\text{window/wall}} \cdot l_{\text{window/wall}} + U_{\text{frame}} \cdot A_{\text{frame}} + \Psi_{\text{window/frame}} \cdot l_{\text{frame/glazing}} + U_{\text{glazing}} \cdot A_{\text{glazing}} \quad (10)$$

or

$$Q_2 = U_{\text{glazing}} \cdot (A_{\text{glazing}} + A_{\text{frame}}) + L \cdot l_{\text{window/wall}} \quad (11)$$

with

$$A_{\text{glazing}} = (h - 2 \cdot b_{\text{frame}})(w - 2 \cdot b_{\text{frame}})$$

$$A_{\text{frame}} = h \cdot w - A_{\text{glazing}}$$

$$l_{\text{window/wall}} = 2 \cdot (h + w)$$

$$l_{\text{frame/glazing}} = 2 \cdot (h - 2 \cdot b_{\text{frame}} + w - 2 \cdot b_{\text{frame}})$$

h Height of window [m]

w Width of window [m]

The results are shown in Table 5-2 and Table 5-3. It is seen that the specific heat losses are very similar even though the derived values for the thermal transmittance of the frame,  $U_{\text{frame}}$ , the linear thermal transmittance in the assembly between the frame and the glazing,  $\Psi_{\text{frame/glazing}}$ , the linear thermal transmittance between the window and wall,  $\Psi_{\text{window/wall}}$ , and the extended linear thermal transmittance,  $L$ , differ in the calculations from the different institutes. The specific heat losses calculated using the extended linear thermal transmittance is slightly larger than the values calculated using the standard method. This is a result of the fact that the perimeter of the window-wall assembly,  $l_{\text{window/wall}}$ , is slightly larger than the perimeter of the glazing,  $l_{\text{frame/glazing}}$ . Both the standard method and the method using the extended linear thermal transmittance are simplified methods that does not consider the 3-dimensional effects in the corners.

Table 5-2: Heat loss through window and assembly for two window sizes using standard method.

| Standard  | TNO  | FRG  | DTU  | DTU  | EMPA | VELUX |
|---|------|------|------|------|------|-------|
| $Q_1$ ( $h \times w = 1.23 \times 1.48$ ) [W/K] | 3.07 | 3.08 | 3.07 | 3.07 | 3.03 | 3.02  |
| $Q_1$ ( $h \times w = 1.80 \times 1.85$ ) [W/K] | 5.18 | 5.20 | 5.18 | 5.18 | 5.13 | 5.12  |

Table 5-3: Heat loss through window and assembly for two window sizes using the extended linear thermal transmittance.

| Extended linear thermal transmittance           | TNO  | FRG  | DTU  | DTU  | EMPA | VELUX |
|---|------|------|------|------|------|-------|
| $Q_2$ ( $h \times w = 1.23 \times 1.48$ ) [W/K] | 3.15 | 3.16 | 3.15 | 3.16 | 3.11 | 3.10  |
| $Q_2$ ( $h \times w = 1.80 \times 1.85$ ) [W/K] | 5.26 | 5.28 | 5.26 | 5.27 | 5.21 | 5.20  |



|   |                    |         |        |        |
|---|--------------------|---------|--------|--------|
| Wall segment width                        | m                  | b_wal   | 1.000  | 1.000  |
| Frame segment width                       | m                  | b_frame | 0.134  | 0.134  |
| Glazing segment width                     | m                  | b_glaz  | 0.489  | 0.489  |
| U-value wall (1D)                         | W/m <sup>2</sup> K | U_wall  | 0.2887 | 0.183  |
| U-value glazing (1D)                      | W/m <sup>2</sup> K | U_glaz  | 1.2068 | 1.2068 |
| U-value insulation replacing glazing (1D) | W/m <sup>2</sup> K | U_panel | 1.211  | 1.211  |

Three numerical calculations are needed to obtain the full breakdown into components:

- 4) complete wall segment+frame+glazing segment
- 5) frame+glazing segment
- 6) frame + thermal insulation panel replacing glazing

Table 5-5: Numerical results

| Numerical calculation output         | unit | symbol   | Case a | Case b |
|--------------------------------------|------|----------|--------|--------|
| total heat flow wal + frame + window | W    | Q_tot    | 26.210 | 24.270 |
| heat flow frame + window             | W    | Q_nowall | 18.910 | 18.910 |
| heat flow frame + window             | W    | Qglazing | 16.850 | 16.850 |

Table 5-6: The derived U-, L- and  $\psi$ -values for the two cases.

| Derived quantities:                               | unit               | symbol     | Case a | Case b |
|---|--------------------|------------|--------|--------|
| linear transmittance total wall-window connection | W/mK               | L_windwall | 0.2700 | 0.2787 |
| U-value frame                                     | W/m <sup>2</sup> K | U_frame    | 1.8681 | 1.8681 |
| linear transmittance frame-glazing connection     | W/mK               | PSI_fg     | 0.1051 | 0.1051 |
| linear transmittance wall-frame connection        | W/mK               | PSI_wf     | 0.0763 | 0.0850 |

## 2.4.2 Finland

Fig. 5- 13 and Fig. 5- 14 show a typical example of a Finnish window and window-wall connection. The window has a three layered glazing mounted in an aluminum and wooden frame. The wall construction is a concrete wall with cavity insulation.

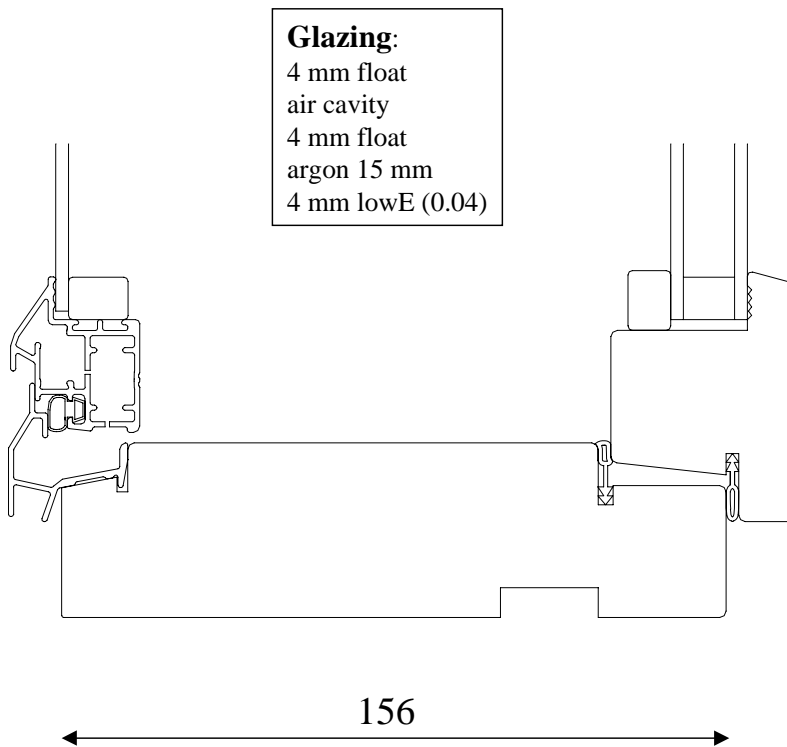


Fig. 5- 13: Structure of Finnish window.

Table 5-7: Results for Finnish window-wall assembly.

|  | Results               |
|--|-----------------------|
| $b_{\text{wallpart}}$ [m]                              | 1.010                 |
| $b_{\text{windowpart}}$ [m]                            | 0.2815                |
| $b_{\text{total}}$ [m]                                 | 1.2915                |
| $d$ (normally 1m) [m]                                  | 1.000                 |
| $\Delta T$ [K]   | 20 (default value)    |
| $U_{\text{glazing}}$ [ $\text{W}/\text{m}^2\text{K}$ ] | 0.925 (default value) |
| $U_{2\text{-dim}}$ [W]                                 | 0.5592 (with THERM)   |
| $U_{\text{wall}}$ [ $\text{W}/\text{m}^2\text{K}$ ]    | 0.2856 (with THERM)   |
| $L$ [W/mK]   | (calculated)          |

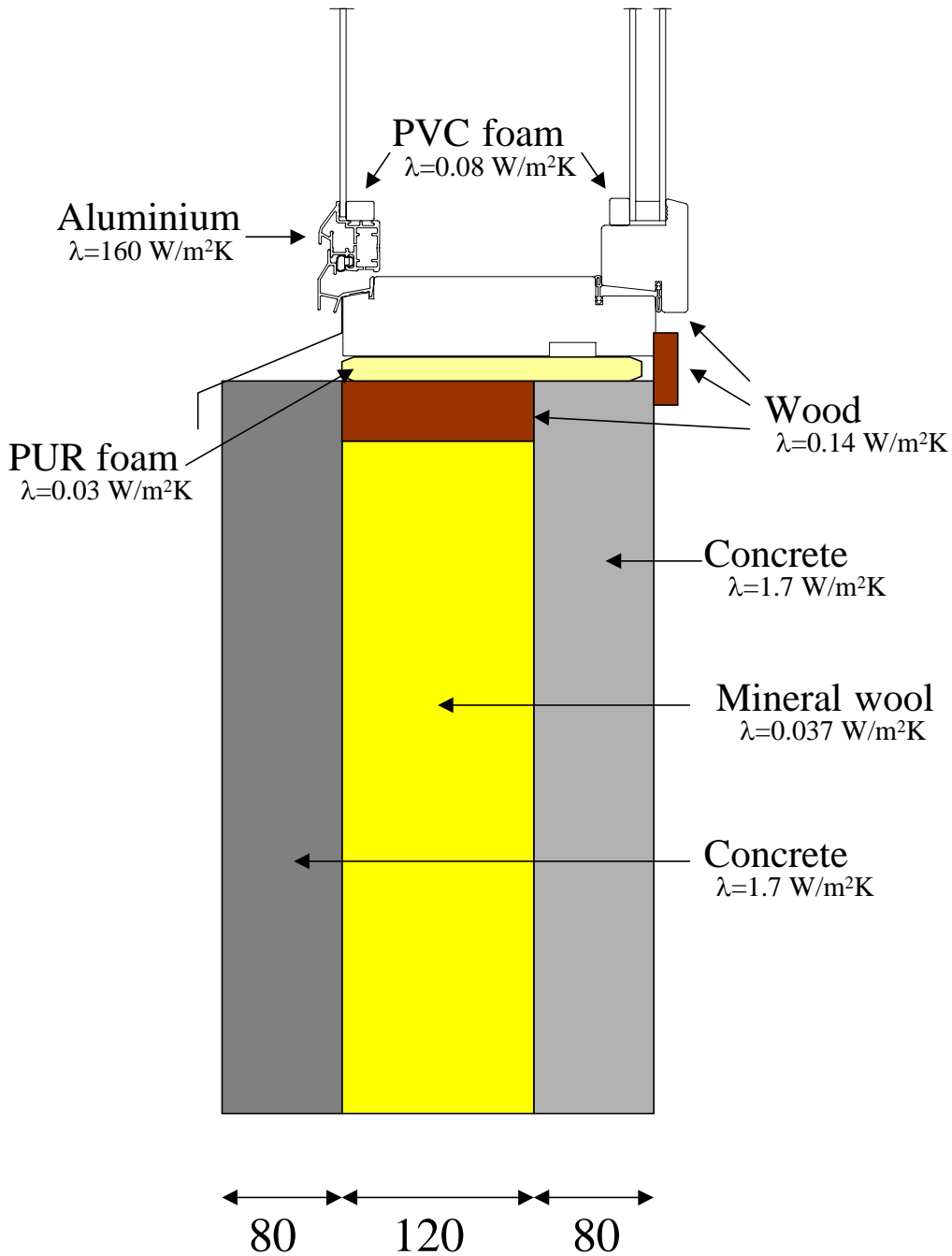


Fig. 5- 14: Finnish window-wall assembly.

### 3 Effects of window wall/roof assembly on solar transmittance

The effects of self-shading and the incidence angle on the transmitted solar energy are in general not included in the energy data describing fenestration products. These effects are normally only included when modeling is carried out on complete buildings or rooms using detailed building energy simulation tools. However, using such tools is usually time consuming and not very suited for initial product comparisons. The following proposes a simplified method to determine the effects of incidence angle and self-shading on solar transmittance for specific window–wall/roof assemblies for different window orientations and climates. Presenting the results in tabular or graphical form will facilitate a direct and more accurate product comparison and will also be helpful in product development e.g. when the resulting effects of a reduced frame area are evaluated. The effects of incidence angle and self-shading can be expressed by corrections to the transmitted solar energy at normal incidence. One correction is applied for the effect of incidence angle on the glazing part and a second correction is applied for the self-shading due to the window – wall/roof assembly. Both corrections depend on the actual climate and window orientation and the latter also depends on the geometry of the assembly.

#### 3.1 Correction for incidence angle and self-shading

The proposed method corrects the transmitted solar energy with respect to incidence angle and effects of self-shading. The correction with respect to incidence angle is performed for the direct, diffuse and reflected parts of the solar energy. The correction for self-shading is simplified and only considers the direct part of the solar energy.

The corrected transmitted solar radiation,  $I_{\text{corr}}$ , at a given time can be found as

$$I_{\text{corr}} = g_0 \cdot (I_{\text{dir}} \cdot F_{i,\text{dir}} \cdot F_{s,\text{dir}} + (I_{\text{dif}} + I_{\text{ref}}) \cdot F_{i,\text{dif}}) \quad (12)$$

$I_{\text{corr}}$  Corrected transmitted solar radiation with respect to self-shading and incidence angle [ $\text{W}/\text{m}^2$ ]

$g_0$  Total solar energy transmittance of the window at normal incidence

$I_{\text{dir}}$  Direct solar irradiance [ $\text{W}/\text{m}^2$ ]

$I_{\text{dif}}$  Diffuse solar irradiance [ $\text{W}/\text{m}^2$ ]

$I_{\text{ref}}$  Ground reflected solar irradiance [ $\text{W}/\text{m}^2$ ]

$F_{i,\text{dir}}$  Correction with respect to incidence angle for direct solar radiation

$F_{i,\text{dif}}$  Correction with respect to incidence angle for diffuse and reflected solar radiation

$F_{s,dir}$  Correction with respect to self-shading for direct solar radiation

Correction of direct solar radiation with respect to incidence angle is described by Karlsson and Roos (2000)

$$F_{i,dir} = 1 - a \cdot z^\alpha - b \cdot z^\beta - c \cdot z^\gamma \quad (13)$$

$$z = i/90 \quad (14)$$

$$a = 8, b = 0.25/q, c = 1 - a - b \quad (15)$$

$$\alpha = 5.2 + 0.7q, \beta = 2, \gamma = (5.26 + 0.06p) + (0.73 + 0.04p)q \quad (16)$$

$i$  Incidence angle [deg]

$p$  Number of panes

$q$  Category parameter between 1 and 10 (see Karlsson and Roos (2000))

A simplified correction of direct solar radiation with respect to incidence angle have been used to calculate results presented in this paper but the method described by Karlsson and Roos (2000) gives a better fit and will be used in future work. The simplified formula is given below

$$F_{i,dir} = (1 - \tan^a(i/2)) \quad (17)$$

$i$  Incidence angle [deg]

$a$  Factor of the dependency of the incidence angle

Correction of diffuse and reflected solar radiation with respect to incidence angle

$$F_{i,dif} = g_{dif}/g_0 \quad (18)$$

$g_{dif}$  Total solar energy transmittance for diffuse solar radiation (can be calculated e.g. by WIS (van Dijk and Goulding (eds), 1996))

Correction of direct solar radiation with respect to self-shading

$$F_{s,dir} = 1 - A_s/A_g \quad (19)$$

$A_s$  Shaded area of the glazing

$A_g$  Glazing area

The solar irradiation and the correction factors are all time dependent. The transmitted solar energy is found by integrating the transmitted solar radiation for a given period of time. The transmitted solar energy,  $E_{\text{sun}}$ , for a given period can be estimated as a sum of discrete steps in time

$$E_{\text{sun}} = g_0 \cdot \Sigma (I_{\text{dir}} \cdot F_{i,\text{dir}} \cdot F_{s,\text{dir}} + (I_{\text{dif}} + I_{\text{ref}}) \cdot F_{i,\text{dif}}) \cdot dt \quad (20)$$

$E_{\text{sun}}$  Transmitted solar energy for a period corrected with respect to incidence angle and effects of self-shading [Wh/m<sup>2</sup>]

The used time step (e.g. 1 hour) [h]

### 3.2 Characterizing self-shading by linear shading coefficients

The general method presented in the previous section is in the following used to characterize the effects of self-shading for a given window-wall/roof assembly. The effects of self-shading is characterized by a linear shading coefficient,  $f_s$ , defined similar to the linear transmission loss. The linear shading coefficient expresses the solar energy lost due to shading pr. length of the glazing for a given period of time.

The linear shading coefficients are found for the right, left and upper sides of the window. The solar energy lost due to shading,  $E_{\text{shaded}}$ , from one side of the window can be found as

$$E_{\text{shaded}} = g_g \cdot \Sigma (I_{\text{dir}} \cdot F_{i,\text{dir}} \cdot dt \cdot A_s) = g_g \cdot f_s \cdot l_s \cdot \Sigma (I_{\text{dir}} \cdot F_{i,\text{dir}} \cdot dt) \quad (21)$$

$g_g$  Total solar energy transmittance of the glazing at normal incidence

$A_s$  The shaded area at the given time step from the investigated side of the window [m<sup>2</sup>]

$f_s$  Linear shading coefficient [m]

$l_s$  Length of glazing [m]

The first expression use the actual shaded area and the second expression use the linear shading coefficient. This result in a linear shading coefficient defined as

$$f_s = \frac{\Sigma I_{\text{dir}} \cdot F_{i,\text{dir}} \cdot A_s \cdot dt}{l_s \cdot \Sigma I_{\text{dir}} \cdot F_{i,\text{dir}} \cdot dt} \quad (22)$$

The linear shading coefficient can be evaluated for a given period of time or at a given time. At a given time the linear shading coefficient is found as

$$f_s = \frac{A_s}{l_s} \quad (23)$$

The total shading coefficient for direct solar radiation is given by

$$F_{s,dir} = 1 - (f_{s,upper} \cdot l_{s,upper} + f_{s,left} \cdot l_{s,left} + f_{s,right} \cdot l_{s,right}) / A_g \quad (24)$$

If the direct solar radiation and the sum of diffuse and reflected solar radiation are given with respect to the incidence angle then the transmitted solar energy,  $E_{sun}$ , for a given period can then be estimated as

$$E_{sun} = g_0 \cdot (F_{s,dir} \cdot E_{dir,corr} + E_{dif,corr}) \quad (25)$$

where

$$E_{dir,corr} = \sum I_{dir} \cdot F_{i,dir} \cdot dt \quad (26)$$

$$E_{dif,corr} = \sum (I_{dif} + I_{ref}) \cdot F_{i,dif} \cdot dt \quad (27)$$

### 3.3 Evaluation of the shaded area caused by self-shading

The correction with respect to self-shading depends on an evaluation of the shaded area of the glazing. A simplified method is used to evaluate the shaded area. Evaluating the shaded area as always having a rectangular form depending only on the length of the glazing and the length of the shade gives a simple way to evaluate the shaded part of the glazing at a given time from the upper, lower, right and left side of the window.

$$F_{s,dir} = 1 - (X_{s,upper} \cdot l_{s,upper} + X_{s,lower} \cdot l_{s,lower} + X_{s,left} \cdot l_{s,left} + X_{s,right} \cdot l_{s,right}) / A_g \quad (28)$$

$l_s$  length of glazing [m]

$x_s$  length of shade on glazing [m]

The shades on the window can be divided into a primary shade from the wall and a secondary shadow from the frame. The situation is shown in Fig. 5- 13.

The length of the shades can for vertical windows be found as described in the following. For vertical windows no shades from the lower part of the window exist.

The solar azimuth, the window azimuth, the solar height and the shadow angle are used in the calculations. Calculation of the solar azimuth and the solar height can be performed by solar algorithms e.g. in The European solar radiation atlas (Scharmer and Geeif, 2000). The variables used in the following formulas are illustrated in Fig. 5-13.

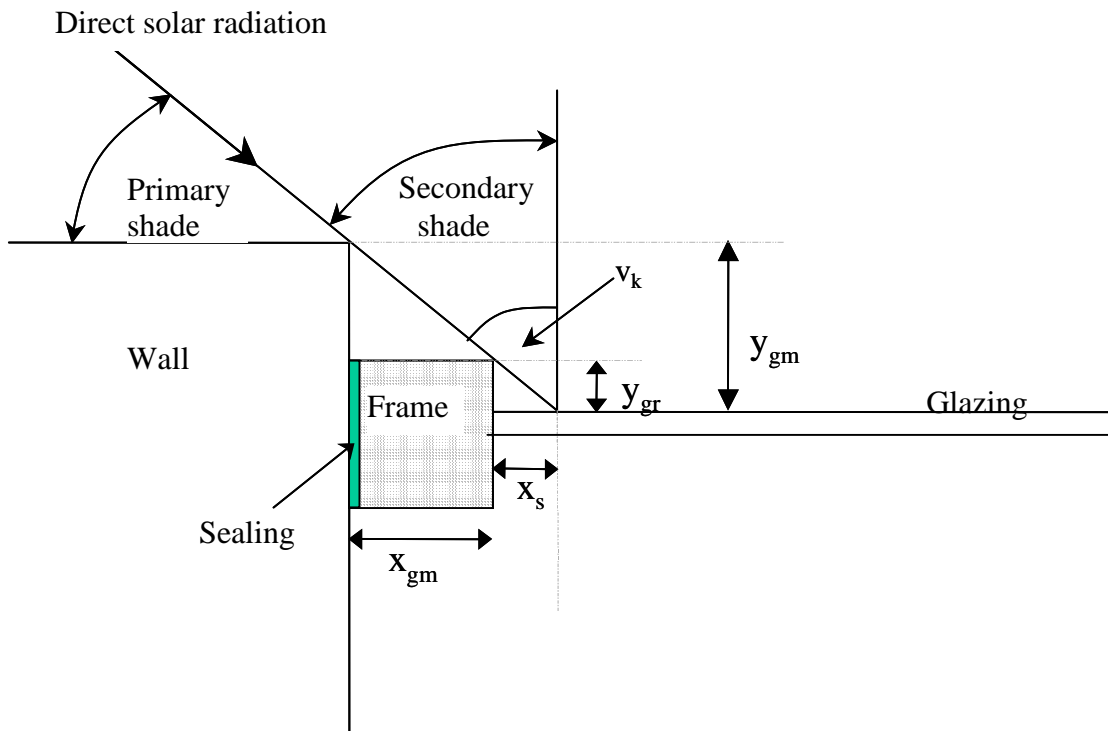


Fig. 5- 13: Shades from wall and frame. Either the wall or the frame shades the window.

The difference between the solar azimuth and the window azimuth is given as

$$\alpha_{s-w} = \alpha_s - \alpha_w \tag{29}$$

- $\alpha_s$  Solar azimuth [deg]
- $\alpha_w$  Window azimuth [deg]
- $\gamma_s$  Solar elevation [deg]
- $v_s$  Shadow angle [deg]

Shades from the left and right side of the window:

$$v_k = \arctan\left(\frac{x_{gm}}{y_{gm} - y_{gr}}\right) \quad (30)$$

$$v_s \geq v_k: \quad x_s = y_{gm} \cdot \tan(\alpha_{s-w}) - x_{gm} \quad (31)$$

$$v_s < v_k: \quad x_s = y_{gr} \cdot \tan(\alpha_{s-w}) \quad (32)$$

Shades from the top of the window:

$$v_k = \arctan\left(\frac{x_{gm}}{(y_{gm} - y_{gr}) / \cos(\alpha_{s-w})}\right) \quad (33)$$

$$v_s \geq v_k: \quad x_s = y_{gm} \cdot \frac{\tan(\gamma_s)}{\cos(\alpha_{s-w})} - x_{gm} \quad (34)$$

$$v_s < v_k: \quad x_s = y_{gr} \cdot \frac{\tan(\gamma_s)}{\cos(\alpha_{s-w})} \quad (35)$$

$x_{gm}$  Length from wall to visible part of glazing [m]

$x_s$  Length of shade on glazing [m]

$y_{gm}$  Length from glazing to wall perpendicular to the glazing [m]

$y_{gr}$  Length from glazing to frame perpendicular to glazing [m]

The shades from the top may also originate from an overhang. The length of the shade can in this case be found similar to the above. The overhang is now the primary shade and the wall is the secondary shade. The shade only originating from the frame is not included. In Fig. 5- 36 the shade from an overhang is shown.

When the length of the shade for one side of the window has been estimated the linear shading coefficient can be expressed as

$$f_s = \frac{\sum I_{dir} \cdot F_{i,dir} \cdot x_s \cdot dt}{\sum I_{dir} \cdot F_{i,dir} \cdot dt} \quad (36)$$

Evaluation of the shaded area as always having a rectangular form is an approximation. The length of the shade is not always the same as the length of the glazing at the investigated side of the window. Also overlapping shades from the sides and top of the window are not considered with the result that areas of the window that are shaded both from the side and top is included twice. Therefore the calculated shaded area is larger than in reality. To avoid this the actual shaded area at a given time step from the

investigated side of the window must be used including the shape of the shade on the glazing

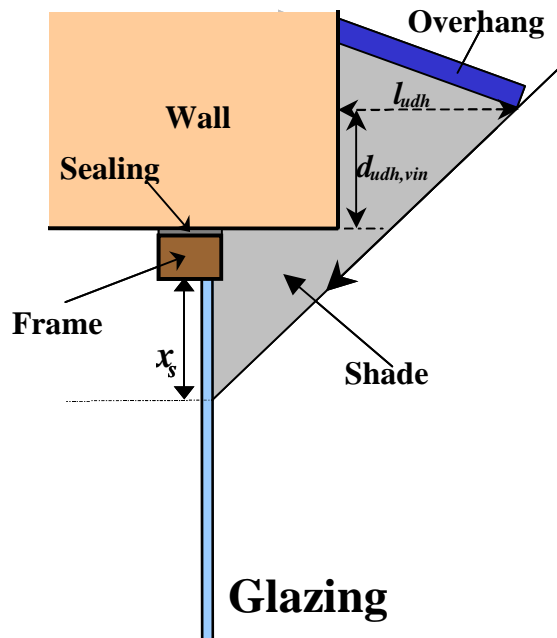
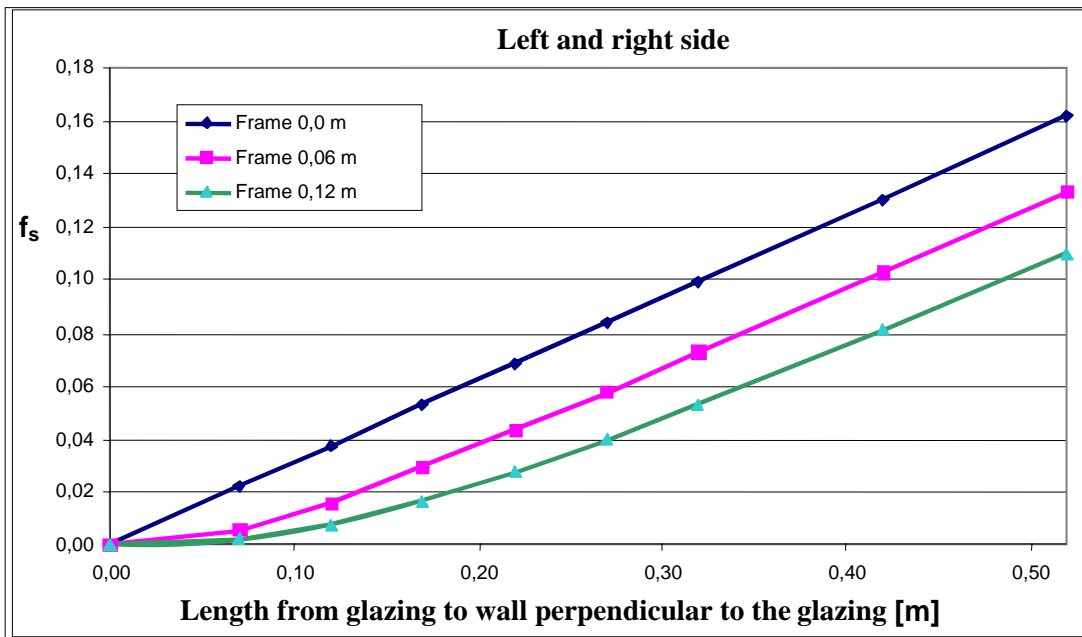


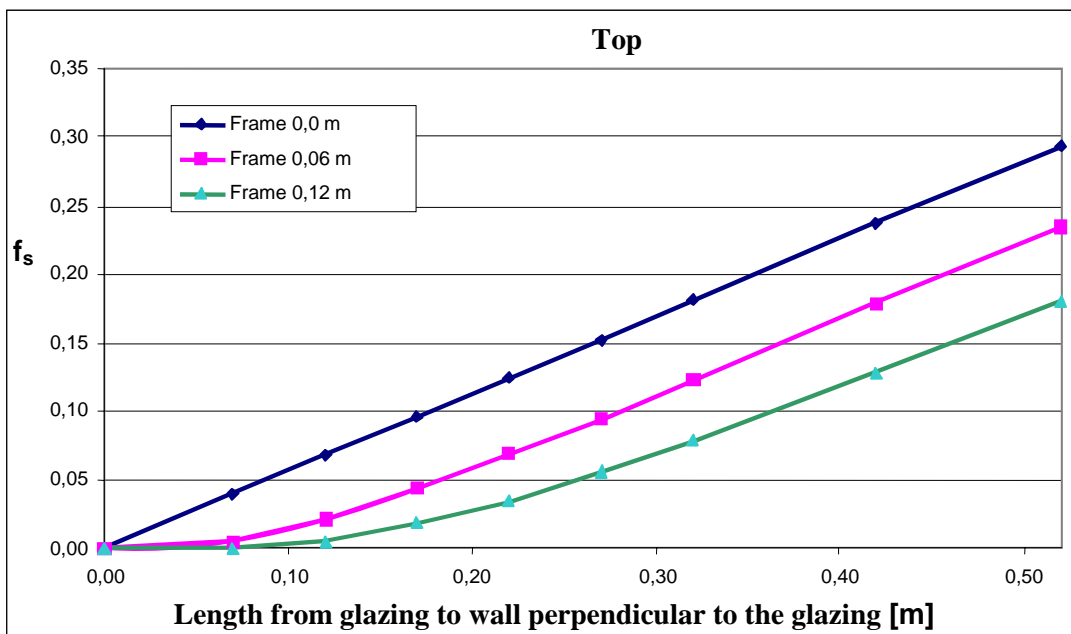
Fig. 5-14: Shades from overhang.

Also the calculation of the shaded areas does not take into account that the length of the shade may at times be larger than the width of the window. This also results in an estimated shaded area larger than in reality.

Diagrams can be used to give the linear shading coefficient in different cases. An example is shown in Fig. 5- 15. The diagram shows the linear shading coefficient for windows oriented towards south for the Danish heating season. Only the primary shade from the wall has been used to estimate  $f_s$ , neglecting the secondary shade from the frame. The linear shading coefficient is shown as a function of the length from wall to visible part of glazing,  $x_{gm}$ , and the length from glazing to wall perpendicular to the glazing,  $y_{gm}$ . The diagrams must be made for different orientations and different periods of time e.g. the heating and cooling season.



A.  $f_s$  for shades from the left and right sides



B.  $f_s$  for shades from the top

Fig. 5- 15: Diagram showing the linear shading coefficient for windows oriented towards south for the Danish heating season. The linear shading coefficient can be found for different widths of the frame and different lengths from the glazing to the wall.

### 3.4 Example

To give an example the linear shading coefficients are found for a window that measures 2m×2m oriented towards south. The window-wall assembly is shown in Fig. 5- 16 and has the same geometry on all four sides of the window. The width of the frame (including the sealing) is 0.06m and the distance from the glazing to the wall is 0.15m. The glazing length on all for sides is  $(2\text{m}-2\cdot 0.06\text{m}) = 1.88\text{ m}$ .

The linear shading coefficients can be found in Fig. 5-15:

$$f_{s,\text{left}} = 0.025$$

$$f_{s,\text{right}} = 0.025$$

$$f_{s,\text{top}} = 0.04$$

This results in a total shading coefficient for direct solar radiation during the heating season of

$$\begin{aligned} F_{s,\text{dir}} &= 1 - (f_{s,\text{upper}} \cdot l_{s,\text{upper}} + f_{s,\text{left}} \cdot l_{s,\text{left}} + f_{s,\text{right}} \cdot l_{s,\text{right}}) / A_g \\ &= 1 - (0.04 \cdot 1.88 + 0.025 \cdot 1.88 + 0.025 \cdot 1.88) / (1.88 \cdot 1.88) \\ &= 0.95 \end{aligned}$$

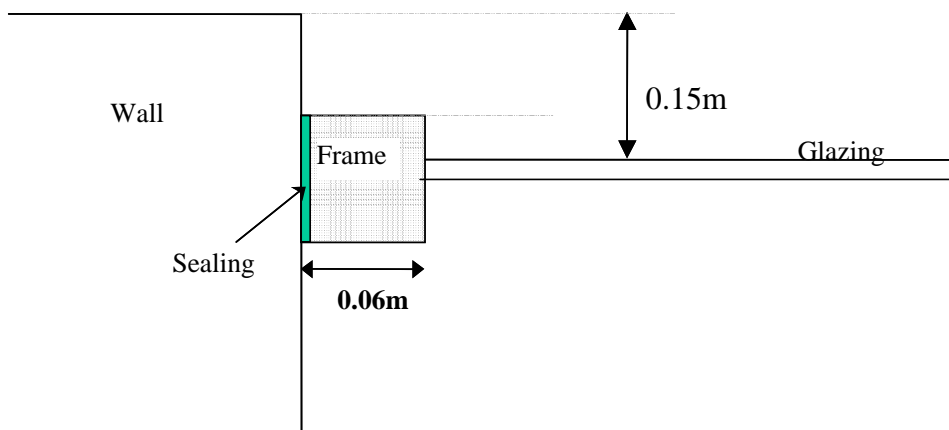


Fig. 5- 16: Example window-wall assembly.

### 3.5 Investigation of the linear shading coefficient

The shaded areas calculated by the method in chapter 4 does not take into account that the length of the shade may at times be larger than the width of the window. The result is that the evaluated shaded area at times is larger than in reality. For small windows this may be a problem. To address this problem the linear shading coefficients are calculated with regard to the total window geometry using eq. 11. The linear shading coefficients are calculated for a small window measuring 1m×1m and a large window measuring 10m×10m. Table 8 shows the deviations depending on the length from glazing to wall perpendicular to the glazing,  $y_{gm}$ . It can be seen that the deviations are small as long as  $y_{gm}$  is no larger than 0.4m. In normal Danish window-wall assemblies the length,  $y_{gm}$ , rarely exceeds 0.2m. Therefore, it is concluded that the error of not including the total window geometry in the evaluation of the linear shading coefficients is acceptable.

Table 5-8: Deviations between linear shading coefficients

| $y_{gm}$ [m] | $f_{s,1\times1}/f_{s,10\times10}$ |       |      |
|--------------|-----------------------------------|-------|------|
|              | Left                              | Right | Top  |
| 0.05         | 1                                 | 1     | 1    |
| 0.1          | 1                                 | 1     | 1    |
| 0.15         | 1                                 | 0.99  | 1    |
| 0.2          | 0.99                              | 0.99  | 1    |
| 0.25         | 0.98                              | 0.98  | 1    |
| 0.3          | 0.97                              | 0.97  | 1    |
| 0.4          | 0.95                              | 0.95  | 1    |
| 0.5          | 0.93                              | 0.93  | 1    |
| 1            | 0.79                              | 0.80  | 0.91 |
| 2            | 0.56                              | 0.57  | 0.68 |

### 3.6 Relation to other methods

In the European standard EN 832 correction for shading and incidence angel is done by correction of the total solar energy transmittance. The corrected total solar energy transmittance,  $g_{corr}$ , is defined as

$$g_{corr} = F_w \cdot F_s \cdot g_0 \quad (37)$$

$F_s$  Shading correction factor

$F_w$  Incidence angle correction factor

$g_0$  Total solar energy transmittance of the window at normal incidence

The transmitted solar energy corrected for shades and incidence angle is found as

$$E_{\text{sun}} = F_{\text{corr}} \cdot g_0 \cdot \Sigma(I_{\text{dir}} + I_{\text{dif}} + I_{\text{ref}}) \cdot dt \quad (38)$$

$$F_{\text{corr}} = F_w \cdot F_s \quad (39)$$

Values for  $F_s$  and  $F_w$  are given in tables. The linear shading coefficients can be used to find  $F_{\text{corr}}$ .

Combining the method in EN832 with the method described in this paper gives

$$F_{\text{corr}} \cdot g_0 \cdot \Sigma(I_{\text{dir}} + I_{\text{dif}} + I_{\text{ref}}) \cdot dt = g_0 \cdot \Sigma(I_{\text{dir}} \cdot F_{i,\text{dir}} \cdot F_{s,\text{dir}} + (I_{\text{dif}} + I_{\text{ref}}) \cdot F_{i,\text{dif}}) \cdot dt \quad (40)$$

which for  $F_{\text{corr}}$  gives

$$F_{\text{corr}} = \frac{\Sigma(I_{\text{dir}} \cdot F_{i,\text{dir}} \cdot F_{s,\text{dir}} + (I_{\text{dif}} + I_{\text{ref}}) \cdot F_{i,\text{dif}}) \cdot dt}{\Sigma(I_{\text{dir}} + I_{\text{dif}} + I_{\text{ref}})} \quad (41)$$

where

$$F_{s,\text{dir}} = 1 - (f_{s,\text{upper}} \cdot l_{s,\text{upper}} + f_{s,\text{left}} \cdot l_{s,\text{left}} + f_{s,\text{right}} \cdot l_{s,\text{right}}) / A_g \quad (42)$$

### 3.7 Simplifications and further work

The correction with respect to self-shading only corrects the part of the direct solar radiation blocked by constructions near the window. Fig. 5- 17 shows the influence from the wall on the solar radiation in more detail. Apart from blocking direct solar radiation the wall also blocks diffuse solar radiation and reflects direct and diffuse solar radiation onto the glazing. The effects of a correction with regard to diffuse solar radiation and reflected solar energy from the wall are expected to be small compared to the correction with regard to direct solar radiation.

View factors may be used to correct the diffuse solar radiation. The correction may be done by subtracting the view factor from the glazing to the wall from the view factor from the unblocked glazing to the diffuse radiation source. The view factors may have to be calculated with respect to an anisotropic radiation distribution.

Evaluation of the solar radiation reflected by the wall depends on the properties of the wall surface.

As further work it is proposed to investigate the influence of the wall-window assembly on the diffuse solar radiation and the solar energy reflected by the wall. A ray-tracing program may be used to investigate these effects. Hopefully the effects are small and as they have opposite signs they may cancel out.

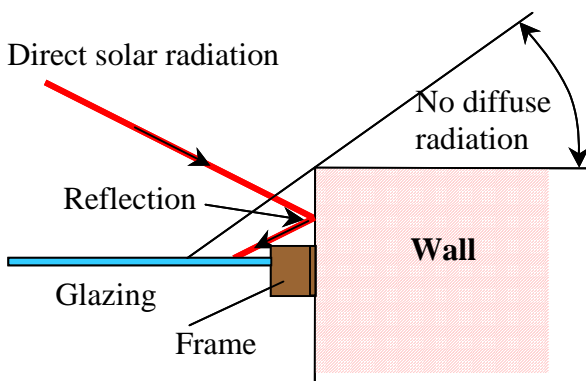


Fig. 5- 17: Solar radiation near the window. The wall block both direct and diffuse solar radiation giving rise to shades but at the same time the wall reflects direct and diffuse solar radiation onto the glazing.

## 3.8 Ray tracing

### 3.8.1 Model description

Ray tracing on complex structures is conveniently carried out using the commercial software package OptiCAD<sup>1</sup>. The program is structured in a computer-aided design (CAD) format in which the user defines objects, then places and orients them in a global-coordinate system. The optical system is not constrained to any rotational symmetry. As the rays interact with the objects, the program keeps track of the energy associated with each ray, including all secondary rays that may be generated (for example at a partially transmitting and partially reflecting surface). OptiCAD includes elements called radiometers that can be attached to or placed in front of individual surfaces to record the energy of the rays striking that surface. The results, including the energy distribution on the radiometers, can be output to file in a form compatible with spreadsheet and other programs for further analysis.

The model of a vertical glazing unit, surrounded by a frame with a sill and set in a wall is conveniently defined in an Excel spreadsheet. This allows the number and dimensions of the building components to be changed easily. When saved as a text file, this is directly readable by OptiCAD. The full model includes a double-glazing element so that light transmission can be studied, but this was not needed for the present work, in which we restrict ourselves to an analysis of the light distribution striking the outer surface of the glazing. The dimensions of the building components relevant to this study are given in Table 9. A rectangular film of the same dimensions as the glazing was placed immediately in front of the glazing. A radiometer attached to the film was divided into a square array of 20 times 20 bins. The reflectance of the wall, frame and sill were assumed to be diffuse (Lambertian). Fig. 5- 18 shows the model. A ground plane is shown in the figure to aid visualisation, but in the study the ground reflectance was set to zero.

Table 5-9: Dimensions, in m, of building components used in the model.

|                          |                |                                      |       |
|--------------------------|----------------|--------------------------------------|-------|
| Glazing Width            | 1.23           | Glazing Height                       | 1.48  |
| Frame width              | 0.15           | Frame depth to outer glazing surface | 0.02  |
| Wall width               | 5              | Wall height                          | 5     |
| Wall depth to frame face | 0.078 or 0.156 |                                      |       |
| Sill height, inner       | 0.025          | Sill height, outer                   | 0.015 |
| Sill depth               | 0.03           |                                      |       |

<sup>1</sup> OptiCAD 7, OptiCAD Corporation, Santa Fe, NM, 87501 USA.

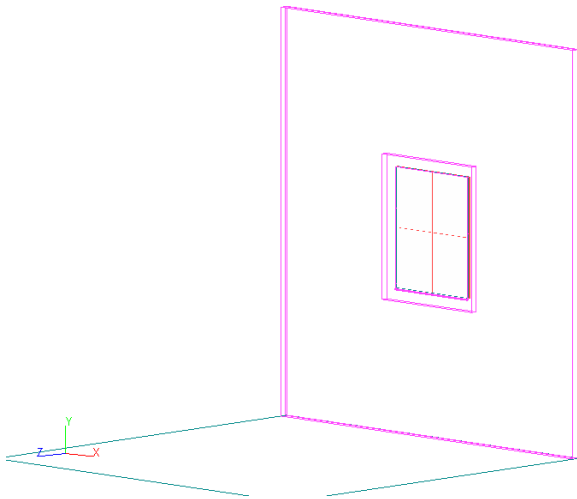


Fig. 5-18: Model of vertical wall with frame, sill and glazing.

The light source used in OptiCAD to simulate the sun generates rays distributed randomly across a disk, with a mean beam divergence of  $0.28^\circ$ . To ensure that the beam of rays covered the window and surrounding frame and wall, the “sun”'s diameter was set to 1.6m. Because of the random distribution of the rays across the disk, repeat runs for the same conditions do not give exactly the same result. To ensure that the effect of including reflections in the calculated shading factor could be determined to better than 1%,  $3 \times 10^7$  rays were used in each ray trace.

### 3.8.2 Simple method compared to results from ray tracing with zero reflectance

The wall was placed facing south. The sun's position was varied. For convenient comparison with the simplified method, the solar altitude and azimuth were calculated for two (arbitrarily chosen) days at latitude  $55.5^\circ\text{N}$ . The angles for each calculation are given in Table 10.

Ray traces were carried out first with the wall, frame and sill reflectances set to 0. At each solar position a second ray trace was carried out with the wall, frame and sill deactivated (i.e. OptiCAD ignores them in the ray trace). The latter calculation gives the irradiance on an unobstructed glazing. The ratio gives the shading factor,  $F(0)$ , due to the geometrical shading of the glazing by the wall, frame and sill. The results are given in Table 10.

The simple method does not take into account overlapping shadows and therefore the shaded area evaluated by the simple method is always larger than or equal to the actual shaded area, leading to a smaller shading factor.

Table 5-10: Shading factors from simple calculation compared to shading factors evaluated using ray tracing with zero reflectance.

| Date                          | Solar azimuth, ° | Solar altitude, ° | $F(0)_{\text{ray traced}}$ | $F(0)_{\text{simple}}^2$ |
|-------------------------------|------------------|-------------------|----------------------------|--------------------------|
| 21. June                      | 0                | 58.00             | 0.978                      | 0.978                    |
|                               | 15               | 57.30             | 0.974                      | 0.974                    |
|                               | 30               | 55.28             | 0.968                      | 0.968                    |
|                               | 45               | 51.66             | 0.960                      | 0.960                    |
|                               | 60               | 46.14             | 0.937                      | 0.935                    |
|                               | 75               | 38.24             | 0.742                      | 0.724                    |
| 21. August                    | 0                | 46.40             | 0.986                      | 0.986                    |
|                               | 15               | 45.46             | 0.981                      | 0.981                    |
|                               | 30               | 43.02             | 0.976                      | 0.976                    |
|                               | 45               | 38.76             | 0.968                      | 0.968                    |
|                               | 60               | 32.48             | 0.955                      | 0.955                    |
|                               | 75               | 24.17             | 0.805                      | 0.801                    |
| 21. June<br>Double wall width | 0                | 58.00             | 0.911                      | 0.911                    |
|                               | 45               | 51.66             | 0.869                      | 0.868                    |
|                               | 65               | 43.82             | 0.678                      | 0.646                    |

### 3.8.3 Influence of reflectance

The correction with respect to self-shading only corrects the part of the direct solar radiation blocked by constructions near the window. Fig. 5- 19 shows the influence from the wall on the solar radiation in more detail. Apart from blocking direct solar radiation the wall also blocks diffuse solar radiation and reflects direct and diffuse solar radiation onto the glazing. In this study, diffuse radiation has not been considered.

The reflectance was varied between 0 and 1 for all three elements, and results are also reported for the more realistic mixed case with a wall reflectance of 0.2 (brick, say) and frame and sill reflectances of 0.8 (glossy white paint, for example). The effect of reflections from wall, frame and sill can be seen from the results of ray-tracings shown in Fig. 5- 20. The left picture shows the shaded glazing with zero reflectance. The blue area is shaded whereas the red area is in sun. The right picture shows the same situation only with the reflectance of the wall, frame and sill set to 1. It is seen that the reflections change the

<sup>2</sup> The shaded area is calculated without taking overlapping shades into account [Nielsen, 2001 pp. 4-6]. Therefore the deviation between the ray-traced and simple results increases with the shaded area.

pattern of the incident solar radiation. The lower right corner of the window now has a contribution from the reflected radiation.

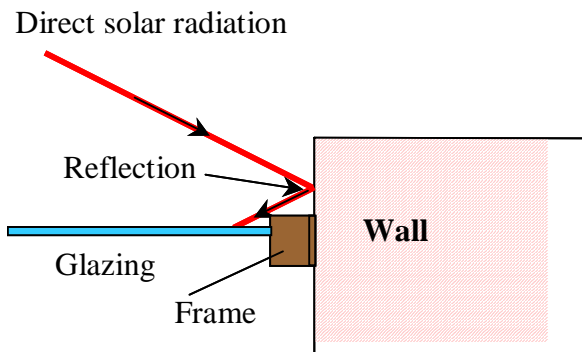


Fig. 5- 19: Solar radiation near the window. The wall and frame reflect direct solar radiation onto the glazing.

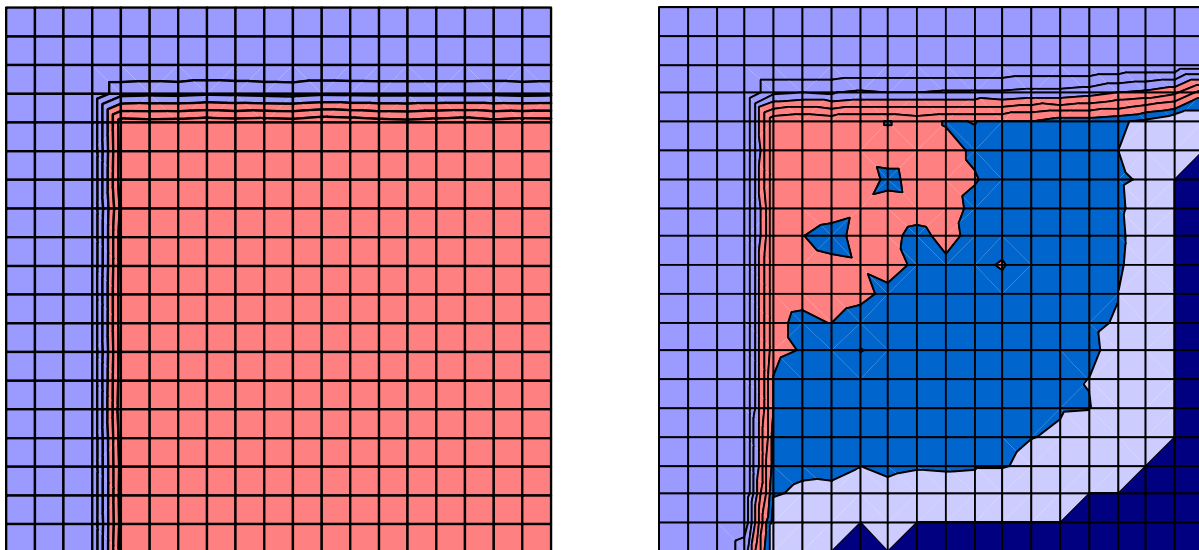


Fig. 5- 20: Solar radiation distribution on the radiometer placed in front of the glazing. Sun at azimuth 65°, altitude 43.82°: Wall depth 0.158m. Left: Incident radiation on shaded glazing with zero reflectance. Right: Incident radiation on shaded glazing with wall.

Table 11 shows the results of the ray tracings performed for two days and two wall depths. In Fig. 5- 21 the shading factor is plotted as a function of the reflectance. It is seen that for any particular geometry (this includes size and shape of building components and sun’s position), the correction to the shading factor with regard to the reflectance is a linear function of reflectance:

$$f_r(\rho) \equiv \frac{F(\rho)}{F(0)} = 1 + b\rho \quad (43)$$

with

$$b = \frac{F(1) - F(0)}{F(0)} \quad (44)$$

Fig. 5- 22 shows  $b$  plotted against  $F(0)$ . It can be seen that  $b$  is a function of the geometry. This will be the subject of future studies.

Table 5-11: Shading factors for two different days and wall depths as function of the wall and frame reflectances.

| Date   | Azimuth,<br>° | Solar<br>altitude,<br>° | Shading factor $F(\rho)$                |       |       |       |             | $F(1)/F(0)$ |
|--------|---------------|-------------------------|---|-------|-------|-------|-------------|-------------|
|        |               |                         | Reflectance $\rho$ (diffuse Lambertian) |       |       |       |             |             |
|        |               |                         | 0                                       | 0.2   | 0.5   | 1     | $0.2/0.8^3$ |             |
| 21-jun | 75            | 38.24                   | 0.742                                   | 0.759 | 0.784 | 0.832 | 0.786       | 1.121       |
|        | 70            | 41.27                   | 0.841                                   | 0.855 | 0.875 | 0.915 | 0.878       | 1.087       |
|        | 65            | 43.82                   | 0.905                                   | 0.917 | 0.933 | 0.968 | 0.936       | 1.070       |
|        | 60            | 46.14                   | 0.937                                   | 0.946 | 0.962 | 0.994 | 0.966       | 1.060       |
|        | 45            | 51.66                   | 0.960                                   | 0.967 | 0.979 | 1.003 | 0.982       | 1.045       |
|        | 30            | 55.28                   | 0.968                                   | 0.974 | 0.983 | 1.004 | 0.985       | 1.037       |
|        | 15            | 57.30                   | 0.974                                   | 0.979 | 0.987 | 1.005 | 0.989       | 1.032       |
|        | 0             | 58.00                   | 0.978                                   | 0.983 | 0.989 | 1.005 | 0.990       | 1.028       |
| 21-aug | 75            | 24.17                   | 0.805                                   | 0.820 | 0.841 | 0.883 | 0.844       | 1.097       |
|        | 70            | 27.15                   | 0.884                                   | 0.896 | 0.912 | 0.948 | 0.916       | 1.072       |
|        | 65            | 29.93                   | 0.933                                   | 0.944 | 0.957 | 0.987 | 0.960       | 1.058       |
|        | 60            | 32.48                   | 0.955                                   | 0.964 | 0.975 | 1.002 | 0.978       | 1.049       |
|        | 45            | 38.76                   | 0.968                                   | 0.975 | 0.984 | 1.004 | 0.985       | 1.037       |
|        | 30            | 43.02                   | 0.976                                   | 0.980 | 0.988 | 1.005 | 0.989       | 1.030       |
|        | 15            | 45.46                   | 0.981                                   | 0.985 | 0.992 | 1.006 | 0.993       | 1.025       |
|        | 0             | 46.40                   | 0.986                                   | 0.989 | 0.994 | 1.007 | 0.994       | 1.021       |
| 21-jun | 65            | 43.82                   | 0.678                                   |       |       | 0.812 | 0.719       | 1.198       |
| Double | 45            | 51.66                   | 0.869                                   |       |       | 0.961 | 0.898       | 1.106       |

<sup>3</sup> Different reflectance of wall and frame. Wall reflectance of 0.2 and frame and sill reflectance of 0.8.

|            |   |       |       |  |  |       |       |       |
|------------|---|-------|-------|--|--|-------|-------|-------|
| wall depth | 0 | 58.00 | 0.911 |  |  | 0.974 | 0.930 | 1.070 |
|------------|---|-------|-------|--|--|-------|-------|-------|

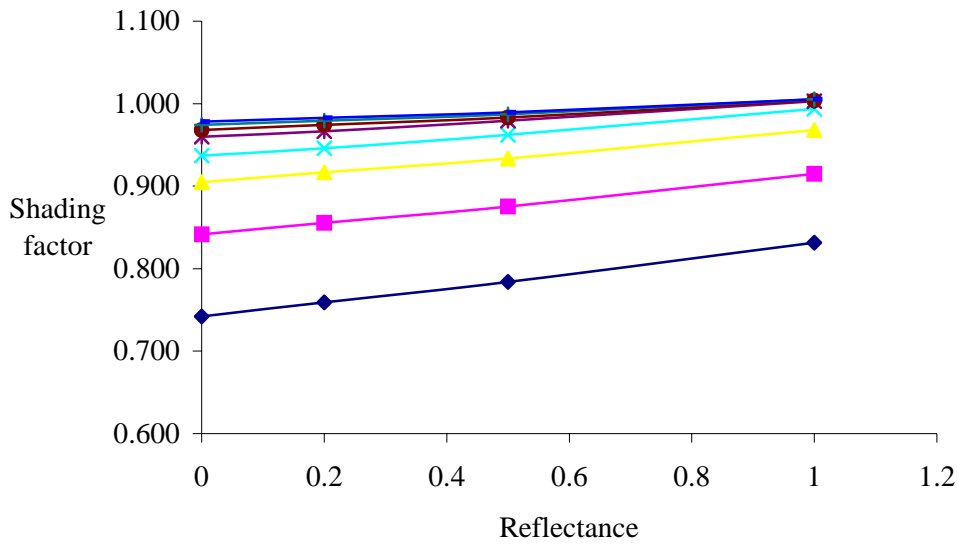


Fig. 5- 21: Shading factor as a function of the reflectance.

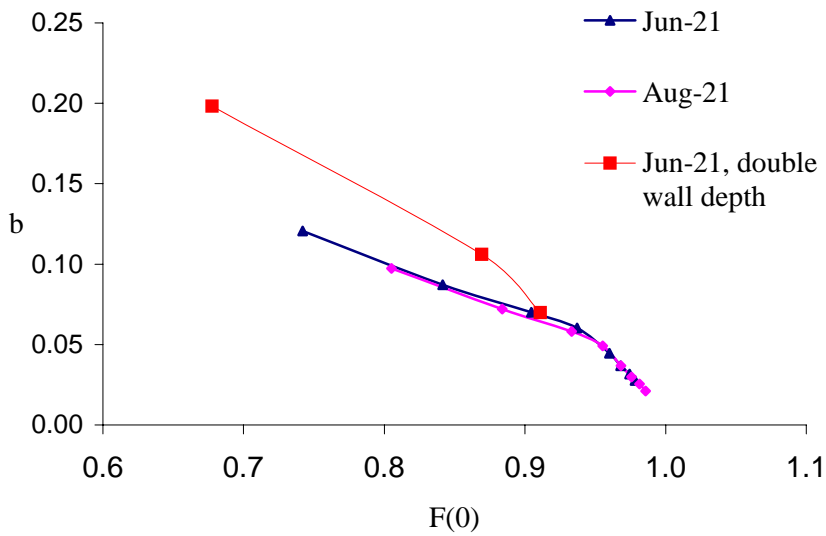


Fig. 5- 22: The function b (equation (2)) versus F(0) for the cases shown in table 11.

In the spirit of the method developed in (Nielsen, 2001), we wish to calculate a weighted average correction factor,  $f_r$ , for the effect of reflections. Analogously to Equation (9) of Nielsen (2001) the direct solar radiation's contribution to the total solar energy transmitted through the glazing during a time  $dt$  is written as:

$$E_{sun,dir} = g_0 \sum I_{dir} F_{i,dir} F_{s,dir} dt \quad (45)$$

Where the symbols have the following meanings

- $g_0$  Total solar energy transmittance of the window at normal incidence
- $I_{dir}$  Direct solar irradiance [ $W/m^2$ ]
- $F_{i,dir}$  Correction with respect to incidence angle for direct solar radiation
- $F_{s,dir}$  Correction with respect to self-shading for direct solar radiation.

The correction with regard to the incidence angle can be estimated as

$$F_{i,dir} = 1 - \tan^a(i/2) \quad (46)$$

where

- $i$  Incidence angle [deg]
- $a$  Factor of the dependency of the incidence angle. For a two-pane low-e coated glazing  $a \cong 3$ .

We now write

$$F_{s,dir} = F(0) f_r \quad (47)$$

where  $F(0)$  is the shading factor with reflectance equal to zero.

Table 12 shows the weighted influence of the reflected solar energy for two days. The last column shows  $\bar{f}_r(1)$  which is the value of  $f_r$  averaged over the day, weighted by the product  $[I_{dir} F_{i,dir} F(0)]$  for each hour. It is seen that reflected solar energy increases the incident solar energy by a few percent on a daily basis.

Table 5-12: Influence of reflections on incident solar radiation.

| Date          | Time <sup>4</sup> | Azimuth,<br>° | Solar<br>altitude, ° | Incidence<br>angle | Direct solar<br>radiation<br>[W/m <sup>2</sup> ] <sup>5</sup> | F <sub>i,dir</sub> | E <sub>sun, dir</sub><br>[Wh/m <sup>2</sup> ] <sup>6</sup> |            | $\bar{f}_r$ <sup>7</sup> (1) |
|---------------|-------------------|---------------|----------------------|--------------------|---|--------------------|--|------------|------------------------------|
|               |                   |               |                      |                    |   |                    | $\rho = 0$   | $\rho = 1$ |                              |
| 21.<br>June   | 7                 | -75           | 38.24                | 78                 | 0   | 0.47               | 0.0  | 0.0        |                              |
|               | 8                 | -60           | 46.14                | 70                 | 31.4  | 0.66               | 19.4   | 20.6       |                              |
|               | 9                 | -45           | 51.66                | 64                 | 16.8  | 0.76               | 12.3   | 12.8       |                              |
|               | 10                | -30           | 55.28                | 60                 | 42.2  | 0.81               | 33.1   | 34.3       |                              |
|               | 11                | -15           | 57.30                | 59                 | 18.0  | 0.82               | 14.4   | 14.9       |                              |
|               | 12                | 0             | 58.00                | 58                 | 17.9  | 0.83               | 14.6   | 15.0       |                              |
|               | 13                | 15            | 57.30                | 59                 | 5.0   | 0.82               | 4.0  | 4.1        |                              |
|               | 14                | 30            | 55.28                | 60                 | 4.4   | 0.81               | 3.5  | 3.6        |                              |
|               | 15                | 45            | 51.66                | 64                 | 0   | 0.76               | 0.0  | 0.0        |                              |
|               | 16                | 60            | 46.14                | 70                 | 8.2   | 0.66               | 5.1  | 5.4        |                              |
|               | 17                | 75            | 38.24                | 78                 | 1.4   | 0.47               | 0.5  | 0.6        |                              |
| Sum           |                   |               |                      |                    |   |                    | 106.8  | 111.3      | 1.04                         |
| 21.<br>August | 7                 | -75           | 24.17                | 76                 | 14.1  | 0.52               | 5.9  | 6.4        |                              |
|               | 8                 | -60           | 32.48                | 65                 | 102.5   | 0.74               | 72.5   | 76.1       |                              |
|               | 9                 | -45           | 38.76                | 57                 | 172.1   | 0.84               | 140.0  | 145.2      |                              |
|               | 10                | -30           | 43.02                | 51                 | 401.6   | 0.89               | 348.8  | 359.2      |                              |
|               | 11                | -15           | 45.46                | 47                 | 567.5   | 0.92               | 512.4  | 525.4      |                              |
|               | 12                | 0             | 46.40                | 46                 | 632.9   | 0.92               | 574.0  | 586.2      |                              |
|               | 13                | 15            | 45.46                | 47                 | 620.6   | 0.92               | 560.3  | 574.6      |                              |
|               | 14                | 30            | 43.02                | 51                 | 520.5   | 0.89               | 452.0  | 465.5      |                              |
|               | 15                | 45            | 38.76                | 57                 | 226.7   | 0.84               | 184.4  | 191.2      |                              |
|               | 16                | 60            | 32.48                | 65                 | 76.9  | 0.74               | 54.4   | 57.0       |                              |
|               | 17                | 75            | 24.17                | 76                 | 37.1  | 0.52               | 15.5   | 17.0       |                              |
| Sum           |                   |               |                      |                    |   |                    | 2920.2   | 3003.8     | 1.03                         |

<sup>4</sup> The time is based on solar azimuth of 0° at noon.

<sup>5</sup> The direct solar irradiance is evaluated using the Danish design reference year.

<sup>6</sup> E<sub>sun</sub> is calculated with g<sub>0</sub> = 1 and the shading factors are assumed the same for positive and negative values of the azimuth.

<sup>7</sup> The weighted mean daily correction with regard to reflection of direct solar radiation

## 4 References

- [1] Nielsen, T. R. (2001) Self-shading effects from window-wall/roof assembly on the g-value. r-A3(5)-DTU-trn(2). Internal IEA Task 27 report.
- [2] Karlsson, J. and Roos, A. (2000) Modelling the angular behavior of the total solar energy transmittance of windows. Solar energy, Vol. 69, No. 4.
- [3] van Dijk D. and Goulding J. (eds.) (1996) WIS reference manual, TNO Building and Construction Research, Delft and University College Dublin.
- [4] Scharmer, K. and Greif, J. (2000) The European Solar Radiation Atlas, Vol 2, École des Mines, Paris.
- [5] prEN ISO 10211-2 (1995) Thermal bridges in building construction – Heat flows and surface temperatures – Part 2: Calculation of linear thermal bridges, CEN, Brussels.
- [6] prEN ISO 10077-2 (2000) Thermal performance of windows, doors and shutters – Calculation of thermal transmittance – Part 2: Numerical methods for frames, CEN, Brussels.